Spectral Analysis and Computation of Effective Diffusivities for Steady Random Flows

N. B. Murphy* and J. Xin

University of California at Irvine, Department of Mathematics,

340 Rowland Hall, Irvine, CA 92697-3875, USA

E. Cherkaev, J. Zhu, and K. M. Golden

University of Utah, Department of Mathematics,

155 S 1400 E, RM 233, Salt Lake City, UT 84112-0090, USA

Advective diffusion of passive tracers by fluid flow plays a key role in the transport of salt, heat, buoys and markers in geophysical flows, in the dispersion of pollutants and trace gases in the atmosphere, and even in the motion of sea ice floes influenced by winds and ocean currents. The long time, large scale behavior of such systems is equivalent to an enhanced diffusion process with an effective diffusivity tensor D^*. Over twenty five years ago, a Stieltjes integral representation for the homogenized tensor was derived, involving the spectral measure of a self-adjoint operator that depends on the flow characteristics. However, analytical calculations of D^* have been obtained for only a few simple flows, and numerical computations of the effective behavior based on this powerful representation have apparently not been attempted. We overcome these limitations by providing a mathematical foundation for rigorous computation of D^*. We explore two different approaches and for each approach we derive Stieltjes integral representations for the symmetric and antisymmetric parts of D^*, involving a spectral measure of a self-adjoint random operator. In discrete formulations of each approach, we express the spectral measure explicitly in terms of standard (or generalized) eigenvalues and eigenvectors of Hermitian matrices. We develop and implement a numerically efficient projection method that significantly reduces the dimension of the random matrix in computations of spectral statistics. We use this method to compute the effective behavior for several model flows and relate spectral characteristics to flow geometry and transport properties.

* University of Utah, Department of Mathematics, 155 S 1400 E, RM 233, Salt Lake City, UT 84112-0090, USA

I. INTRODUCTION

The enhancement in diffusive transport of passive scalars by complex fluid flow plays a key role in many important processes in the global climate system [55] and Earth's ecosystems [14]. Advection of geophysical fluids intensifies the dispersion and large scale transport of heat [36], pollutants [7, 12, 48], and nutrients [14, 21] diffusing in their environment. Advective processes also enhance the large scale transport of plankton [21], which is an important component of the food web that sustains life in the polar oceans. The transport of vast sea ice floes in the polar oceans is driven by a seasonally and regionally changing balance in oceanic and atmospheric forces [28, 55]. These forces can enhance the transport of sea ice floes by eddie fluxes in the atmosphere and ocean currents [28, 44, 45, 56].

Complex interactions between shearing ocean waves, tidal currents, and wind drift, for example, gives rise to complex, behavior of the flow fields [11, 27, 59]. It was discovered in the early 1900s [53] that complex fluid flows transport passive scalars in much the same way as molecular diffusion. The mathematical description of this phenomenon [54] demonstrated that the long time, large scale behavior of a diffusing particle or tracer being advected by an *incompressible* fluid velocity field is equivalent to an enhanced diffusion process with an effective diffusivity tensor D^*. Describing the enhancement of the effective transport properties by fluid advection is a challenging problem with theoretical and practical importance in many fields of science and engineering, ranging from turbulent combustion [1, 10, 43, 52, 57, 58] to mass, heat, and salt transport in geophysical flows [36].

A broad range of mathematical techniques have been developed that reduce the analysis of complex fluid flows, with rapidly varying structures in space and time, to solving averaged or *homogenized* equations that do not have rapidly varying data, and involve an effective parameter [9, 15, 16, 29–31, 41, 58]. Homogenization of the advection-diffusion equation for passive scalar transport by random, time-independent, *mean-zero* fluid velocity fields was treated in [31]. This reduced the analysis of advective diffusion to solving a diffusion equation involving a homogenized temperature and a (constant) effective diffusivity tensor D^*.

An important consequence of this analysis is that the effective diffusivity D^* is given in terms of a random "cell problem" involving a curl-free stationary stochastic process [31], which satisfies a steady state diffusion equation involving a skew-symmetric random matrix H [2, 3, 15, 16]. By adapting the analytic continuation method of homogenization theory

for composite materials [19], it was shown [2, 3] that the cell problem could be written as a resolvent formula involving a self-adjoint random operator acting on the Hilbert space of *curl-free vector fields*. This, in turn, led to a Stieltjes integral representation for the *symmetric* part of D*, involving the Péclet number Pe of the flow and a *spectral measure* of the operator. A key feature of the integral representation for D* is that parameter information in Pe is *separated* from the geometry of the fluid velocity field, which is encoded in the spectral measure through its moments. This parameter separation has led [2, 3] to rigorous forward bounds for the diagonal components of D*.

The mathematical framework developed in [31] was adapted [41] to the case of a periodic, time-dependent fluid velocity field with *non-zero mean*. It was shown [41] that, depending on the strength of the fluctuations relative to the mean flow, the effective diffusivity tensor D* can be constant or a function of both space and time. When D* is constant, only its symmetric part appears in the homogenized equation as an enhancement in the diffusivity. However, when D* is a function of space and time, its antisymmetric part also plays a key role in the homogenized equation. Based on [8], the cell problem associated with a *time-independent* flow was transformed [41] into a resolvent formula involving a self-adjoint operator, acting on a Sobolev space [17, 33] of spatially periodic *scalar fields*, which is also a Hilbert space. This, in turn, led to a discrete Stieltjes integral representation for the *antisymmetric* part of D*, involving the Péclet number of the flow and a spectral measure of the operator.

Such methods have been extended to steady flows where particles diffuse according to linear collisions [42], solute transport in porous media [8], anelastic (weakly compressible) flows [32], and to the setting of a time-dependent fluid velocity field [4, 38]. All these approaches yield integral representations of the symmetric and, when appropriate, the antisymmetric part of D*. Variational formulations of the effective parameter problem for D* are given in [3, 15, 16].

Here we adapt and extend the mathematical frameworks developed in both [3] and [41] to the case of a time-independent periodic flow. We also discuss how the frameworks are extended to randomly perturbed periodic flows. In particular, for each approach in [3, 41], we develop Stieltjes integral representations for both the symmetric and antisymmetric parts of D*, involving the molecular diffusivity and a spectral measure of a self-adjoint operator that depends only on the fluid velocity field. Moreover, for each approach in [3, 41],

we provide a mathematical foundation for rigorous computation of D^* through discrete, matrix formulations of these effective parameter problems. For an alternative computational method that is accurate for large Péclet numbers see [20].

We demonstrate for the setting introduced in [3], that the discrete spectral measure is given explicitly in terms of the eigenvalues and eigenvectors of a *standard* eigenvalue problem. We develop a projection method which allows the spectral measure to be obtained from the eigenvalues and eigenvectors of a much smaller matrix, greatly increasing the efficiency of numerical computations. For the setting described in [41], we show that the spectral measure is instead given in terms of the eigenvalues and eigenvectors of a *generalized* eigenvalue problem.

We provide a detailed matrix analysis that demonstrates the two approaches yield equivalent spectral representations of the effective diffusivity tensor D^* when the matrix Laplacian, at the heart of both approaches, is of full rank. Moreover, we demonstrate that both approaches can be formulated in terms of a common, *standard* eigenvalue problem. However, the matrix Laplacian becomes rank deficient when periodic boundary conditions are imposed. We generalize both approaches to this rank deficient setting and show that the two generalized approaches again yield equivalent spectral representations of D^*. This analysis provides a numerically efficient way to compute the discrete spectral measure underlying the integral representation for D^*. We utilize this unified mathematical framework to compute the effective diffusivity for some model flows.

A. Synopsis of the paper

In Section II, we formulate the effective parameter problem for advection enhanced diffusion by random, incompressible flows. In particular, we review the problem of homogenizing the advection-diffusion equation for such flows, developed in [31], which yields a rigorous functional representation for the effective diffusivity tensor D^* in terms of the solution of a random "cell problem" which arises in the homogenization procedure.

In Section III A, we discuss how the incompressibility of the fluid velocity field allows it to be expressed in terms of the divergence of an antisymmetric random matrix. This, in turn, allows the cell problem to be written as a steady state diffusion equation involving a curl-free random field. Moreover, we demonstrate how this leads to functional formulas for

the symmetric and antisymmetric parts of the effective diffusivity tensor D^*, involving the curl-free field and a self-adjoint random operator. In Section III B, we discuss how the cell problem can be transformed into a resolvent formula involving this self-adjoint operator, which acts on the Hilbert space of curl-free, random *vector fields* [2, 3]. We then discuss how this result and the spectral theorem [46, 51] yields Stieltjes integral representations for both the symmetric [2, 3] and antisymmetric parts of D^*, involving a *spectral measure* of the operator. We utilize analytical properties of the Stieltjes integrals to provide rigorous bounds for the components of these homogenized tensors.

In Section IV A, we provide a mathematical foundation for rigorous computation of D^* associated with this approach. In particular, a discrete representation of the cell problem involving a Hermitian random matrix leads to Stieltjes integral representations for the symmetric and antisymmetric parts of D^*, involving a discrete spectral measure which is given explicitly in terms of the eigenvalues and eigenvectors of the matrix. In Section IV B, we develop a projection method which allows spectral statistics to be obtained by diagonalizing a much smaller random matrix, greatly increasing the efficiency of numerical computations.

In Section V, we formulate another approach to the effective parameter problem [41], which is different from the approach discussed in Section IV. We demonstrate this approach also provides Stieltjes integral representations for the symmetric and antisymmetric parts of D^*. In particular, we transform the cell problem into a resolvent formula involving a self-adjoint random operator acting on a Sobolev space of random *scalar fields*, which is also a Hilbert space. This leads to functional formulas for D^* and a resolvent formula for the cell problem. This, in turn, leads to Stieltjes integral representations for the symmetric and antisymmetric parts of D^*, involving a spectral measure of the random operator.

The symmetry of the random operator depends intimately on the Sobolev-type inner-product in this approach. Consequently, its matrix formulation is substantially different from that of Section IV. This technical difficulty is overcome in Section VI by casting the effective parameter problem in terms of a *generalized* eigenvalue problem, which has the Sobolev-type inner-product as a key feature. This leads to Stieltjes integral representations for the symmetric and antisymmetric parts of D^*, involving a discrete spectral measure which is given explicitly in terms of the associated generalized eigenvalues and eigenvectors.

The inverse Laplacian operator is central to both of the continuum formulations of the effective parameter problems described in Sections III and V. Consequently, the matrix

Laplacian is also central to both of the discrete formulations described in Sections IV and VI, which is assumed to be of full rank so that it is invertible. Given this condition, we demonstrate in Section VII that the two discrete formulations of the effective parameter problems given in Sections IV and VI produce equivalent spectral representations for the effective diffusivity tensor D^*.

In Section VIII, we generalize the mathematical frameworks formulated in Sections IV and VI to the case of a rank deficient matrix Laplacian. This is important in computations of the effective diffusivity tensor D^* for randomly perturbed periodic flows, as the matrix Laplacian with periodic boundary conditions is rank deficient. A detailed matrix analysis shows that both approaches yield equivalent spectral representations of D^* and that the spectral statistics can be obtained from a standard eigenvalue problem of a much smaller random matrix. When the matrix Laplacian is of full rank, these generalized formulations reduce to the formulations in Sections IV and VI.

In Section IX we numerically compute the spectral measures and effective diffusivity tensors for several non-random periodic flows as well as randomly perturbed periodic flows. Our computations are in excellent agreement with theoretical results [3] for shear flow. We relate spectral characteristics of our computations to flow geometry and transport properties.

II. HOMOGENIZATION OF THE ADVECTION-DIFFUSION EQUATION

The dispersion of a cloud of passive scalars with density ϕ diffusing with molecular diffusivity ε and being advected by a incompressible velocity field $\boldsymbol{u}$ satisfying $\boldsymbol{\nabla}\cdot\boldsymbol{u} = 0$ is described by the advection-diffusion equation

$$\phi_t(t,\boldsymbol{x}) = \boldsymbol{u}(\boldsymbol{x})\cdot\boldsymbol{\nabla}\phi(t,\boldsymbol{x}) + \varepsilon\Delta\phi(t,\boldsymbol{x}), \quad \phi(0,\boldsymbol{x}) = \phi_0(\boldsymbol{x}), \qquad \boldsymbol{x}\in\mathbb{R}^d, \quad t > 0, \quad (1)$$

with initial density $\phi_0(\boldsymbol{x})$ given. Here, ϕ_t denotes partial differentiation of ϕ with respect to time t, $\Delta = \boldsymbol{\nabla}\cdot\boldsymbol{\nabla} = \nabla^2$ is the Laplacian, $\varepsilon > 0$, d is the system dimension, and we denote by 0 the null element on all linear spaces in question. Moreover, $\boldsymbol{\xi}\cdot\boldsymbol{\zeta} = \boldsymbol{\xi}^\dagger\boldsymbol{\zeta}$ and $\dagger$ is the operation of complex-conjugate-transpose, with $\boldsymbol{\xi}\cdot\boldsymbol{\xi} = |\boldsymbol{\xi}|^2$. Later, we will extensively use this form of the dot product over complex fields, with built in complex conjugation. However, we stress that all quantities considered in this section are *real-valued*. We assume for now that the time-independent fluid velocity field $\boldsymbol{u}$ is spatially periodic on the region

$\mathcal{V} \subset \mathbb{R}^d$. Later, we will discuss the case of an array of randomly perturbed, periodic flows.

The long time, large scale dispersion of the passive scalars can be described [54] by an effective diffusivity tensor D^*. An explicit representation for D^* can be found using methods of homogenization theory [6, 39]. These methods have demonstrated that the averaged or *homogenized* behavior of the advection-diffusion equation in (1) is determined by a diffusion equation involving an averaged scalar density $\bar{\phi}$ and a (constant) effective diffusivity tensor D^* [31]

$$\bar{\phi}_t(t, \boldsymbol{x}) = \boldsymbol{\nabla} \cdot [\mathsf{D}^* \boldsymbol{\nabla} \bar{\phi}(t, \boldsymbol{x})], \quad \bar{\phi}(0, \boldsymbol{x}) = \phi_0(\boldsymbol{x}). \tag{2}$$

The components D^*_{jk}, $j, k = 1, \ldots, d$, of D^* are given by [31]

$$D^*_{jk} = \varepsilon \delta_{jk} + \langle u_j \chi_k \rangle, \tag{3}$$

where $\langle \cdot \rangle$ denotes volume averaging over the period cell $\mathcal{V}$. The function χ_j in (3) satisfies a cell problem which is a steady state advection-diffusion equation with a forcing term involving u_j, the jth component of the fluid velocity field $\boldsymbol{u}$ [16, 31],

$$\boldsymbol{u} \cdot \boldsymbol{\nabla} \chi_j + \varepsilon \Delta \chi_j = -u_j, \quad \langle \boldsymbol{\nabla} \chi_j \rangle = 0. \tag{4}$$

Equations (2)–(4) follow from the assumption that the initial density ϕ_0 is slowly varying relative to the variations of the velocity field $\boldsymbol{u}$ [16, 31]. This information is incorporated into equation (1) by introducing a small dimensionless parameter $\delta \ll 1$ and writing [31]

$$\phi(0, \boldsymbol{x}) = \phi_0(\delta \boldsymbol{x}). \tag{5}$$

Anticipating that ϕ will have diffusive dynamics as $t \to \infty$, space and time are rescaled by $\boldsymbol{x} \mapsto \boldsymbol{x}/\delta$ and $t \mapsto t/\delta^2$. As $\delta \to 0$, the associated solution $\phi^\delta(t, \boldsymbol{x}) = \phi(t/\delta^2, \boldsymbol{x}/\delta)$ of equation (1) (in the rescaled variables) converges to $\bar{\phi}(t, \boldsymbol{x})$ which satisfies equation (2). The convergence is in an L^2 sense that depends on the technical assumptions made about the fluid velocity field $\boldsymbol{u}$ [3, 15, 16, 29, 31, 41].

We stress that the cell problem in (4) involves only the fast variables $\boldsymbol{x}/\delta$ and t/δ^2 [31]. Other space-time scalings have also been considered, which have lead to space-time dependent D^* [41] and even anomalous diffusive dynamics [29]. Homogenization theorems for space-time dependent fluid velocity fields are treated in [9, 29, 41].

In our analysis of the effective diffusivity tensor D^*, it will be convenient to use non-dimensional parameters. We therefore assume that equation (1) has been non-dimensionalized as follows. Let ℓ and τ be typical length and time scales associated with the problem of interest. Mapping to the non-dimensional variables $t \mapsto t/\tau$ and $\boldsymbol{x} \mapsto \boldsymbol{x}/\ell$, one finds that ϕ satisfies the advection-diffusion equation in (1) with a non-dimensional molecular diffusivity and fluid velocity field,

$$\varepsilon \mapsto \tau\varepsilon/\ell^2, \quad \boldsymbol{u} \mapsto \tau\,\boldsymbol{u}/\ell. \tag{6}$$

In the case of a time-independent, spatially periodic flow, a natural choice for ℓ and τ is, respectively, the maximum cell period and $\tau = \ell/\langle|\boldsymbol{u}|^2\rangle^{1/2}$, so that (6) is given by $\varepsilon \mapsto \varepsilon/(\ell\,\langle|\boldsymbol{u}|^2\rangle^{1/2})$ and $\boldsymbol{u} \mapsto \boldsymbol{u}/\langle|\boldsymbol{u}|^2\rangle^{1/2}$. In this case, a natural definition of the Péclet number Pe is

$$Pe = \frac{\ell\langle|\boldsymbol{u}|^2\rangle^{1/2}}{\varepsilon}, \tag{7}$$

so that the scaled molecular diffusivity satisfies $\varepsilon = Pe^{-1}$.

III.   CURL-FREE FIELDS AND THE EFFECTIVE DIFFUSIVITY TENSOR

In this section, we adapt and extend a method [2, 3] which leads to integral representations for the effective diffusivity tensor D^*. More specifically, in Section III A we provide functional formulas for the symmetric and antisymmetric parts of D^*, involving the curl-free vector field $\boldsymbol{\nabla}\chi_j$ in equation (4). We review a Hilbert space formulation of this effective parameter problem [2, 3, 15, 16] in Section III B, which leads to a resolvent formula for $\boldsymbol{\nabla}\chi_j$, involving a self-adjoint operator. Moreover, we use this result and the spectral theorem [46, 51] to provide Stieltjes integral representations for both the symmetric and antisymmetric parts of D^*, involving a spectral measure of the operator.

A.   Functional formulas for the effective diffusivity tensor

Since $\boldsymbol{u}(\boldsymbol{x})$ is incompressible, $\boldsymbol{\nabla}\!\cdot\!\boldsymbol{u} = 0$, there is a real (non-dimensional) *antisymmetric* matrix $\mathsf{H}(\boldsymbol{x})$ [2, 3] such that

$$\boldsymbol{u} = \boldsymbol{\nabla}\!\cdot\!\mathsf{H}, \qquad \mathsf{H}^T = -\mathsf{H}, \tag{8}$$

where H^T denotes transposition of the matrix H. Due to the anti-symmetry of the matrix H and the symmetry of the Hessian operator $\nabla\nabla$ when acting on a sufficiently smooth space of functions, we have that $H : \nabla\nabla\varphi = 0$ for all such smooth functions φ. Consequently, $\nabla\cdot[H\nabla\varphi] = [\nabla\cdot H]\cdot\nabla\varphi + H : \nabla\nabla\varphi = [\nabla\cdot H]\cdot\nabla\varphi$, or $\nabla\cdot[H\nabla] = [\nabla\cdot H]\cdot\nabla$ as operators acting on such functions. Using this identity and the representation of the fluid velocity field $\boldsymbol{u}$ in (8), equation (1) can be written as a diffusion equation,

$$\phi_t = \nabla\cdot[D\nabla\phi], \quad \phi(0, \boldsymbol{x}) = \phi_0(\boldsymbol{x}), \qquad D = \varepsilon I + H. \tag{9}$$

Moreover, the cell problem in (4) can be written as a steady-state diffusion equation [15, 16],

$$\nabla\cdot[D(\nabla\chi_k + \boldsymbol{e}_k)] = 0, \quad \langle\nabla\chi_k\rangle = 0, \quad k = 1,\ldots,d. \tag{10}$$

Here, $\langle\cdot\rangle$ denotes volume averaging over the period cell $\mathcal{V}$, $\boldsymbol{e}_k$ is a standard basis vector, $k = 1,\ldots,d$, and $D(t, \boldsymbol{x}) = \varepsilon I + H(t, \boldsymbol{x})$ can be viewed as a local diffusivity tensor with coefficients

$$D_{jk} = \varepsilon\delta_{jk} + H_{jk}, \quad j, k = 1,\ldots,d, \tag{11}$$

where δ_{jk} is the Kronecker delta and I is the identity operator on $\mathbb{R}^d$.

The symmetric S^* and antisymmetric A^* parts of the effective diffusivity tensor D^* are defined by

$$D^* = S^* + A^*, \qquad S^* = \frac{1}{2}\left(D^* + [D^*]^T\right), \quad A^* = \frac{1}{2}\left(D^* - [D^*]^T\right). \tag{12}$$

Substituting into equation (3) the expression for u_j in (4) and using equation (8), $\boldsymbol{u} = \nabla\cdot H$, one finds that the components S^*_{jk} and A^*_{jk}, $j, k = 1,\ldots,d$, of S^* and A^* can be written in terms of the following functionals involving the *real-valued* vector field $\nabla\chi_k$

$$S^*_{jk} = \varepsilon(\delta_{jk} + \langle\nabla\chi_j\cdot\nabla\chi_k\rangle), \qquad A^*_{jk} = \langle H\nabla\chi_j\cdot\nabla\chi_k\rangle. \tag{13}$$

The symmetry $S^*_{jk} = S^*_{kj}$ of the tensor S^* in (13) follows from the fact that the vector field $\nabla\chi_k$ is real-valued so that $\langle\nabla\chi_j\cdot\nabla\chi_k\rangle = \langle\nabla\chi_k\cdot\nabla\chi_j\rangle$. Moreover, the positivity condition $\langle\nabla\chi_k\cdot\nabla\chi_k\rangle = \langle|\nabla\chi_k|^2\rangle \geq 0$ demonstrates that the effective transport of the scalar density ϕ is always *enhanced* in all of the principle directions $\boldsymbol{e}_k$, $k = 1,\ldots,d$, by the presence of an incompressible velocity field, $D^*_{kk} = S^*_{kk} \geq \varepsilon$. The equality $D^*_{kk} = S^*_{kk}$ follows from the skew-symmetry of the matrix A^*, $A^*_{kj} = -A^*_{jk}$, hence $A^*_{kk} = 0$. This, in turn, follows from

the skew-symmetry of the *real-valued* matrix H, which implies that $\mathsf{A}^*_{jk} = \langle \mathsf{H}\boldsymbol{\nabla}\chi_j \cdot \boldsymbol{\nabla}\chi_k \rangle = -\langle \boldsymbol{\nabla}\chi_j \cdot \mathsf{H}\boldsymbol{\nabla}\chi_k \rangle = -\langle \mathsf{H}\boldsymbol{\nabla}\chi_k \cdot \boldsymbol{\nabla}\chi_j \rangle = -\mathsf{A}^*_{kj}$.

We conclude this section by noting that the cell problem in equation (10) is equivalent [2, 3, 15, 16] to the quasi-static limit of Maxwell's equations [19, 24, 35], which describe the transport properties of an electromagnetic wave in a composite material,

$$\boldsymbol{\nabla}\times\boldsymbol{E}_k = 0, \quad \boldsymbol{\nabla}\cdot\boldsymbol{J}_k = 0, \quad \boldsymbol{J}_k = \mathsf{D}\boldsymbol{E}_k, \quad \langle\boldsymbol{E}_k\rangle = \boldsymbol{e}_k, \qquad \mathsf{D} = \varepsilon\mathsf{I} + \mathsf{H}. \tag{14}$$

Here, $\boldsymbol{E}_k = \boldsymbol{\nabla}\chi_k + \boldsymbol{e}_k$ plays the role of the local electric field, $\boldsymbol{J}_k = \mathsf{D}\boldsymbol{E}_k$ plays the role of the local current density, and $\mathsf{D} = \varepsilon\mathsf{I} + \mathsf{H}$ plays the role of the local conductivity tensor of the medium. Since H is skew-symmetric, the intensity-flux relation $\boldsymbol{J}_k = \mathsf{D}\boldsymbol{E}_k$ is not the usual Fourier law, but instead resembles that of a Hall medium [15, 16, 23, 35]. In Section III B, we employ the representation of the cell problem in (10) and adapt the analytic continuation method [19] for characterizing transport in composites to provide Stieltjes integral representations for both the symmetric and antisymmetric parts of the effective diffusivity tensor D^*, involving a spectral measure of a self-adjoint operator.

B. Hilbert space and integral representations

The analytic continuation method provides Stieltjes integral representations for the bulk transport coefficients of composite media [19]. This method is based on the spectral theorem of Hilbert space theory and a resolvent formula for, say, the electric field, involving a self-adjoint operator [19] or matrix [37] which depends only on the composite geometry. In this section, we adapt this method [2, 3] to provide Stieltjes integral representations for both the symmetric and antisymmetric parts of the effective diffusivity tensor D^*, which encodes the complicated geometry of the fluid velocity field in a spectral measure of a self-adjoint operator.

The analytical platform of the analytic continuation method is a Hilbert space $\mathscr{H}$. In the effective parameter problem for effective diffusivity, the mathematical structure of $\mathscr{H}$ depends on the specific details of the fluid velocity field of interest. When one considers a fluid velocity field that is spatially periodic on a region $\mathcal{V} \subset \mathbb{R}^d$, the Hilbert space $\mathscr{H}$ can be taken to be [29]

$$\mathscr{H} = \{\boldsymbol{\xi} \in \otimes^d_{n=1} L^2(\mathcal{V}, \mathrm{m}) \,:\, \boldsymbol{\xi}(\boldsymbol{x}) \text{ is periodic in } \mathcal{V}\}, \tag{15}$$

where m is the normalized Lebesgue measure (uniform distribution) on $\mathbb{R}^d$, restricted to $\mathcal{V}$, and $L^2(\mathcal{V}, \mathrm{m})$ is the space of complex-valued scalar functions that are square-integrable with respect to m. The Hilbert space $\mathscr{H}$ is equipped with a sesquilinear inner-product $\langle \cdot, \cdot \rangle$ defined by $\langle \boldsymbol{\xi}, \boldsymbol{\zeta} \rangle = \langle \boldsymbol{\xi} \cdot \boldsymbol{\zeta} \rangle$, with $\langle \boldsymbol{\zeta}, \boldsymbol{\xi} \rangle = \overline{\langle \boldsymbol{\xi}, \boldsymbol{\zeta} \rangle}$ for $\boldsymbol{\xi}, \boldsymbol{\zeta} \in \mathscr{H}$, which induces a norm $\| \cdot \|$ defined by $\| \boldsymbol{\xi} \| = \langle \boldsymbol{\xi}, \boldsymbol{\xi} \rangle^{1/2}$ and $\boldsymbol{\xi} \in \mathscr{H}$ implies that $\| \boldsymbol{\xi} \| < \infty$. Here, $\langle \cdot \rangle$ denotes volume average over the period cell $\mathcal{V}$ with respect to the measure m, $\overline{a}$ is the complex-conjugate of the scalar a, and we stress that the dot product $\boldsymbol{\xi} \cdot \boldsymbol{\zeta} = \boldsymbol{\xi}^\dagger \boldsymbol{\zeta}$ includes the operation $\dagger$ of complex-conjugate-transpose.

One could also imagine a random fluid flow filling all of $\mathbb{R}^d$, with a velocity field $\boldsymbol{u}$ determined by the probability space (Ω, P) with σ-algebra generated by the sets $\{\boldsymbol{u}(\boldsymbol{x}) \in B\}$, where $\boldsymbol{x} \in \mathbb{R}^d$ and B is a Borel subset of $\mathbb{R}^d$ [3]. Here, Ω is the set of all geometric realizations of $\boldsymbol{u}$, which is indexed by the parameter $\omega \in \Omega$ representing one particular geometric realization, and P is the associated probability measure. The underlying Hilbert space in this case can be taken to be $\mathscr{H} = L^2(\Omega, P)$, i.e., the space of all P-measurable vector-valued functions $\boldsymbol{\xi}$ satisfying $\| \boldsymbol{\xi} \| = \langle |\boldsymbol{\xi}|^2 \rangle^{1/2} < \infty$, where $\langle \cdot \rangle$ denotes ensemble averaging and the underlying sesquilinear inner-product is defined by $\langle \boldsymbol{\xi}, \boldsymbol{\zeta} \rangle = \langle \boldsymbol{\xi} \cdot \boldsymbol{\zeta} \rangle$. In this case, one could consider a random fluid flow with a velocity field $\boldsymbol{u}$ that is stationary [31] or ergodic [2, 3], for example, with regularity conditions at infinity, i.e., as $|\boldsymbol{x}| \to \infty$. In these cases, one works with an infinite medium directly, which presents substantial computational difficulties.

A more computationally tractable, random system is given by a $n \times n$ array of randomly perturbed periodic flows [16]. In this case, the σ-algebra associated with the underlying probability space is generated by the Lebesgue measurable subsets of $\mathbb{R}^d$. Here, the Hilbert space $\mathscr{H}$ is given by equation (15) and averaged quantities depend on the realization of the random medium because $\langle \cdot \rangle$ is given by volume averaging over the period cell $\mathcal{V}$ [16]. The effective diffusivity tensor D^* is obtained by taking an infinite volume limit, $\mathsf{D}^* = \lim_{n \to \infty} \mathsf{D}_n^*$, of the finite volume effective diffusivity tensor D_n^* and evoking an ergodic theorem [16, 19]. Numerically, it is natural to spatially average each statistical trial and then ensemble average over all of the sampled random realizations.

In any case, once the Hilbert space $\mathscr{H}$ is established, with associated average $\langle \cdot \rangle$, inner-product $\langle \cdot, \cdot \rangle$, and norm $\| \cdot \|$, the spectral theory presented in the remainder of this section progresses independent of the underlying details, as it lays on an axiomatic foundation [51]. For the sake of numerical tractability, we will assume that the Hilbert space $\mathscr{H}$ is given by

equation (15). The fluid velocity field $\boldsymbol{u}$ can be assumed to represent a periodic or randomly perturbed periodic flow.

Now consider the associated Hilbert space $\mathscr{H}_\times$ of curl-free fields [3, 15, 16, 19, 35],

$$\mathscr{H}_\times = \{\boldsymbol{\xi} \in \mathscr{H} \ : \ \boldsymbol{\nabla}\times\boldsymbol{\xi} = 0 \ \text{ weakly and } \langle\boldsymbol{\xi}\rangle = 0\}. \tag{16}$$

The curl-free vector field $\boldsymbol{\nabla}\chi_k$ in the cell problem in (10) is mean-zero $\langle\boldsymbol{\nabla}\chi_k\rangle = 0$. When the matrix D in equation (9) is bounded in the operator norm $\|\cdot\|$ induced by the $\mathscr{H}$-inner-product [18], $\|\mathsf{D}\| < \infty$, then there exists unique $\boldsymbol{\nabla}\chi_k \in \mathscr{H}_\times$ satisfying equation (10) [19, 39]. We assume that

$$0 < \varepsilon < \infty, \quad \|\mathsf{H}\| < \infty, \tag{17}$$

which together imply that $\|\mathsf{D}\| < \infty$.

The linear operator $\boldsymbol{\Gamma} = \boldsymbol{\nabla}(\Delta^{-1})\boldsymbol{\nabla}\cdot$ is a projection onto the Hilbert space $\mathscr{H}_\times$ in the sense that $\boldsymbol{\Gamma} : \mathscr{H} \mapsto \mathscr{H}_\times$ and $\boldsymbol{\Gamma}\boldsymbol{\xi} = \boldsymbol{\xi}$ (weakly) for all $\boldsymbol{\xi} \in \mathscr{H}_\times$, in particular $\boldsymbol{\Gamma}\boldsymbol{\nabla}\chi_k = \boldsymbol{\nabla}\chi_k$. It is based on convolution with respect to the Green's function for the Laplacian Δ [34, 49]. Applying the integro-differential operator $\boldsymbol{\nabla}\Delta^{-1}$ to the cell problem in equation (10) yields $\boldsymbol{\Gamma}[(\varepsilon\mathsf{I} + \mathsf{H})(\boldsymbol{\nabla}\chi_k + \boldsymbol{e}_k)] = 0$. Since $\boldsymbol{\Gamma}\boldsymbol{e}_k = 0$ and $\boldsymbol{\Gamma}\boldsymbol{\nabla}\chi_k = \boldsymbol{\nabla}\chi_k$, this is equivalent to $(\varepsilon\mathsf{I} + \boldsymbol{\Gamma}\mathsf{H}\boldsymbol{\Gamma})\boldsymbol{\nabla}\chi_k = -\boldsymbol{\Gamma}\mathsf{H}\boldsymbol{e}_k$, which yields the following resolvent formula for $\boldsymbol{\nabla}\chi_k$

$$\boldsymbol{\nabla}\chi_k = (\varepsilon\mathsf{I} + \mathbf{A})^{-1}\boldsymbol{g}_k, \qquad \mathbf{A} = \boldsymbol{\Gamma}\mathsf{H}\boldsymbol{\Gamma}, \quad \boldsymbol{g}_k = -\boldsymbol{\Gamma}\mathsf{H}\boldsymbol{e}_k. \tag{18}$$

Since $\boldsymbol{\Gamma}$ is a projection operator onto $\mathscr{H}_\times \subset \mathscr{H}$ it is bounded by unity in operator norm on $\mathscr{H}$, $\|\boldsymbol{\Gamma}\| \leq 1$ [18, 47]. Integration by parts and the symmetry of the operator $(-\Delta)^{-1}$ [49] shows that $\boldsymbol{\Gamma}$ is also a *symmetric* operator, i.e., $\langle\boldsymbol{\Gamma}\boldsymbol{\xi}\cdot\boldsymbol{\zeta}\rangle = \langle\boldsymbol{\xi}\cdot\boldsymbol{\Gamma}\boldsymbol{\zeta}\rangle$ for all $\boldsymbol{\xi}, \boldsymbol{\zeta} \in \mathscr{H}$. These two properties of $\boldsymbol{\Gamma}$ show that it is a *self-adjoint* operator on $\mathscr{H}$ [46]. Using this property and $\boldsymbol{\Gamma}\boldsymbol{\nabla}\chi_k = \boldsymbol{\nabla}\chi_k$, we may write A^*_{jk} in equation (13) as $\mathsf{A}^*_{jk} = \langle\mathbf{A}\boldsymbol{\nabla}\chi_j\cdot\boldsymbol{\nabla}\chi_k\rangle$. Consequently, substituting the resolvent formula for $\boldsymbol{\nabla}\chi_k$ in equation (18) into the functional formulas in equation (13) yields

$$\mathsf{S}^*_{jk} = \varepsilon(\delta_{jk} + \langle(\varepsilon\mathsf{I} + \mathbf{A})^{-1}\boldsymbol{g}_j\cdot(\varepsilon\mathsf{I} + \mathbf{A})^{-1}\boldsymbol{g}_k\rangle), \tag{19}$$
$$\mathsf{A}^*_{jk} = \langle\mathbf{A}(\varepsilon\mathsf{I} + \mathbf{A})^{-1}\boldsymbol{g}_j\cdot(\varepsilon\mathsf{I} + \mathbf{A})^{-1}\boldsymbol{g}_k\rangle.$$

Since $\boldsymbol{\Gamma}$ is self-adjoint on $\mathscr{H}$, the anti-symmetry of the matrix H implies that $\mathbf{A} = \boldsymbol{\Gamma}\mathsf{H}\boldsymbol{\Gamma}$ is an *antisymmetric* operator on $\mathscr{H}$, i.e., $\langle\mathbf{A}\boldsymbol{\xi}\cdot\boldsymbol{\zeta}\rangle = -\langle\boldsymbol{\xi}\cdot\mathbf{A}\boldsymbol{\zeta}\rangle$. We stress that the operator

A depends only on the fluid velocity field via equation (8). By equation (17), the operator **A** is bounded on $\mathscr{H}$ with $\|\mathbf{A}\| \leq \|\mathsf{H}\| < \infty$. This, the skew-symmetry of **A**, and the sesquilinearity of the $\mathscr{H}$-inner-product imply that $\mathbf{M} = -\imath \mathbf{A}$, where $\imath = \sqrt{-1}$, is a bounded symmetric operator, hence self-adjoint on $\mathscr{H}$ with $\|\mathbf{M}\| = \|\mathbf{A}\| < \infty$. The spectrum Σ of the self-adjoint operator **M** is real-valued with spectral radius equal to its operator norm [46], i.e.,

$$\Sigma \subseteq [-\|\mathsf{H}\|, \|\mathsf{H}\|]. \tag{20}$$

The spectral theorem for bounded linear self-adjoint operators in Hilbert space states that there is a one-to-one correspondence between the operator **M** and a family of self-adjoint projection operators $\{\mathbf{Q}(\lambda)\}_{\lambda \in \Sigma}$ — the resolution of the identity — satisfying [51]

$$\lim_{\lambda \to \inf \Sigma} \mathbf{Q}(\lambda) = 0, \quad \lim_{\lambda \to \sup \Sigma} \mathbf{Q}(\lambda) = \mathsf{I}. \tag{21}$$

Furthermore, for all $\boldsymbol{\xi}, \boldsymbol{\zeta} \in \mathscr{H}_\times$, the *complex-valued* function of the spectral variable λ defined by $\mu_{\xi\zeta}(\lambda) = \langle \mathbf{Q}(\lambda)\boldsymbol{\xi}, \boldsymbol{\zeta} \rangle$ has real and imaginary parts that are strictly increasing and of bounded variation [51]. Therefore, there is a *complex* Radon–Stieltjes measure $\mu_{\xi\zeta}$ associated with $\mu_{\xi\zeta}(\lambda)$ [18, 50, 51]. The spectral theorem also states that, for all complex-valued functions $f \in L^2(\mu_{\xi\xi})$ and $h \in L^2(\mu_{\zeta\zeta})$, there exist linear operators denoted by $f(\mathbf{M})$ and $h(\mathbf{M})$ which are defined in terms of the sesquilinear functional $\langle f(\mathbf{M})\boldsymbol{\xi}, h(\mathbf{M})\boldsymbol{\zeta} \rangle$ [51]. In particular, this functional has the following integral representation involving the Stieltjes measure $\mu_{\xi\zeta}$, for all $\boldsymbol{\xi}, \boldsymbol{\zeta} \in \mathscr{H}_\times$,

$$\langle f(\mathbf{M})\boldsymbol{\xi}, h(\mathbf{M})\boldsymbol{\zeta} \rangle = \int_{-\infty}^{\infty} \overline{f}(\lambda)\, h(\lambda)\, \mathrm{d}\mu_{\xi\zeta}(\lambda), \quad \mu_{\xi\zeta}(\lambda) = \langle \mathbf{Q}(\lambda)\boldsymbol{\xi}, \boldsymbol{\zeta} \rangle, \tag{22}$$

where the integration is over the spectrum Σ of **M** [46, 51] and $\overline{f}$ denotes complex conjugation of the scalar function f.

Since a Stieltjes measure ν has the property [51] $\int_a^b d\nu(\lambda) = \nu(b) - \nu(a)$, equation (21) implies that the mass $\mu_{\xi\zeta}^0$ of the measure $\mu_{\xi\zeta}$ is given by

$$\mu_{\xi\zeta}^0 = \int_{-\infty}^{\infty} \mathrm{d}\mu_{\xi\zeta}(\lambda) = \int_{-\infty}^{\infty} \mathrm{d}\langle \mathbf{Q}(\lambda)\boldsymbol{\xi}, \boldsymbol{\zeta} \rangle = \langle \boldsymbol{\xi}, \boldsymbol{\zeta} \rangle, \tag{23}$$

which is bounded in the sense that $|\mu_{\xi\zeta}^0| \leq \|\boldsymbol{\xi}\| \|\boldsymbol{\zeta}\| < \infty$ for all $\boldsymbol{\xi}, \boldsymbol{\zeta} \in \mathscr{H}_\times$. Due to the sesquilinearity of the inner-product and the fact that the projection operator $\mathbf{Q}(\lambda)$ is self-adjoint on $\mathscr{H}_\times$, the complex-valued function $\mu_{\zeta\xi}(\lambda)$ satisfies $\mu_{\zeta\xi}(\lambda) = \overline{\mu}_{\xi\zeta}(\lambda)$ and

$\mu_{\xi\xi}(\lambda) = \|\mathbf{Q}(\lambda)\boldsymbol{\xi}\|^2$. Consider the associated *positive* Stieltjes measure $\mu_{\xi\xi}$ and the real-valued functions

$$\text{Re } \mu_{\xi\zeta}(\lambda) = \frac{1}{2}\left(\mu_{\xi\zeta}(\lambda) + \overline{\mu}_{\xi\zeta}(\lambda)\right), \quad \text{Im } \mu_{\xi\zeta}(\lambda) = \frac{1}{2\imath}\left(\mu_{\xi\zeta}(\lambda) - \overline{\mu}_{\xi\zeta}(\lambda)\right), \tag{24}$$

with associated *signed* Stieltjes measures Re $\mu_{\xi\zeta}$ and Im $\mu_{\xi\zeta}$ [18].

For notational simplicity we denote by $\mu_{jk}(\lambda) = \langle \mathbf{Q}(\lambda)\boldsymbol{g}_j, \boldsymbol{g}_k \rangle$ instead of $\mu_{g_j g_k}(\lambda)$. We now demonstrate that the spectral theorem in (22) provides Stieltjes integral representations for the functional formulas in equation (19), involving a spectral measure μ_{jk} associated with the function $\mu_{jk}(\lambda)$, where the real-valued vector field $\boldsymbol{g}_k = -\boldsymbol{\Gamma}\mathsf{H}\boldsymbol{e}_k$ is defined in equation (18). From equation (23), the mass μ_{jk}^0 of the measure μ_{jk} is real-valued and satisfies

$$\mu_{jk}^0 = \langle \boldsymbol{g}_j, \boldsymbol{g}_k \rangle = \langle \boldsymbol{\Gamma}\mathsf{H}\boldsymbol{e}_j \cdot \boldsymbol{\Gamma}\mathsf{H}\boldsymbol{e}_k \rangle = \langle \mathsf{H}^T\boldsymbol{\Gamma}\mathsf{H}\boldsymbol{e}_j \cdot \boldsymbol{e}_k \rangle, \qquad |\mu_{jk}^0| \leq \|\mathsf{H}\|^2 < \infty, \tag{25}$$

where we have used that $\boldsymbol{\Gamma}$ is a self-adjoint projection operator on $\mathscr{H}_\times$. In equation (22), set $\mathbf{M} = -\imath\mathbf{A}$, $\boldsymbol{\xi} = \boldsymbol{g}_j$, and $\boldsymbol{\zeta} = \boldsymbol{g}_k$. Moreover, for the first formula in equation (19) set $f(\lambda) = h(\lambda) = (\varepsilon + \imath\lambda)^{-1}$, and in the second formula set $f(\lambda) = \imath\lambda(\varepsilon + \imath\lambda)^{-1}$ and $h(\lambda) = (\varepsilon + \imath\lambda)^{-1}$, with $\lambda \in \mathbb{R}$ and $|\lambda| \leq \|\mathsf{H}\| < \infty$. Since $(\varepsilon^2 + \lambda^2)^{-1} \leq 1/\varepsilon^2 < \infty$ and $\lambda^2(\varepsilon^2 + \lambda^2)^{-1} \leq 1$ for all $0 < \varepsilon < \infty$, it is clear from equation (25) that the functions f and h defined above satisfy $f, h \in L^2(\mu_{kk})$ for all $k = 1, \ldots, d$ and $0 < \varepsilon < \infty$. Consequently, the spectral theorem in (22) implies that the functional formulas for S_{jk}^* and A_{jk}^* in equation (19) have the following Stieltjes integral representations

$$\mathsf{S}_{jk}^* = \varepsilon\left(\delta_{jk} + \int_{-\infty}^{\infty}\frac{\mathrm{d}\mu_{jk}(\lambda)}{\varepsilon^2 + \lambda^2}\right), \quad \mathsf{A}_{jk}^* = -\int_{-\infty}^{\infty}\frac{\imath\lambda\,\mathrm{d}\mu_{jk}(\lambda)}{\varepsilon^2 + \lambda^2}, \tag{26}$$

which involve the *complex measure* μ_{jk}.

We now show how the integrals in (26) for S_{jk}^* and A_{jk}^* can be represented in terms of the *signed measures* Re μ_{jk} and Im μ_{jk}, respectively, associated with the functions in (24). Since $\boldsymbol{\nabla}\chi_k$ and H in (13) are *real-valued*, we have from (18) the following symmetry conditions

$$\langle(\varepsilon\mathsf{I} + \mathbf{A})^{-1}\boldsymbol{g}_j \cdot (\varepsilon\mathsf{I} + \mathbf{A})^{-1}\boldsymbol{g}_k\rangle = \langle(\varepsilon\mathsf{I} + \mathbf{A})^{-1}\boldsymbol{g}_k \cdot (\varepsilon\mathsf{I} + \mathbf{A})^{-1}\boldsymbol{g}_j\rangle \tag{27}$$

$$\langle\mathbf{A}(\varepsilon\mathsf{I} + \mathbf{A})^{-1}\boldsymbol{g}_j \cdot (\varepsilon\mathsf{I} + \mathbf{A})^{-1}\boldsymbol{g}_k\rangle = \langle(\varepsilon\mathsf{I} + \mathbf{A})^{-1}\boldsymbol{g}_k \cdot \mathbf{A}(\varepsilon\mathsf{I} + \mathbf{A})^{-1}\boldsymbol{g}_j\rangle.$$

These symmetries, the sesquilinearity of the $\mathscr{H}$-inner-product, the linearity [51] of the Stieltjes integral in (22) with respect to the function $\mu_{\xi\zeta}(\lambda)$ and equation (26) yield

$$\mathsf{S}_{jk}^* = \varepsilon\left(\delta_{jk} + \int_{-\infty}^{\infty}\frac{\mathrm{dRe }\,\mu_{jk}(\lambda)}{\varepsilon^2 + \lambda^2}\right), \quad \mathsf{A}_{jk}^* = \int_{-\infty}^{\infty}\frac{\lambda\,\mathrm{dIm }\,\mu_{jk}(\lambda)}{\varepsilon^2 + \lambda^2}, \tag{28}$$

where we have used Re $\mu_{jk}(\lambda) = (\mu_{jk}(\lambda) + \overline{\mu}_{jk}(\lambda))/2$ and Im $\mu_{jk}(\lambda) = (\mu_{jk}(\lambda) - \overline{\mu}_{jk}(\lambda))/(2\imath)$.

The formulas for S_{jk}^* and A_{jk}^* in (28) were computed with respect to the standard basis $\{e_j\}$, through the definition of $\mu_{jk}(\lambda) = \langle \mathbf{Q}(\lambda) g_j, g_k \rangle$ with $g_k = -\mathbf{\Gamma} \mathsf{H} e_k$. We now show that, given S_{jk}^* and A_{jk}^*, $j, k = 1, \ldots, d$, the effective diffusivity tensor can be computed relative to any directions. This is due to the bilinearity of the inner-product underlying the definition of $\mu_{jk}(\lambda)$. More specifically, if $\boldsymbol{\xi}, \boldsymbol{\zeta} \in \mathbb{R}^d$ are arbitrary directions of interest, then $\langle \mathbf{Q}(\lambda) \mathbf{\Gamma} \mathsf{H} \boldsymbol{\xi}, \mathbf{\Gamma} \mathsf{H} \boldsymbol{\zeta} \rangle = \sum_{jk} a_j b_k \langle \mathbf{Q}(\lambda) g_j, g_k \rangle$, where the constants a_j and b_k, $j, k = 1, \ldots, d$, are the coordinates of the vectors $\boldsymbol{\xi}$ and $\boldsymbol{\zeta}$ with respect to the standard basis. This immediately leads to integral representations for the effective diffusivity tensor relative to any desired directions.

We conclude this section with a discussion regarding some rigorous bounds for S_{jk}^* and A_{jk}^*, $j, k = 1, \ldots, d$, that follow from the integral representations in (28). We assume that $0 < \varepsilon < \infty$ throughout our discussion. From equation (20), the spectrum Σ of the operator $\mathbf{M} = -\imath \mathbf{A}$ is a bounded subset of $\mathbb{R}$. Denote $\lambda_+ = \sup \Sigma$ and $|\lambda|_+ = \sup_{\lambda \in \Sigma} |\lambda|$, and recall that $\inf_{\lambda \in \Sigma} \lambda^2 = 0$ as $\lambda = 0$ is a limit point [49] of the *compact* operator $\mathbf{M}$ [8, 29]. Since μ_{kk} is a positive measure with finite mass μ_{kk}^0, the inequalities $1/(\varepsilon^2 + \lambda_+^2) \leq 1/(\varepsilon^2 + \lambda^2) \leq 1/\varepsilon^2$, holding for all $\lambda \in \Sigma$, yield [18]

$$\varepsilon \left[1 + \mu_{kk}^0/(\varepsilon^2 + \lambda_+^2) \right] \leq \mathsf{S}_{kk}^* \leq \varepsilon \left[1 + \mu_{kk}^0/\varepsilon^2 \right]. \tag{29}$$

It may be that $\mu_{kk}^0 = 0$, hence $\mathsf{S}_{kk}^* = \varepsilon$, e.g., shear flow orthogonal to the kth direction [3, 15].

When $j \neq k$, Re μ_{jk} is a signed measure. There are unique, *positive* measures Re μ_{jk}^+ and Re μ_{jk}^- such that Re $\mu_{jk} = $ Re $\mu_{jk}^+ - $ Re μ_{jk}^- [18]. Moreover, associated with the signed measure Re μ_{jk} is its *total variation* $|$Re $\mu|_{jk}$ [18]

$$\text{Re } \mu_{jk} = \text{Re } \mu_{jk}^+ - \text{Re } \mu_{jk}^-, \qquad |\text{Re } \mu|_{jk} = \text{Re } \mu_{jk}^+ + \text{Re } \mu_{jk}^-. \tag{30}$$

From equation (25) the measures Re μ_{jk}^+ and Re μ_{jk}^- have bounded mass, $[\text{Re } \mu_{jk}^+]^0$ and $[\text{Re } \mu_{jk}^-]^0$, respectively, thus the mass $|\text{Re } \mu|_{jk}^0$ of the measure $|\text{Re } \mu|_{jk}$ is also bounded. Since $|\mathsf{S}_{jk}^*| \leq \int \mathrm{d}|\text{Re } \mu|_{jk}(\lambda)/(\varepsilon^2 + \lambda^2)$ [18], the upper bound in equation (29) with μ_{kk}^0 replaced by $|\text{Re } \mu|_{jk}^0$ holds for the positive quantity $|\mathsf{S}_{jk}^*|$. Our numerical results in Section IX indicate that $\mu_{kk} = |\text{Re } \mu|_{jk}$, $j \neq k$, for 2D flows that are symmetric about the line $y = x$, such as as cat's eye flow, yielding the bound $|\mathsf{S}_{jk}^*| \leq \mathsf{S}_{kk}^*$ which holds for such flows (see Figures 3 and 4 below). These bounds for S_{jk}^* can be improved upon by separately considering the positive

and negative contributions of the integral representation for S_{jk}^*, yielding

$$\varepsilon \frac{[\text{Re }\mu_{jk}^+]^0}{\varepsilon^2 + \lambda_+^2} - \frac{[\text{Re }\mu_{jk}^-]^0}{\varepsilon} \leq S_{jk}^* \leq \frac{[\text{Re }\mu_{jk}^+]^0}{\varepsilon} - \varepsilon \frac{[\text{Re }\mu_{jk}^-]^0}{\varepsilon^2 + \lambda_+^2}, \qquad j \neq k. \tag{31}$$

In a similar way, we obtain the following bounds for A_{jk}^*

$$-\frac{|\lambda|_+ |\text{Im }\mu|_{jk}^0}{\varepsilon^2} \leq A_{jk}^* \leq \frac{|\lambda|_+ |\text{Im }\mu|_{jk}^0}{\varepsilon^2}, \qquad j \neq k, \tag{32}$$

where $|\text{Im }\mu|_{jk}^0$ is the finite mass of the total variation $|\text{Im }\mu|_{jk} = \text{Im }\mu_{jk}^+ + \text{Im }\mu_{jk}^-$ of the signed measure $\text{Im }\mu_{jk} = \text{Im }\mu_{jk}^+ - \text{Im }\mu_{jk}^-$ [18]. Bounds on S_{kk}^* can also be obtained using variational methods [3, 15, 16] as well as Padé approximants [3, 5] of Stieltjes functions.

IV.   DISCRETE SETTING: HILBERT SPACE OF CURL-FREE FIELDS

Here, we provide a discrete formulation of the effective parameter problem in Section III B, which will be used in Section IX to compute a discrete spectral measure μ_{jk} involved in discrete versions of the Stieltjes integral representations for the effective diffusivity tensor D^* in equation (28). More specifically, we use the cell problem in equations (10) and (18), written as $(\varepsilon I + A)\nabla\chi_k = g_k$, to express the discrete spectral measure explicitly in terms of the eigenvalues and eigenvectors of a matrix representation A of the operator $A = \Gamma H \Gamma$, not to be confused with the antisymmetric part A^* of the effective diffusivity tensor. In Section IV A, we discuss the spectral properties of the matrix A and provide the Stieltjes integral representations for the effective diffusivity tensor D^* in (28), involving the discrete spectral measure μ_{jk}. A projection method is formulated in Section IV B, which shows that the discrete measure μ_{jk} is determined by the eigenvalues and eigenvectors of a matrix that is much smaller than the matrix A. This greatly increases the efficiency of our numerical computations of D^* in Section IX.

A.   Matrix formulation of the effective parameter problem

In the discrete setting [37], H is represented by a banded antisymmetric matrix. For simplicity we will not make a notational distinction between the two cases, as the context will be made clear. The differential operator ∇ is represented by a finite difference matrix ∇ [13, 37], where $\nabla^T = (\nabla_1^T, \ldots, \nabla_d^T)$ and $\nabla_j, j = 1, \ldots, d$, are also finite difference matrices.

Moreover, the divergence operator $\boldsymbol{\nabla}\cdot$ is given by $-\nabla^T$ and the matrix representation of the negative Laplacian $-\Delta$ is given by $\nabla^T\nabla$. Consequently, the projection operator $\boldsymbol{\Gamma} = \boldsymbol{\nabla}(\Delta^{-1})\boldsymbol{\nabla}\cdot$ is represented by the symmetric projection matrix $\Gamma = \nabla(\nabla^T\nabla)^{-1}\nabla^T$, satisfying $\Gamma^2 = \Gamma$ and $\Gamma\nabla = \nabla$, where $(\nabla^T\nabla)^{-1}$ is now interpreted as a matrix inversion. We assume here that the matrix ∇ is of full rank so that $(\nabla^T\nabla)^{-1}$ exists. The rank deficient case, where the matrix $\nabla^T\nabla$ is singular, is examined in detail in Section VIII. In this way, the integro-differential operator $\mathbf{A}$ is represented by an antisymmetric matrix $\mathsf{A} = \Gamma\mathsf{H}\Gamma$ satisfying $\mathsf{A}^T = -\mathsf{A}$, which is not to be confused with the antisymmetric part A^* of the effective diffusivity tensor D^*. In a similar way, the vectors $\boldsymbol{g}_k = -\boldsymbol{\Gamma}\mathsf{H}\boldsymbol{e}_k$, $k = 1, \dots, d$, are redefined in this matrix setting and, for simplicity, we will not make a notational distinction between the two cases for the vectors $\boldsymbol{g}_k$ and $\boldsymbol{e}_k$, as the context will be made clear.

The spectrum Σ of the antisymmetric matrix A, of size N, say, consists solely of eigenvalues υ_n, $n = 1, \dots, N$, with corresponding eigenvectors $\boldsymbol{w}_n$ satisfying $\mathsf{A}\boldsymbol{w}_n = \upsilon_n\boldsymbol{w}_n$. It is well known [22] that its eigenvalues υ_n are purely imaginary, $\upsilon_n = \imath\lambda_n$ with $\lambda_n \in \mathbb{R}$. Therefore, the matrix $\mathsf{M} = -\imath\mathsf{A}$ is Hermitian ($\mathsf{M}^\dagger = \mathsf{M}$) and it has the same eigenvectors $\boldsymbol{w}_n$ as the matrix A and real eigenvalues given by $\lambda_n = \mathrm{Im}\,\upsilon_n$. It is also well known [25] that the eigenvectors $\boldsymbol{w}_n$, $n = 1, \dots, N$, form an orthonormal basis for $\mathbb{C}^N$, i.e., $\boldsymbol{w}_n^\dagger\boldsymbol{w}_m = \delta_{nm}$ and for every $\boldsymbol{\xi} \in \mathbb{C}^N$ we have $\boldsymbol{\xi} = \sum_n(\boldsymbol{w}_n^\dagger\boldsymbol{\xi})\boldsymbol{w}_n = \left(\sum_n \boldsymbol{w}_n\boldsymbol{w}_n^\dagger\right)\boldsymbol{\xi}$. Consequently, defining $\mathsf{Q}_n = \boldsymbol{w}_n\boldsymbol{w}_n^\dagger$, $n = 1, \dots, N$, to be the mutually orthogonal projection matrices onto the eigenspaces spanned by the $\boldsymbol{w}_n$,

$$\sum_{n=1}^N \mathsf{Q}_n = \mathsf{I}, \qquad \mathsf{Q}_n = \boldsymbol{w}_n\boldsymbol{w}_n^\dagger, \qquad \mathsf{Q}_l\mathsf{Q}_m = \mathsf{Q}_l\,\delta_{lm}. \tag{33}$$

We now use equation (33) to prove the spectral theorem in (22) for this matrix setting. From $\mathsf{M}\boldsymbol{w}_n = \lambda_n\boldsymbol{w}_n$ and equation (33) we have that $\mathsf{M}\mathsf{Q}_n = \lambda_n\mathsf{Q}_n$. This formula and (33) then imply that the matrix M has the spectral decomposition $\mathsf{M} = \sum_n \lambda_n\mathsf{Q}_n$. By the mutual orthogonality of the projection matrices Q_n and by induction, we have that $\mathsf{M}^m = \sum_n \lambda_n^m\mathsf{Q}_n$ for all $m \in \mathbb{N}$. This, in turn, implies that $f(\mathsf{M}) = \sum_n f(\lambda_n)\mathsf{Q}_n$ for any polynomial $f : \mathbb{R} \mapsto \mathbb{C}$. From the mutual orthogonality and the symmetry of the projection matrices Q_n it follows that, for all $\boldsymbol{\xi}, \boldsymbol{\zeta} \in \mathbb{C}^N$ and complex-valued polynomials $f(\lambda)$ and $h(\lambda)$, the bilinear functional $\langle f(\mathsf{M})\boldsymbol{\xi}\cdot h(\mathsf{M})\boldsymbol{\zeta}\rangle$ has the integral representation in equation (22), with $\mathbf{M}$ substituted by M. Moreover, the complex-valued function $\mu_{\xi\zeta}(\lambda) = \langle\mathbf{Q}(\lambda)\boldsymbol{\xi}, \boldsymbol{\zeta}\rangle$ in equation (22) is now given by $\mu_{\xi\zeta}(\lambda) = \langle\mathsf{Q}(\lambda)\boldsymbol{\xi}\cdot\boldsymbol{\zeta}\rangle$, where the associated matrix representation $\mathsf{Q}(\lambda)$ of the projection

operator $\mathbf{Q}(\lambda)$ and the discrete spectral measure $\mathrm{d}\mu_{\xi\zeta}(\lambda)$ are given by

$$\mathsf{Q}(\lambda) = \sum_{n:\,\lambda_n \leq \lambda} \theta(\lambda - \lambda_n)\mathsf{Q}_n, \qquad \mathrm{d}\mu_{\xi\zeta}(\lambda) = \sum_{n:\,\lambda_n \leq \lambda} \langle \delta_{\lambda_n}(\mathrm{d}\lambda)[\mathsf{Q}_n\boldsymbol{\xi}{\cdot}\boldsymbol{\zeta}]\rangle. \tag{34}$$

Here, $\theta(\lambda)$ is the Heaviside function, satisfying $\theta(\lambda) = 0$ for $\lambda < 0$ and $\theta(\lambda) = 1$ for $\lambda \geq 0$, and $\delta_{\lambda_n}(\mathrm{d}\lambda)$ is the δ-measure centered at λ_n.

The spectral theorem for symmetric matrices also holds for functions of the form $f(\lambda) = a\lambda^l(b + c\lambda)^{-m}$, with $l, m \in \mathbb{N}$, $a, b, c \in \mathbb{C}$, and $b + c\lambda \neq 0$ for all $\lambda \in \Sigma$. We will demonstrate this for the special cases that arise in the functional formulas for S^*_{jk} and A^*_{jk} in equation (19), with $\mathbf{A}$ substituted with A, which yield the integral representations in (26) involving a discrete spectral measure $\mathrm{d}\mu_{jk}(\lambda)$ associated with the measure in (34). The argument involving the function $f(\lambda)$ above is a simple extension of that given here.

As A is a real-valued matrix, its eigenvalues $\upsilon_n = \imath\lambda_n$, $n = 1, \ldots, N$, and eigenvectors $\boldsymbol{w}_n$ come in complex-conjugate pairs [22]. Therefore, if the size N of A is even, then we may re-number the index set I_N as $I_N = \{-N/2, \ldots, -1, 1, \ldots, N/2\}$ such that $\upsilon_{-n} = \overline{\upsilon_n} = -\upsilon_n$ and $\boldsymbol{w}_{-n} = \overline{\boldsymbol{w}_n}$. If N is odd then $\upsilon_0 = 0$ is also an eigenvalue with a *real-valued* eigenvector $\boldsymbol{w}_0$. Denoting by W the matrix with columns consisting of the eigenvectors $\boldsymbol{w}_n$, $\Upsilon = \mathrm{diag}(\upsilon_{-N/2}, \ldots, \upsilon_{N/2})$ the diagonal matrix with eigenvalues υ_n on the main diagonal, and $\Lambda = \mathrm{diag}(\lambda_{-N/2}, \ldots, \lambda_{N/2})$, we have that $\mathsf{A} = \mathsf{W}\Upsilon\mathsf{W}^\dagger = \imath\mathsf{W}\Lambda\mathsf{W}^\dagger$, where the matrix W is unitary $\mathsf{W}^\dagger\mathsf{W} = \mathsf{W}\mathsf{W}^\dagger = \mathsf{I}$ [22]. Therefore, the matrix $\mathsf{M} = -\imath\mathsf{A} = \mathsf{W}\Lambda\mathsf{W}^\dagger$ is Hermitian $(\mathsf{M}^\dagger = \mathsf{M})$.

This spectral decomposition of A demonstrates that the matrix $(\varepsilon\mathsf{I} + \mathsf{A})^{-1}$, is well defined for all $0 < \varepsilon < \infty$. In particular, since $\mathsf{W}^\dagger = \mathsf{W}^{-1}$, it has the following useful representation $(\varepsilon\mathsf{I} + \mathsf{A})^{-1} = \mathsf{W}(\varepsilon\mathsf{I} + \imath\Lambda)^{-1}\mathsf{W}^\dagger$, where $(\varepsilon\mathsf{I} + \imath\Lambda)^{-1}$ is a diagonal matrix with entries $1/(\varepsilon + \imath\lambda)$. This allows the discrete version of the resolvent formula in equation (18) to be written as

$$\nabla\boldsymbol{\chi}_j = \mathsf{W}(\varepsilon\mathsf{I} + \imath\Lambda)^{-1}\mathsf{W}^\dagger\boldsymbol{g}_j, \quad \boldsymbol{g}_j = -\Gamma\mathsf{H}\boldsymbol{e}_j. \tag{35}$$

Substituting the resolvent formula for $\nabla\boldsymbol{\chi}_k$ in equation (35) into the discrete version of (13) and using $\Gamma\nabla = \nabla$ to write $\langle\mathsf{H}\,\nabla\boldsymbol{\chi}_j{\cdot}\nabla\boldsymbol{\chi}_k\rangle = \langle\mathsf{A}\,\nabla\boldsymbol{\chi}_j{\cdot}\nabla\boldsymbol{\chi}_k\rangle$, we obtain the following analogue of equation (19),

$$\mathsf{S}^*_{jk} = \varepsilon\big(\,\delta_{jk} + \langle(\varepsilon\mathsf{I} + \imath\Lambda)^{-1}\mathsf{W}^\dagger\boldsymbol{g}_j{\cdot}(\varepsilon\mathsf{I} + \imath\Lambda)^{-1}\mathsf{W}^\dagger\boldsymbol{g}_k\rangle\,\big), \tag{36}$$

$$\mathsf{A}^*_{jk} = \langle\imath\Lambda(\varepsilon\mathsf{I} + \imath\Lambda)^{-1}\mathsf{W}^\dagger\boldsymbol{g}_j{\cdot}(\varepsilon\mathsf{I} + \imath\Lambda)^{-1}\mathsf{W}^\dagger\boldsymbol{g}_k\rangle,$$

where we have used that $W^\dagger = W^{-1}$. The quadratic form $W^\dagger \boldsymbol{g}_j \cdot W^\dagger \boldsymbol{g}_k$ arising in (36) can be written in terms of the projection matrices Q_n defined in (33) as follows

$$W^\dagger \boldsymbol{g}_j \cdot W^\dagger \boldsymbol{g}_k = \sum_{n \in I_N} \overline{(\boldsymbol{w}_n^\dagger \boldsymbol{g}_j)}(\boldsymbol{w}_n^\dagger \boldsymbol{g}_k) = \sum_{n \in I_N} Q_n \, \boldsymbol{g}_j \cdot \boldsymbol{g}_k. \tag{37}$$

This implies that the functional formulas for S_{jk}^* and A_{jk}^* in equation (36) have the integral representations in equation (26) with discrete spectral measure $d\mu_{jk}(\lambda)$ defined in equation (34) with $\boldsymbol{\xi} = \boldsymbol{g}_j = -\Gamma H \boldsymbol{e}_j$ and $\boldsymbol{\zeta} = \boldsymbol{g}_k = -\Gamma H \boldsymbol{e}_k$.

As in the abstract Hilbert space setting discussed in Section III B, we may use the fact that the matrix A, the vector $\boldsymbol{g}_j$, and the molecular diffusivity ε are real-valued to obtain the symmetry relations in equation (27), with $\mathbf{A}$ changed to A. This allows us to rewrite the integral representations for S_{jk}^* and A_{jk}^* in (26) involving the discrete, *complex measure* $d\mu_{jk}(\lambda)$, as the integral representations in equation (28) involving the real *signed measures* $\text{Re} \, \mu_{jk}$ and $\text{Im} \, \mu_{jk}$. As in the abstract Hilbert space setting, these signed measures are determined by the functions $\text{Re} \, \mu_{jk}(\lambda)$ and $\text{Im} \, \mu_{jk}(\lambda)$ in equation (24), where in this matrix setting $\mu_{jk}(\lambda) = \langle Q(\lambda)\boldsymbol{g}_j \cdot \boldsymbol{g}_k \rangle$ and $Q(\lambda)$ is defined in equation (34). As the projection matrix Q_n is Hermitian, we have $[Q_n \boldsymbol{g}_k \cdot \boldsymbol{g}_j] = [\overline{Q}_n \boldsymbol{g}_j \cdot \boldsymbol{g}_k]$. Consequently, from equations (24) and (34) we have that

$$\text{Re} \, \mu_{jk}(\lambda) = \frac{1}{2} \sum_{n: \, \lambda_n \leq \lambda} \langle \theta(\lambda - \lambda_n)[(Q_n + \overline{Q}_n)\boldsymbol{g}_j \cdot \boldsymbol{g}_k] \rangle \tag{38}$$

$$\text{Im} \, \mu_{jk}(\lambda) = \frac{1}{2\imath} \sum_{n: \, \lambda_n \leq \lambda} \langle \theta(\lambda - \lambda_n)[(Q_n - \overline{Q}_n)\boldsymbol{g}_j \cdot \boldsymbol{g}_k] \rangle,$$

where $[(Q_n + \overline{Q}_n)\boldsymbol{g}_j \cdot \boldsymbol{g}_k] = 2\text{Re} \, [Q_n \boldsymbol{g}_j \cdot \boldsymbol{g}_k]$ and $[(Q_n - \overline{Q}_n)\boldsymbol{g}_j \cdot \boldsymbol{g}_k] = 2\imath \text{Im} \, [Q_n \boldsymbol{g}_j \cdot \boldsymbol{g}_k]$.

Since the eigenvalues $\upsilon_n = \imath \lambda_n$ and eigenvectors $\boldsymbol{w}_n$ of the matrix A come in complex conjugate pairs, the representations of the measures $\text{Re} \, \mu_{jk}$ and $\text{Im} \, \mu_{jk}$, which follow from the functions in equation (38), can be simplified and shown [41] to depend only on the restricted index set $\{n \geq 0 : \lambda_n \leq \lambda\}$. This is clear from equations (28) and (38), since for $n \geq 0$ we have $\lambda_{-n}^2 = (-\lambda_n)^2 = \lambda_n^2$ and $\boldsymbol{w}_{-n} = \overline{\boldsymbol{w}_n}$, thus $Q_{-n} = \overline{Q}_n$. Consequently, we have that

$$\text{Re} \, [Q_n \boldsymbol{g}_j \cdot \boldsymbol{g}_k] + \text{Re} \, [Q_{-n}\boldsymbol{g}_j \cdot \boldsymbol{g}_k] = 2\text{Re} \, [Q_n \boldsymbol{g}_j \cdot \boldsymbol{g}_k] \tag{39}$$

$$\lambda_n \text{Im} \, [Q_n \boldsymbol{g}_j \cdot \boldsymbol{g}_k] + \lambda_{-n} \text{Im} \, [Q_{-n}\boldsymbol{g}_j \cdot \boldsymbol{g}_k] = 2\lambda_n \text{Im} \, [Q_n \boldsymbol{g}_j \cdot \boldsymbol{g}_k],$$

with $\lambda_0 \text{Im} [Q_0 \boldsymbol{g}_j \cdot \boldsymbol{g}_k] \equiv 0$.

B. Projection method

We now formulate a projection method which demonstrates that the discrete spectral measure μ_{jk} in (38) is determined by the eigenvalues and eigenvectors of a matrix that is much smaller than the matrix A. This will be used in Section IX to greatly increases the efficiency of our numerical computations of D^*. This method follows from the projective nature of the matrix Γ, which causes $\mathsf{A} = \Gamma\mathsf{H}\Gamma$ to have a large null space associated with the null space of Γ. We demonstrate that the spectral weights $[\mathsf{Q}_n\boldsymbol{g}_j\cdot\boldsymbol{g}_k]$ associated with this null space are identically zero and therefore do not need to be computed at all.

Since Γ is a real-symmetric projection matrix of size N, its eigenvalues γ_n, $n = 1, \ldots, N$, satisfy $\gamma_n = 0, 1$ [22]. Consequently, Γ has the spectral decomposition $\Gamma = \mathsf{P}\mathsf{G}\mathsf{P}^T$, where P is an orthogonal matrix, $\mathsf{P}\mathsf{P}^T = \mathsf{P}^T\mathsf{P} = \mathsf{I}$, with columns consisting of the eigenvectors of Γ, and the diagonal matrix G has the eigenvalues γ_n along its main diagonal. Write $\mathsf{P} = [\mathsf{P}_0 \ \mathsf{P}_1]$, where the columns of the $N \times N_0$ matrix P_0 and the $N \times N_1$ matrix P_1 are orthonormal eigenvectors that span the null space and range of Γ, respectively, with $N_0 + N_1 = N$ [22]. It follows that $\mathsf{G} = \mathrm{diag}(\mathbf{0}_{N_0}, \mathbf{1}_{N_1})$, where $\mathbf{0}_{N_0}$ and $\mathbf{1}_{N_1}$ are vectors of zeros and ones of length N_0 and N_1, respectively. This, in turn, implies that the matrix Γ can be written as

$$\Gamma = \mathsf{P}_1\mathsf{P}_1^T. \tag{40}$$

The matrix P being orthogonal implies that $\mathsf{P}_1^T\mathsf{P}_1 = I_{11}$, where I_{11} is the identity matrix of size $N_1 \times N_1$. This demonstrates that the matrix Γ satisfies $\Gamma^2 = \Gamma$. Moreover, Γ projects vectors in $\mathbb{R}^N$ on to the subspace spanned by the columns of P_1.

Using the spectral decomposition $\Gamma = \mathsf{P}\mathsf{G}\mathsf{P}^T$ of Γ, we may write the matrix $\mathsf{A} = \Gamma\mathsf{H}\Gamma$ as $\mathsf{A} = \mathsf{P}[\mathsf{G}(\mathsf{P}^T\mathsf{H}\mathsf{P})\mathsf{G}]\mathsf{P}^T$. The block matrix form of the matrix $\mathsf{G}(\mathsf{P}^T\mathsf{H}\mathsf{P})\mathsf{G} = \mathsf{P}^T\mathsf{A}\mathsf{P}$ is given by

$$\mathsf{G}(\mathsf{P}^T\mathsf{H}\mathsf{P})\mathsf{G} = \begin{bmatrix} \mathsf{O}_{00} & \mathsf{O}_{01} \\ \mathsf{O}_{10} & \mathsf{I}_{11} \end{bmatrix} \begin{bmatrix} \mathsf{P}_0^T \\ \mathsf{P}_1^T \end{bmatrix} \mathsf{H} \begin{bmatrix} \mathsf{P}_0 & \mathsf{P}_1 \end{bmatrix} \begin{bmatrix} \mathsf{O}_{00} & \mathsf{O}_{01} \\ \mathsf{O}_{10} & \mathsf{I}_{11} \end{bmatrix} = \begin{bmatrix} \mathsf{O}_{00} & \mathsf{O}_{01} \\ \mathsf{O}_{10} & \mathsf{P}_1^T\mathsf{H}\mathsf{P}_1 \end{bmatrix}, \tag{41}$$

where O_{ab} is a matrix of zeros of size $N_a \times N_b$, $a, b = 0, 1$.

Due to the skew-symmetry of H, the matrix $\mathsf{P}_1^T\mathsf{H}\mathsf{P}_1$ of size $N_1 \times N_1$ is also antisymmetric and consequently has the spectral decomposition

$$\mathsf{P}_1^T\mathsf{H}\mathsf{P}_1 = \imath\mathsf{R}_{11}\Lambda_{11}\mathsf{R}_{11}^\dagger, \tag{42}$$

where R_{11} is a unitary matrix, $\mathsf{R}_{11}^\dagger \mathsf{R}_{11} = \mathsf{R}_{11}\mathsf{R}_{11}^\dagger = \mathsf{I}_{11}$, and Λ_{11} is a real-valued diagonal matrix. Equations (41) and (42) allow the matrix A to be written as

$$\mathsf{A} = \imath\mathsf{W}\Lambda\mathsf{W}^\dagger, \quad \mathsf{W} = \mathsf{P}\mathsf{R}, \qquad \mathsf{R} = \begin{bmatrix} \mathsf{I}_{00} & \mathsf{O}_{01} \\ \mathsf{O}_{10} & \mathsf{R}_{11} \end{bmatrix}, \quad \Lambda = \begin{bmatrix} \mathsf{O}_{00} & \mathsf{O}_{01} \\ \mathsf{O}_{10} & \Lambda_{11} \end{bmatrix}, \qquad (43)$$

where I_{00} is the identity matrix of size $N_0 \times N_0$. Since R_{11} is a unitary matrix, the matrix R also is. Consequently, since P is orthogonal, W is a unitary matrix $\mathsf{W}^\dagger\mathsf{W} = \mathsf{W}\mathsf{W}^\dagger = \mathsf{I}$.

Equation (43) demonstrates that the eigenvalues $\imath\lambda_n$ of the matrix A are zero for all $n = 1, \ldots, N_0$. We now show that the associated spectral weights $[\mathsf{Q}_n\boldsymbol{g}_j \cdot \boldsymbol{g}_k]$ are also zero for all $n = 1, \ldots, N_0$. Here, $\boldsymbol{g}_j = -\Gamma\mathsf{H}\boldsymbol{e}_j$, $\mathsf{Q}_n = \boldsymbol{w}_n\boldsymbol{w}_n^\dagger$, and $\boldsymbol{w}_n$, $n = 1, \ldots, N$, are the eigenvectors of A which comprise the columns of the matrix W. From equation (43), we see that $\mathsf{W}^\dagger = \mathsf{R}^\dagger\mathsf{P}^T$. Since $\Gamma = \mathsf{P}\mathsf{G}\mathsf{P}^T$ and P is an orthogonal matrix, this implies that $\mathsf{W}^\dagger\Gamma = \mathsf{R}^\dagger\mathsf{G}\mathsf{P}^T$. It follows from the block forms of the matrices G, P, and R in equations (41) and (43), that $\mathsf{W}^\dagger\Gamma$ is given by

$$\mathsf{W}^\dagger\Gamma = \mathsf{R}^\dagger\mathsf{G}\mathsf{P}^T = \begin{bmatrix} \mathsf{I}_{00} & \mathsf{O}_{01} \\ \mathsf{O}_{10} & \mathsf{R}_{11}^\dagger \end{bmatrix} \begin{bmatrix} \mathsf{O}_{00} & \mathsf{O}_{01} \\ \mathsf{O}_{10} & \mathsf{I}_{11} \end{bmatrix} \begin{bmatrix} \mathsf{P}_0^T \\ \mathsf{P}_1^T \end{bmatrix} = \begin{bmatrix} \mathsf{O}_{0N} \\ \mathsf{R}_{11}^\dagger\mathsf{P}_1^T \end{bmatrix}, \qquad (44)$$

where O_{0N} is a matrix of zeros of size $N_0 \times N$. It follows from $\boldsymbol{g}_j = -\Gamma\mathsf{H}\boldsymbol{e}_j$ and equation (44) that $\boldsymbol{w}_n^\dagger\boldsymbol{g}_j = 0$ for all $n = 1, \ldots, N_0$. This and equation (37) imply that $[\mathsf{Q}_n\boldsymbol{g}_j \cdot \boldsymbol{g}_k] = 0$ for all $n = 1, \ldots, N_0$, as claimed.

In Section IX we will employ this projection method to compute the discrete spectral measure $d\mu_{jk}(\lambda)$ by directly computing the eigenvectors and eigenvalues of the matrix $\mathsf{P}_1^T\mathsf{H}\mathsf{P}_1$. Our analysis demonstrates that the discrete spectral measure $d\mu_{jk}(\lambda)$ associated with equation (34) does not depend on components $[\mathsf{Q}_n\boldsymbol{g}_j \cdot \boldsymbol{g}_k]$, $n = 1, \ldots, N_0$, and therefore do not need to be computed at all. Moreover, in the case of a randomly perturbed, periodic velocity field, since the matrix Γ is non-random, the spectral decomposition $\Gamma = \mathsf{P}\mathsf{G}\mathsf{P}^T$ needs to be computed only once, while the spectral decomposition in (42) of the much smaller matrix $\mathsf{P}_1^T\mathsf{H}\mathsf{P}_1$ of size $N_1 \times N_1$ is performed repeatedly to gather spectral statistics. This greatly increases the efficiency of our associated computations.

V. SOBOLEV SPACE AND THE EFFECTIVE DIFFUSIVITY TENSOR

In this section, we adapt and extend an alternate method [8, 41] to the method presented in Section III, which provides integral representations for the effective diffusivity tensor

D^*, and leads to a more direct approach for its computation than the projection method discussed in Section IV B. We provide functional formulas that are analogous to the formulas in equation (13) for the symmetric S^* and antisymmetric A^* parts of D^*, involving the scalar field χ_j in equation (4). We also provide a Sobolev space formulation of the effective parameter problem [41] which yields a resolvent formula for χ_j that is analogous to the formula in (18), involving a self-adjoint operator that depends only on the fluid velocity field. This leads to the Stieltjes integral representations in (28), involving a spectral measure of the operator.

In contrast to Section III B, which defined the effective tensor D^* in terms of the *vector field* $\boldsymbol{\nabla}\chi_j$, here we define D^* in terms of the *scalar field* χ_j. Consider the Hilbert space $\mathcal{H}$,

$$\mathcal{H} = \{f \in L^2(\mathcal{V}, \mathrm{m}) \, : \, f(\boldsymbol{x}) \text{ is periodic in } \mathcal{V}\}, \tag{45}$$

where m is the Lebesgue measure on $\mathbb{R}^d$, restricted to $\mathcal{V}$, and the σ-algebra associated with the underlying probability space is generated by the Lebesgue measurable subsets of $\mathbb{R}^d$. The Hilbert space $\mathcal{H}$ is equipped with a sesquilinear inner product $\langle \cdot, \cdot \rangle$ defined by $\langle f, h \rangle = \langle \overline{f} \, h \rangle$, with $\langle h, f \rangle = \overline{\langle f, h \rangle}$ for $f, h \in \mathcal{H}$, which induces a norm $\| \cdot \|$ defined by $\|f\| = \langle f, f \rangle^{1/2}$ and $f \in \mathcal{H}$ implies $\|f\| < \infty$. Now consider the associated Sobolev space $\mathcal{H}^{1,2}$, which itself is a Hilbert space [8],

$$\mathcal{H}^{1,2} = \{f \in \mathcal{H} \, : \, \|f\|_{1,2} < \infty, \, \langle f \rangle = 0\}, \qquad \|f\|_{1,2} = \langle |\boldsymbol{\nabla} f|^2 \rangle^{1/2}, \tag{46}$$

where $\| \cdot \|_{1,2}$ is the norm induced by the underlying sesquilinear inner-product $\langle \cdot, \cdot \rangle_{1,2}$ defined by $\langle f, h \rangle_{1,2} = \langle \boldsymbol{\nabla} f \cdot \boldsymbol{\nabla} h \rangle$, with $\langle h, f \rangle_{1,2} = \overline{\langle f, h \rangle_{1,2}}$.

Recall the definition of the components $D^*_{jk} = \varepsilon \delta_{jk} + \langle u_j \chi_k \rangle$, $j, k = 1, \ldots, d$, of the effective diffusivity tensor D^* in (3). Rewrite the functional $\langle u_j \chi_k \rangle$ as [41],

$$\langle u_j \chi_k \rangle = \langle [\Delta \Delta^{-1} u_j] \chi_k \rangle = -\langle \boldsymbol{\nabla} \Delta^{-1} u_j \cdot \boldsymbol{\nabla} \chi_k \rangle = -\langle \Delta^{-1} u_j, \chi_k \rangle_{1,2}, \tag{47}$$

where we have used the periodicity of the functions u_j and χ_k. Substituting into equation (47) the expression $-u_j = \boldsymbol{u} \cdot \boldsymbol{\nabla} \chi_j + \varepsilon \Delta \chi_j$ for $-u_j$ in (4) yields the following functional formulas for the components S^*_{jk} and A^*_{jk}, $j, k = 1, \ldots, d$, of the symmetric S^* and antisymmetric A^* parts of D^* defined in equation (12),

$$S^*_{jk} = \varepsilon(\delta_{jk} + \langle \chi_j, \chi_k \rangle_{1,2}), \qquad A^*_{jk} = \langle A\chi_j, \chi_k \rangle_{1,2}, \quad A = \Delta^{-1}[\boldsymbol{u} \cdot \boldsymbol{\nabla}]. \tag{48}$$

The functional formulas in (48) are analogous to the functional formulas in equation (13). Due to the incompressibility of the fluid velocity field, $\boldsymbol{\nabla}\cdot\boldsymbol{u} = 0$, the operator A is antisymmetric on $\mathcal{H}^{1,2}$, i.e., $\langle Af, h\rangle_{1,2} = -\langle f, Ah\rangle_{1,2}$ for all $f, h \in \mathcal{H}^{1,2}$ (see equation (A1)). We stress that the operator A is independent of ε. Since the scalar fields χ_j and $A\chi_j$ are *real-valued*, we have that $\langle \chi_j, \chi_k\rangle_{1,2} = \langle \chi_k, \chi_j\rangle_{1,2}$ and $\mathsf{A}^*_{kj} = \langle A\chi_k, \chi_j\rangle_{1,2} = -\langle \chi_k, A\chi_j\rangle_{1,2} = -\langle A\chi_j, \chi_k\rangle_{1,2} = -\mathsf{A}^*_{jk}$, confirming that S^* is symmetric and A^* is antisymmetric.

Applying the operator Δ^{-1} to both sides of the the cell problem $\varepsilon\Delta\chi_j + \boldsymbol{u}\cdot\boldsymbol{\nabla}\chi_j = -u_j$ in equation (4) yields the following resolvent formula for χ_j involving the antisymmetric operator A, which is analogous to equation (18),

$$\chi_j = (\varepsilon + A)^{-1}g_j, \qquad g_j = -\Delta^{-1}u_j. \tag{49}$$

Substituting the resolvent formula for χ_j in (49) into the functionals in equation (48) yields

$$\mathsf{S}^*_{jk} = \varepsilon(\delta_{jk} + \langle(\varepsilon + A)^{-1}g_j, (\varepsilon + A)^{-1}g_k\rangle_{1,2}), \tag{50}$$
$$\mathsf{A}^*_{jk} = \langle A\,(\varepsilon + A)^{-1}g_j, (\varepsilon + A)^{-1}g_k\rangle_{1,2},$$

which is a direct analogue of equation (19).

Since $\mathcal{V}$ is a bounded domain, the linear operator Δ^{-1} is bounded on $\mathcal{H}$ [49]. When $|\boldsymbol{u}|^2$ is uniformly bounded on the period cell $\mathcal{V}$,

$$\sup_{\boldsymbol{x}\in\mathcal{V}} |\boldsymbol{u}(\boldsymbol{x})|^2 < \infty, \tag{51}$$

the linear operator A is bounded on $\mathcal{H}^{1,2}$, with (see equations (A2) and (A3))

$$\|A\|_{1,2} \leq \left[\, \|\Delta^{-1}\| \sup_{\boldsymbol{x}\in\mathcal{V}} |\boldsymbol{u}(\boldsymbol{x})|^2 \,\right]^{1/2} < \infty. \tag{52}$$

All of the fluid velocity fields that we consider in Section IX satisfy equation (51). More generally, for $u_k \in \mathcal{H}$, $k = 1, \ldots, d$, the operator A is compact on $\mathcal{H}^{1,2}$ [8], hence bounded [49]. It follows that $M = -\imath A$ is a bounded linear operator on $\mathcal{H}^{1,2}$ with $\|M\|_{1,2} = \|A\|_{1,2} < \infty$, where $\imath = \sqrt{-1}$. Moreover, the skew-symmetry of A and the sesquilinearity of the $\mathcal{H}^{1,2}$-inner-product imply that M is also symmetric, $\langle Mf, h\rangle_{1,2} = \langle f, Mh\rangle_{1,2}$, hence *self-adjoint* on $\mathcal{H}^{1,2}$ [46]. The spectrum Σ of the self-adjoint operator M is real-valued, with spectral radius equal to its operator norm [46], i.e.,

$$\Sigma \subseteq [-\|A\|_{1,2}, \|A\|_{1,2}]. \tag{53}$$

Exactly as in Section III B, direct analogues of equations (22)–(28) lead to the Stieltjes integral representations in (28), involving a Stieltjes measure μ_{jk} associated with the function of the spectral variable λ defined by $\mu_{jk}(\lambda) = \langle Q(\lambda)g_j, g_k \rangle_{1,2}$, where $g_j = -\Delta^{-1}u_j$ is defined in (49) and $\{Q(\lambda)\}_{\lambda \in \Sigma}$ is the family of self-adjoint projection operators that is in one-to-one correspondence with the bounded linear self-adjoint operator M on the Hilbert space $\mathcal{H}^{1,2}$. From equation (23), the mass μ_{jk}^0 of the measure μ_{jk} is given by $\mu_{jk}^0 = \langle g_j, g_k \rangle_{1,2} = \langle \boldsymbol{\nabla}\Delta^{-1}u_j \cdot \boldsymbol{\nabla}\Delta^{-1}u_k \rangle$ so that

$$\mu_{jk}^0 = \langle [(-\Delta)^{-1}u_j]\, u_k \rangle, \quad |\mu_{jk}^0| \leq \|\Delta^{-1}u_j\|\, \|u_k\| < \infty. \tag{54}$$

VI.   DISCRETE SETTING: SOBOLEV SPACE OF SCALAR FIELDS

In Section IX, we consider a discrete approximation of the cell problem in (4) written as $(\varepsilon + \imath M)\chi_j = g_j$, where $M = -\imath A$, $A = \Delta^{-1}[\boldsymbol{u}\cdot\boldsymbol{\nabla}]$, and $g_j = -\Delta^{-1}u_j$, as defined in equations (48) and (49). From the formula $\boldsymbol{u} = \boldsymbol{\nabla}\cdot\mathsf{H}$ in equation (8) and our discussion in Section IV A, we may write the discrete, matrix representation M of the self-adjoint operator $M = \Delta^{-1}[-\imath\boldsymbol{\nabla}\cdot\mathsf{H}\boldsymbol{\nabla}]$ by $\mathsf{M} = (-\nabla^T\nabla)^{-1}[-\imath\nabla^T\mathsf{H}\nabla]$. As in Section IV A, for simplicity, we do not make a notational distinction for the matrix H, between the continuum and discrete settings as the context will be clear. This composition of the Hermitian matrix $-\imath\nabla^T\mathsf{H}\nabla$ and the real-symmetric matrix $(-\nabla^T\nabla)^{-1}$ is not symmetric. From equation (A1) we see that the symmetry properties of the operator M depend intimately on the inner-product $\langle f, h \rangle_{1,2} = \langle \boldsymbol{\nabla}f\cdot\boldsymbol{\nabla}h \rangle$ of the underlying Sobolev space $\mathcal{H}^{1,2}$ defined in equation (46). Therefore, the properties of this inner-product must be included in the discrete formulation of the effective diffusivity tensor D^*.

In this section, we provide a discrete, matrix formulation of the effective parameter problem introduced in Section V, which involves a *generalized eigenvalue problem* that has the Sobolev-type inner-product as a central feature. In particular, this formulation retains the key properties of the weak form of the eigenvalue problem $\langle M\varphi_n, \varphi_n \rangle_{1,2} = \lambda_n$. Namely, the operator M is self-adjoint *with respect to the inner-product* $\langle \cdot, \cdot \rangle_{1,2}$ defined by $\langle f, h \rangle_{1,2} = \langle \boldsymbol{\nabla}f\cdot\boldsymbol{\nabla}h \rangle$, its eigenfunctions $\varphi_n \in \mathcal{H}^{1,2}$ are orthonormal $\langle \varphi_n, \varphi_m \rangle_{1,2} = \delta_{nm}$, $n, m = 1, 2, 3, \ldots$, with respect to the inner-product $\langle \cdot, \cdot \rangle_{1,2}$, and the spectrum Σ of M is real valued, $\Sigma \subset \mathbb{R}$. Towards this goal, consider the eigenvalue problem $M\varphi_n = \lambda_n\varphi_n$ in the

following form,

$$-\imath \boldsymbol{\nabla}{\cdot}\mathsf{H}\boldsymbol{\nabla}\varphi_n = \lambda_n \Delta \varphi_n. \tag{55}$$

Equation (55) is well defined for $\mathsf{H}_{jk} \in C^1(\mathcal{V})$ and $\varphi_n \in C^2(\mathcal{V})$, where $C^r(\mathcal{V})$ the space of continuously differentiable functions of order r with domain $\mathcal{V}$. Using a discrete version of equation (55), our goal is to establish the integral representations in (28) for the functionals $\mathsf{S}_{jk}^* = \varepsilon(\delta_{jk} + \langle \chi_j, \chi_k \rangle_{1,2})$ and $\mathsf{A}_{jk}^* = \langle \imath M \chi_j, \chi_k \rangle_{1,2}$ in (48), involving a discrete spectral measure which is analogous to the measure in equation (34).

By our discussion in Section IV A, the matrix representation of (55) is given by

$$\mathsf{B}\boldsymbol{z}_n = \lambda_n \mathsf{C}\boldsymbol{z}_n, \qquad \mathsf{B} = -\imath \nabla^T \mathsf{H} \nabla, \quad \mathsf{C} = \nabla^T \nabla. \tag{56}$$

The first formula in equation (56) is a *generalized eigenvalue problem* [40] associated with the pencil $\mathsf{B} - \lambda \mathsf{C}$, where B and C are Hermitian and real-symmetric matrices, respectively, of size K, say. The λ_n and $\boldsymbol{z}_n$, $n = 1, \ldots, K$, are known as generalized eigenvalues and eigenvectors, respectively. The matrix $\mathsf{C} = \nabla^T \nabla$ is clearly positive semi-definite. In this section, we will assume that C is positive definite, hence invertible. We will discuss the case where C is positive semi-definite in Section VIII.

Since the matrices B and C are symmetric and C is positive definite, the generalized eigenvalue problem has properties which are similar to the properties of the standard symmetric eigenvalue problem [40]. In particular, the generalized eigenvalues λ_n are all real, the generalized eigenvectors $\boldsymbol{z}_n$ form a basis for $\mathbb{C}^K$, and the $\boldsymbol{z}_n$ are orthonormal in the following sense $\boldsymbol{z}_n^\dagger \mathsf{C} \boldsymbol{z}_m = \delta_{nm}$, $n, m = 1, \ldots, K$, [40]. Since $\mathsf{C} = \nabla^T \nabla$ is real-valued, this is equivalent to the Sobolev-type orthogonality condition

$$\nabla \boldsymbol{z}_n {\cdot} \nabla \boldsymbol{z}_m = \delta_{nm}. \tag{57}$$

In other words, the generalized eigenvectors $\boldsymbol{z}_n$ are orthonormal with respect to the "discrete inner-product" $\langle \cdot, \cdot \rangle_{1,2}$ defined by $\langle \boldsymbol{\xi}, \boldsymbol{\zeta} \rangle_{1,2} = \nabla \boldsymbol{\xi} {\cdot} \nabla \boldsymbol{\zeta}$, for $\boldsymbol{\xi}, \boldsymbol{\zeta} \in \mathbb{C}^K$. Denoting by Z the matrix with columns consisting of the generalized eigenvectors $\boldsymbol{z}_n$, equation (57) is seen to be equivalent to $[\nabla \mathsf{Z}]^\dagger [\nabla \mathsf{Z}] = \mathsf{I}$, or $\mathsf{Z}^\dagger \mathsf{C} \mathsf{Z} = \mathsf{I}$. A key feature of the generalized eigenvalue problem is that the matrix Z simultaneously diagonalizes B and C. Specifically, if Λ is the diagonal matrix whose elements on the main diagonal are the generalized eigenvalues λ_n, then [40]

$$\mathsf{Z}^\dagger \mathsf{B} \mathsf{Z} = \Lambda, \qquad \mathsf{Z}^\dagger \mathsf{C} \mathsf{Z} = \mathsf{I}. \tag{58}$$

Since the $\boldsymbol{z}_n$, $n = 1, \ldots, K$, form a basis for $\mathbb{C}^K$ and satisfy (57), for all $\boldsymbol{\xi} \in \mathbb{C}^K$, we have that $\boldsymbol{\xi} = \sum_n (\nabla \boldsymbol{z}_n \cdot \nabla \boldsymbol{\xi}) \boldsymbol{z}_n = \sum_n (\boldsymbol{z}_n [\nabla \boldsymbol{z}_n]^\dagger \nabla) \boldsymbol{\xi}$, which implies the following analogue of equation (33)

$$\sum_{n=1}^{K} \mathcal{Q}_n = \mathsf{I}, \qquad \mathcal{Q}_n = \boldsymbol{z}_n [\nabla \boldsymbol{z}_n]^\dagger \nabla, \qquad \mathcal{Q}_l \mathcal{Q}_m = \mathcal{Q}_l \, \delta_{lm}, \tag{59}$$

where the matrices $\mathcal{Q}_n$, $n = 1, \ldots, K$, are self-adjoint with respect to the *discrete* inner-product $\langle \cdot, \cdot \rangle_{1,2}$ defined above, i.e., $\langle \mathcal{Q}_n \boldsymbol{\xi}, \boldsymbol{\zeta} \rangle_{1,2} = \langle \boldsymbol{\xi}, \mathcal{Q}_n \boldsymbol{\zeta} \rangle_{1,2}$ for all $\boldsymbol{\xi}, \boldsymbol{\zeta} \in \mathbb{C}^K$.

We now use equation (59) to prove the spectral theorem in (22) for this generalized eigenvalue problem setting. From $\mathsf{B} \boldsymbol{z}_n = \lambda_n \mathsf{C} \boldsymbol{z}_n$ and equation (59) we have that $\mathsf{B} \mathcal{Q}_n = \lambda_n \mathsf{C} \mathcal{Q}_n$ which is equivalent to $\mathsf{C}^{-1} \mathsf{B} \mathcal{Q}_n = \lambda_n \mathcal{Q}_n$, since the matrix C is invertible. As in the discussion following equation (33), the mutual orthogonality of the projection matrices $\mathcal{Q}_n$ implies that $f(\mathsf{C}^{-1} \mathsf{B}) = \sum_n f(\lambda_n) \mathcal{Q}_n$ for any polynomial $f : \mathbb{R} \mapsto \mathbb{C}$. From the mutual orthogonality of the projection matrices $\mathcal{Q}_n$ and their symmetry with respect to the discrete inner-product $\langle \cdot, \cdot \rangle_{1,2}$ it follows that, for all $\boldsymbol{\xi}, \boldsymbol{\zeta} \in \mathbb{C}^K$ and complex-valued polynomials $f(\lambda)$ and $h(\lambda)$, the bilinear functional $\langle f(\mathsf{C}^{-1} \mathsf{B}) \boldsymbol{\xi}, h(\mathsf{C}^{-1} \mathsf{B}) \boldsymbol{\zeta} \rangle_{1,2}$ has the integral representation in (22), with $\mathbf{M}$ substituted by $\mathsf{C}^{-1} \mathsf{B}$. Moreover, the complex-valued function $\mu_{\xi\zeta}(\lambda) = \langle \mathbf{Q}(\lambda) \boldsymbol{\xi}, \boldsymbol{\zeta} \rangle$ in (22) is now given by $\mu_{\xi\zeta}(\lambda) = \langle \mathcal{Q}(\lambda) \boldsymbol{\xi}, \boldsymbol{\zeta} \rangle_{1,2}$, where the associated matrix representation $\mathcal{Q}(\lambda)$ of the projection operator $\mathbf{Q}(\lambda)$ and the discrete spectral measure $\mathrm{d}\mu_{\xi\zeta}(\lambda)$ are given by the following analogue of equation (34)

$$\mathcal{Q}(\lambda) = \sum_{n: \lambda_n \leq \lambda} \theta(\lambda - \lambda_n) \mathcal{Q}_n, \qquad \mathrm{d}\mu_{\xi\zeta}(\lambda) = \sum_{n: \lambda_n \leq \lambda} \langle \delta_{\lambda_n}(\mathrm{d}\lambda)[\nabla \mathcal{Q}_n \boldsymbol{\xi} \cdot \nabla \boldsymbol{\zeta}] \rangle. \tag{60}$$

We now demonstrate that discrete representations of the functional formulas for S_{jk}^* and A_{jk}^* in equation (48) yield their associated integral representations in (28), involving the discrete spectral measure μ_{jk} in (60). From $A = \Delta^{-1}(\boldsymbol{\nabla} \cdot \mathsf{H} \boldsymbol{\nabla})$ and (56), the matrix representation of the functional formulas $\mathsf{S}_{jk}^* = \varepsilon(\delta_{jk} + \langle \chi_j, \chi_k \rangle_{1,2})$ and $\mathsf{A}_{jk}^* = \langle A \chi_j, \chi_k \rangle_{1,2}$ in equation (48) are given by

$$\mathsf{S}_{jk}^* = \varepsilon(\delta_{jk} + \langle \nabla \boldsymbol{\chi}_j \cdot \nabla \boldsymbol{\chi}_k \rangle) \quad \mathsf{A}_{jk}^* = \langle \nabla \mathsf{C}^{-1}[\imath \mathsf{B}] \boldsymbol{\chi}_j \cdot \nabla \boldsymbol{\chi}_k \rangle. \tag{61}$$

Moreover, the matrix representation of the cell problem $\varepsilon \Delta \chi_j + \boldsymbol{\nabla} \cdot \mathsf{H} \boldsymbol{\nabla} \chi_j = -u_j$, in (4), is given by

$$(\varepsilon \mathsf{C} + \imath \mathsf{B}) \boldsymbol{\chi}_j = \boldsymbol{u}_j, \tag{62}$$

where $\boldsymbol{u}_j$ is the discrete, vector representation of the jth component of the fluid velocity field u_j, for example. The matrix Z is invertible, as the generalized eigenvectors $\boldsymbol{z}_n$ form a basis for $\mathbb{C}^N$. Consequently, by equation (58) we have that $\mathsf{B} = \mathsf{Z}^{-\dagger}\Lambda\mathsf{Z}^{-1}$, $\mathsf{C} = \mathsf{Z}^{-\dagger}\mathsf{Z}^{-1}$. It now follows from equation (62) that $\mathsf{Z}^{-\dagger}(\varepsilon\mathsf{I} + \imath\Lambda)\mathsf{Z}^{-1}\boldsymbol{\chi}_j = \boldsymbol{u}_j$, or equivalently

$$\boldsymbol{\chi}_j = \mathsf{Z}(\varepsilon\mathsf{I} + \imath\Lambda)^{-1}\mathsf{Z}^{\dagger}\boldsymbol{u}_j. \tag{63}$$

Substituting the resolvent formula for $\boldsymbol{\chi}_j$ in (63) into equation (61) yields the following formula that is a direct analogue of equation (36)

$$\mathsf{S}_{jk}^* = \varepsilon(\delta_{jk} + \langle(\varepsilon\mathsf{I} + \imath\Lambda)^{-1}\mathsf{Z}^{\dagger}\boldsymbol{u}_j\cdot(\varepsilon\mathsf{I} + \imath\Lambda)^{-1}\mathsf{Z}^{\dagger}\boldsymbol{u}_k\rangle) \tag{64}$$
$$\mathsf{A}_{jk}^* = \langle\imath\Lambda(\varepsilon\mathsf{I} + \imath\Lambda)^{-1}\mathsf{Z}^{\dagger}\boldsymbol{u}_j\cdot(\varepsilon\mathsf{I} + \imath\Lambda)^{-1}\mathsf{Z}^{\dagger}\boldsymbol{u}_k\rangle,$$

where we have used that $[\nabla\mathsf{Z}]^{\dagger} = [\nabla\mathsf{Z}]^{-1}$. The quadratic form $\mathsf{Z}^{\dagger}\boldsymbol{u}_j\cdot\mathsf{Z}^{\dagger}\boldsymbol{u}_k$ arising in (64) can be written in terms of the projection matrices $\mathcal{Q}_n$ defined in (59) as follows. Analogous to equation (37), we have

$$\mathsf{Z}^{\dagger}\boldsymbol{u}_j\cdot\mathsf{Z}^{\dagger}\boldsymbol{u}_k = \sum_{n=1}^{N}\overline{(\boldsymbol{z}_n^{\dagger}\boldsymbol{u}_j)}(\boldsymbol{z}_n^{\dagger}\boldsymbol{u}_k) = \sum_{n=1}^{N}\boldsymbol{z}_n\boldsymbol{z}_n^{\dagger}\boldsymbol{u}_j\cdot\boldsymbol{u}_k. \tag{65}$$

We now demonstrate that $\boldsymbol{z}_n\boldsymbol{z}_n^{\dagger}\boldsymbol{u}_j\cdot\boldsymbol{u}_k = \nabla\mathcal{Q}_n\boldsymbol{g}_j\cdot\nabla\boldsymbol{g}_k$, where $\boldsymbol{g}_j = (\nabla^T\nabla)^{-1}\boldsymbol{u}_j$,

$$\boldsymbol{z}_n\boldsymbol{z}_n^{\dagger}\boldsymbol{u}_j\cdot\boldsymbol{u}_k = \boldsymbol{z}_n\boldsymbol{z}_n^{\dagger}[\nabla^T\nabla]\boldsymbol{g}_j\cdot[\nabla^T\nabla]\boldsymbol{g}_k = [\nabla\boldsymbol{z}_n][\nabla\boldsymbol{z}_n]^{\dagger}\nabla\boldsymbol{g}_j\cdot\nabla\boldsymbol{g}_k = \nabla\mathcal{Q}_n\boldsymbol{g}_j\cdot\nabla\boldsymbol{g}_k. \tag{66}$$

It follows from equations (65) and (66) that the functional formulas for S_{jk}^* and A_{jk}^* in (64) have the Stieltjes integral representations in equation (26), involving the discrete spectral measure μ_{jk} in (60) with $\boldsymbol{\xi} = \boldsymbol{g}_j = (\nabla^T\nabla)^{-1}\boldsymbol{u}_j$ and $\boldsymbol{\zeta} = \boldsymbol{g}_k = (\nabla^T\nabla)^{-1}\boldsymbol{u}_k$.

Exactly as in Section IV A, we may rewrite these integral representations for S_{jk}^* and A_{jk}^* in equation (26), involving the *complex measure* μ_{jk}, as the integral representations in equation (28) involving the real *signed measures* Re μ_{jk} and Im μ_{jk}. The associated real-valued functions Re $\mu_{jk}(\lambda)$ and Im $\mu_{jk}(\lambda)$ are given by equation (38) with $[(\mathsf{Q}_n + \overline{\mathsf{Q}}_n)\boldsymbol{g}_j\cdot\boldsymbol{g}_k]$ substituted by $[\nabla(\mathcal{Q}_n + \overline{\mathcal{Q}}_n)\boldsymbol{g}_j\cdot\nabla\boldsymbol{g}_k]$. Furthermore, due to the generalized eigenvalues and eigenvectors of the antisymmetric matrix $\imath\mathsf{M} = \nabla^T\mathsf{H}\nabla$ coming in complex conjugate pairs, the discrete measure μ_{jk} depends only on a subset of the index set of the sums in (65) and satisfy equation (39), with $[\mathsf{Q}_n\boldsymbol{g}_j\cdot\boldsymbol{g}_k]$ substituted by $[\nabla\mathcal{Q}_n\boldsymbol{g}_j\cdot\nabla\boldsymbol{g}_k]$.

VII.   DISCRETE EQUIVALENCE OF THE EFFECTIVE PARAMETER PROBLEMS

In Section III, we formulated an effective parameter problem for the effective diffusivity tensor D^* associated with an incompressible fluid velocity field. The discrete version of this effective parameter problem was formulated in Section IV. An alternate approach to the effective parameter problem was formulated in Section V, and its discrete version was formulated in Section VI. In this section, we demonstrate that the discrete versions of these effective parameter problems yield equivalent spectral representations of D^* when the matrix ∇ is of full rank, so that the matrix Laplacian is invertible.

Let $\nabla = \mathsf{U}\Sigma\mathsf{V}^T$ be the singular value decomposition (SVD) of the matrix ∇ of size $N \times K$, say, where $N > K$. Here, $\Sigma = \mathrm{diag}(\sigma_1, \ldots, \sigma_K)$, where $0 \leq \sigma_1 \leq \cdots \leq \sigma_K$, and the matrices U and V are of size $N \times K$ and $K \times K$, respectively, and satisfy [13]

$$\mathsf{U}^T\mathsf{U} = \mathsf{I}, \quad \mathsf{V}^T\mathsf{V} = \mathsf{V}\mathsf{V}^T = \mathsf{I}, \tag{67}$$

where I is the $K \times K$ identity matrix. The columns of U are called left singular vectors, the columns of V are called right singular vectors, and the σ_i are called singular values.

It follows from $\nabla = \mathsf{U}\Sigma\mathsf{V}^T$ and equation (67) that the spectral decomposition of the negative matrix Laplacian $\nabla^T\nabla$ is given by $\nabla^T\nabla = \mathsf{V}\Sigma^2\mathsf{V}^T$ [13]. We assume that ∇ is of full rank so that $\sigma_i > 0$ for all $i = 1, \ldots, K$. This implies that Σ^{-1} exists so that the matrix Laplacian is invertible. In this case, it follows from $\nabla = \mathsf{U}\Sigma\mathsf{V}^T$ and equation (67) that the projection matrix $\Gamma = \nabla(\nabla^T\nabla)^{-1}\nabla^T$ is given by

$$\Gamma = \mathsf{U}\mathsf{U}^T, \tag{68}$$

which is a $N \times N$ symmetric projection matrix satisfying $\Gamma^2 = \Gamma$ and $\Gamma\nabla = \nabla$ (see equation (67)). A key property of the SVD of the *full rank* matrix ∇ is that its range is spanned by the columns of U [13], hence $\Gamma = \mathsf{U}\mathsf{U}^T$ projects subspaces of $\mathbb{R}^N$ onto the range of ∇.

From equations (67) and (68), we can write the eigenvalue problem $-\imath\Gamma\mathsf{H}\Gamma\boldsymbol{w}_n = \lambda_n\boldsymbol{w}_n$ discussed in Section IV A as

$$[-\imath\mathsf{U}^T\mathsf{H}\mathsf{U}][\mathsf{U}^T\boldsymbol{w}_n] = \lambda_n[\mathsf{U}^T\boldsymbol{w}_n]. \tag{69}$$

Now consider the generalized eigenvalue problem $-\imath\nabla^T\mathsf{H}\nabla\boldsymbol{z}_n = \alpha_n\nabla^T\nabla\boldsymbol{z}_n$ discussed in Section VI and recall that $\nabla = \mathsf{U}\Sigma\mathsf{V}^T$ and $\nabla^T\nabla = \mathsf{V}\Sigma^2\mathsf{V}^T$. Since Σ is invertible, by

equation (67), we can write this generalized eigenvalue problem as the following standard eigenvalue problem

$$[-\imath \mathsf{U}^T \mathsf{H} \mathsf{U}][\Sigma \mathsf{V}^T \boldsymbol{z}_n] = \alpha_n [\Sigma \mathsf{V}^T \boldsymbol{z}_n]. \tag{70}$$

Comparing the formulas in equations (69) and (70) indicates that spectrum associated with each of these eigenvalue problems is identical, $\alpha_n = \lambda_n$, and that the eigenvectors are related by $\mathsf{U}^T \boldsymbol{w}_n = \Sigma \mathsf{V}^T \boldsymbol{z}_n$. Since Γ is a projection matrix, $\Gamma^2 = \Gamma$, the eigenvalue problem $\Gamma \mathsf{H} \Gamma \boldsymbol{w}_n = \imath \lambda_n \boldsymbol{w}_n$ can be written as $\Gamma \mathsf{H} \Gamma [\Gamma \boldsymbol{w}_n] = \imath \lambda_n [\Gamma \boldsymbol{w}_n]$, which implies that $\Gamma \boldsymbol{w}_n = \boldsymbol{w}_n$. Consequently, applying the matrix U to both sides of the formula $\mathsf{U}^T \boldsymbol{w}_n = \Sigma \mathsf{V}^T \boldsymbol{z}_n$ and recalling that $\Gamma = \mathsf{U}\mathsf{U}^T$ and $\nabla = \mathsf{U}\Sigma \mathsf{V}^T$ we have

$$\boldsymbol{w}_n = \nabla \boldsymbol{z}_n. \tag{71}$$

In the following lemma we make precise the correspondence between the standard eigenvalue problem $-\imath \Gamma \mathsf{H} \Gamma \boldsymbol{w}_n = \lambda_n \boldsymbol{w}_n$ and the generalized eigenvalue problem $-\imath \nabla^T \mathsf{H} \nabla \boldsymbol{z}_n = \alpha_n \nabla^T \nabla \boldsymbol{z}_n$, as well as the associated spectral measures in equations (34) and (60), respectively.

Lemma 1 *Consider the standard eigenvalue problem and the generalized eigenvalue problem given, respectively, in equations (72) and (73) below*

$$-\imath \Gamma \mathsf{H} \Gamma \boldsymbol{w}_n = \lambda_n \boldsymbol{w}_n, \tag{72}$$

$$-\imath \nabla^T \mathsf{H} \nabla \boldsymbol{z}_n = \lambda_n \nabla^T \nabla \boldsymbol{z}_n. \tag{73}$$

Let $\nabla = \mathsf{U}\Sigma \mathsf{V}^T$ be the SVD of the matrix ∇, which we assume to be of full rank. Then equation (72) implies and is implied by equation (73), with $\boldsymbol{w}_n$ and $\boldsymbol{z}_n$ related as in equation (71). This implies that the spectrum associated with each of these eigenvalue problems is identical. Moreover, the spectral weights in equations (37) and (66) are identical, i.e.,

$$\mathcal{Q}_n \Gamma \mathsf{H} \boldsymbol{e}_j \cdot \Gamma \mathsf{H} \boldsymbol{e}_k = \nabla \mathcal{Q}_n [\nabla^T \nabla]^{-1} \boldsymbol{u}_j \cdot \nabla [\nabla^T \nabla]^{-1} \boldsymbol{u}_k. \tag{74}$$

This, in turn, implies that the associated spectral measures in equations (34) and (60) are identical for all $\boldsymbol{\xi}, \boldsymbol{\zeta} \in \mathbb{C}^N$.

Proof of Lemma 1

Recall that $\nabla = \mathsf{U}\Sigma \mathsf{V}^T$, $\nabla^T \nabla = \mathsf{V}\Sigma^2 \mathsf{V}^T$, and $\Gamma = \mathsf{U}\mathsf{U}^T$, where Σ is invertible, and the matrices V and U satisfy equation (67). First consider equation (72) written as in equation (69),

$[-\imath \mathsf{U}^T \mathsf{H} \mathsf{U}][\mathsf{U}^T \boldsymbol{w}_n] = \lambda_n [\mathsf{U}^T \boldsymbol{w}_n]$. Since the matrix Σ is invertible and $\mathsf{V}^T \mathsf{V} = \mathsf{I}$, we can rewrite equation (69) as

$$\mathsf{V}\Sigma[-\imath \mathsf{U}^T \mathsf{H}\mathsf{U}](\Sigma\mathsf{V}^T)(\mathsf{V}\Sigma^{-1})[\mathsf{U}^T \boldsymbol{w}_n] = \lambda_n(\mathsf{V}\Sigma^2\mathsf{V}^T)(\mathsf{V}\Sigma^{-1})[\mathsf{U}^T \boldsymbol{w}_n], \qquad (75)$$

which is precisely equation (73) written in terms of $\nabla = \mathsf{U}\Sigma\mathsf{V}^T$ with $\boldsymbol{z}_n = \mathsf{V}\Sigma^{-1}\mathsf{U}^T \boldsymbol{w}_n$. This formula for $\boldsymbol{z}_n$, equation (67), and the formula $\Gamma\boldsymbol{w}_n = \boldsymbol{w}_n$ above equation (71) imply that $\boldsymbol{w}_n = \mathsf{U}\Sigma\mathsf{V}^T \boldsymbol{z}_n = \nabla\boldsymbol{z}_n$. Now consider equation (73) written as in (70), $[-\imath \mathsf{U}^T \mathsf{H}\mathsf{U}][\Sigma\mathsf{V}^T \boldsymbol{z}_n] = \lambda_n[\Sigma\mathsf{V}^T \boldsymbol{z}_n]$. Since $\mathsf{U}^T \mathsf{U} = \mathsf{I}$, we can rewrite equation (70) as

$$\mathsf{U}[-\imath \mathsf{U}^T \mathsf{H}\mathsf{U}](\mathsf{U}^T \mathsf{U})[\Sigma\mathsf{V}^T \boldsymbol{z}_n] = \lambda_n \mathsf{U}[\Sigma\mathsf{V}^T \boldsymbol{z}_n], \qquad (76)$$

which is precisely (72) written in terms of $\Gamma = \mathsf{U}\mathsf{U}^T$ with $\boldsymbol{w}_n = \mathsf{U}\Sigma\mathsf{V}^T \boldsymbol{z}_n = \nabla\boldsymbol{z}_n$.

We now establish equation (74). From the formula $\boldsymbol{u} = \boldsymbol{\nabla}\!\cdot\!\mathsf{H}$ in (8), we have that $u_j = \boldsymbol{\nabla}\!\cdot\!\mathsf{H}\boldsymbol{e}_j$. Since $\nabla = \mathsf{U}\Sigma\mathsf{V}^T$, the discrete version of this formula is given by

$$\boldsymbol{u}_j = -\nabla^T \mathsf{H}\boldsymbol{e}_j = -\mathsf{V}\Sigma\mathsf{U}^T \mathsf{H}\boldsymbol{e}_j. \qquad (77)$$

From $\nabla = \mathsf{U}\Sigma\mathsf{V}^T$ and $(\nabla^T\nabla)^{-1} = \mathsf{V}\Sigma^{-2}\mathsf{V}^T$ we have $\nabla(\nabla^T\nabla)^{-1} = \mathsf{U}\Sigma^{-1}\mathsf{V}^T$. Consequently, $\Gamma = \mathsf{U}\mathsf{U}^T$, and equations (67) and (77), yield $-\Gamma\mathsf{H}\boldsymbol{e}_j = \nabla(\nabla^T\nabla)^{-1}\boldsymbol{u}_j$. Equation (74) now follows from the formula $\boldsymbol{w}_n = \nabla\boldsymbol{z}_n$ in (71)

$$\begin{aligned}
\boldsymbol{w}_n\boldsymbol{w}_n^\dagger \nabla(\nabla^T\nabla)^{-1}\boldsymbol{u}_j\!\cdot\!\nabla(\nabla^T\nabla)^{-1}\boldsymbol{u}_k &= [(\nabla^T\nabla)^{-1}\nabla^T \boldsymbol{w}_n][(\nabla^T\nabla)^{-1}\nabla^T \boldsymbol{w}_n]^\dagger \boldsymbol{u}_j\!\cdot\!\boldsymbol{u}_k \\
&= [(\nabla^T\nabla)^{-1}\nabla^T\nabla\boldsymbol{z}_n][(\nabla^T\nabla)^{-1}\nabla^T\nabla\boldsymbol{z}_n]^\dagger \boldsymbol{u}_j\!\cdot\!\boldsymbol{u}_k \\
&= \boldsymbol{z}_n\boldsymbol{z}_n^\dagger \boldsymbol{u}_j\!\cdot\!\boldsymbol{u}_k, \qquad (78)
\end{aligned}$$

where we have used that the inverse of a symmetric matrix is also symmetric [22]. The equivalence of equations (74) and (78) now follows from equations (33), (59), and (66). This concludes our proof of Lemma 1 $\square$.

We conclude this section with a discussion regarding numerical computations of the effective diffusivity D^*. The approach discussed in this section and the projection method discussed in Section IV B combine the computational advantages of the methods discussed in Sections IV A and VI. More specifically, in the full rank setting, the spectral measure underlying the discrete integral representation for D^* was calculated in Section IV A in terms of the *standard* eigenvalue problem $-\imath\Gamma\mathsf{H}\Gamma\boldsymbol{w}_m = \lambda_n\boldsymbol{w}_n$, where the matrix $-\imath\Gamma\mathsf{H}\Gamma$ is of size $N \times N$. In Section VI, D^* was calculated in terms of the *generalized* eigenvalue

problem $-\imath \nabla^T \mathsf{H} \nabla \boldsymbol{z}_n = \lambda_n \nabla^T \nabla \boldsymbol{z}_n$, involving the $K \times K$ matrices $-\imath \nabla^T \mathsf{H} \nabla$ and $\nabla^T \nabla$. Since $\nabla^T = (\nabla_1^T, \ldots, \nabla_d^T)$ is of size $K \times N$ we have that $K = N/d$. However, the generalized eigenvalue problem is more computationally intensive than the standard eigenvalue problem [40]. For the case of randomly perturbed flows, these are not efficient ways to compute spectral statistics for D^*.

The projection method developed in Section IV B demonstrates that, by first computing the standard eigenvalue decomposition of the non-random matrix Γ, the spectral statistics of the eigenvalue problem $-\imath \Gamma \mathsf{H} \Gamma \boldsymbol{w}_n = \lambda_n \boldsymbol{w}_n$ can then be obtained by repeatedly computing the standard eigenvalue decomposition of smaller matrices. They are of size $K \times K$ by equations (40), (41), and (68). We stress that K and N_1 both denote the rank of the matrix Γ in this section and in Section IV B, respectively, i.e., $K = N_1$. Note that computing the matrix $\Gamma = \nabla (\nabla^T \nabla)^{-1} \nabla^T$ involves numerically solving N linear systems of size $K \times K$. Alternatively, the proof of Lemma 1 illustrates that by first computing the SVD of the matrix gradient, $\nabla = \mathsf{U} \Sigma \mathsf{V}^T$, the spectral statistics of the generalized eigenvalue problem $-\imath \nabla^T \mathsf{H} \nabla \boldsymbol{z}_n = \lambda_n \nabla^T \nabla \boldsymbol{z}_n$ can then be obtained by repeatedly computing the standard eigenvalue decomposition of the matrix $-\imath \mathsf{U}^T \mathsf{H} \mathsf{U}$ which is of size $K \times K$. When N is large, these equivalent methods are more numerically efficient than the other approaches discussed in Sections IV A and VI.

In Section VIII, we generalize Lemma 1 to the case where ∇ has rank K_1 with $K_1 < K$, demonstrating that the two formulations yield equivalent spectral representations of the effective diffusivity tensor D^* in the this rank deficient setting. Moreover, we demonstrate that, by first computing the SVD of the matrix gradient, D^* can be computed via a *standard* eigenvalue problem for matrices of size $K_1 \times K_1$. Consequently, the rank deficiency of the problem actually increases the numerical efficiency of computations.

VIII. RANK DEFICIENCY AND A UNIFYING STANDARD EIGENVALUE PROBLEM

In Sections IV and VI we provided two discrete, matrix formulations of the effective parameter problem for the effective diffusivity tensor D^*. These two formulations assume that the $N \times K$ matrix ∇ is of full rank K so that the negative matrix Laplacian $\nabla^T \nabla$ is invertible. Lemma 1 shows that, given this condition, the two formulations yield equivalent

spectral representations of D^*. In this section, we generalize Lemma 1 to the case where ∇ has rank K_1 with $K_1 < K$, again demonstrating that the two formulations are equivalent in this rank deficient setting. This framework is used in Section IX to compute D^* for periodic flows, for which the matrix ∇ with periodic boundary conditions is rank deficient.

Consider the cell problem in (4) written, via (8) and $[\boldsymbol{\nabla}{\cdot}\mathsf{H}]{\cdot}\boldsymbol{\nabla}\varphi = \boldsymbol{\nabla}{\cdot}[\mathsf{H}\boldsymbol{\nabla}\varphi]$, as

$$\boldsymbol{\nabla}{\cdot}\mathsf{H}\boldsymbol{\nabla}\chi_j + \varepsilon\Delta\chi_j = -u_j. \tag{79}$$

Discretizing equation (79) yields (see Section IV A for details)

$$\nabla^T\mathsf{H}\nabla\boldsymbol{\chi}_j + \varepsilon\nabla^T\nabla\boldsymbol{\chi}_j = \boldsymbol{u}_j, \tag{80}$$

where $\boldsymbol{u}_j$ is the discrete, vector representation of the jth component of the fluid velocity field u_j, and similarly for $\boldsymbol{\chi}_j$. Substituting the formula for $\boldsymbol{u}_j$ in (80) into the discrete version $D_{jk}^* = \varepsilon\delta_{jk} + \langle\boldsymbol{u}_j{\cdot}\boldsymbol{\chi}_k\rangle$ of equation (3) yields

$$D_{jk}^* = \mathsf{S}_{jk}^* + \mathsf{A}_{jk}^*, \qquad \mathsf{S}_{jk}^* = \varepsilon(\delta_{jk} + \langle\nabla^T\nabla\boldsymbol{\chi}_j{\cdot}\boldsymbol{\chi}_k\rangle), \quad \mathsf{A}_{jk}^* = \langle\nabla^T\mathsf{H}\nabla\boldsymbol{\chi}_j{\cdot}\boldsymbol{\chi}_k\rangle, \tag{81}$$

where, as before, $\mathsf{S}_{kj}^* = \mathsf{S}_{jk}^*$ and $\mathsf{A}_{kj}^* = -\mathsf{A}_{jk}^*$.

We first work with equation (80) directly and develop a mathematical framework which parallels the framework of Section VI. We then transform equation (80) into a discrete analogue of equation (18) written as $(\varepsilon\mathsf{I} + \Gamma\mathsf{H}\Gamma)\nabla\boldsymbol{\chi}_j = -\Gamma\mathsf{H}\boldsymbol{e}_j$, with a suitable generalization of the formula for the matrix Γ in (68), and develop a mathematical framework which parallels the framework of Section IV. We then generalize Lemma 1 of Section VII, establishing the equivalence of these two formulations for the rank deficient setting.

Let $\nabla = \mathsf{U}\Sigma\mathsf{V}^T$ be the SVD of the $N \times K$ matrix ∇ discussed in Section VII. We assume that ∇ is rank deficient so that $\nabla^T\nabla = \mathsf{V}\Sigma^2\mathsf{V}^T$ is singular, with K_1 non-zero eigenvalues and $K_0 = K - K_1$ zero eigenvalues, and write

$$\mathsf{U} = [\mathsf{U}_0\ \mathsf{U}_1], \quad \Sigma = \begin{bmatrix} \mathsf{O}_{00} & \mathsf{O}_{01} \\ \mathsf{O}_{10} & \Sigma_1 \end{bmatrix}, \quad \mathsf{V} = [\mathsf{V}_0\ \mathsf{V}_1]. \tag{82}$$

Here, O_{ab} are matrices of zeros of size $K_a \times K_b$, $a, b = 0, 1$, U_a is $N \times K_a$, V_a is $K \times K_a$, and Σ_1 is a $K_1 \times K_1$ diagonal, *invertible* matrix. By equation (67) the matrices U_1 and V_1 satisfy

$$\mathsf{U}_1^T\mathsf{U}_1 = \mathsf{I}_1, \quad \mathsf{V}_1^T\mathsf{V}_1 = \mathsf{I}_1, \tag{83}$$

where I_1 is the $K_1 \times K_1$ identity matrix. An important property of the SVD of the matrix ∇ is that its null space is spanned by the columns of V_0 and its range is spanned by the columns of U_1 [13].

Due to the blocks of zeros of Σ in (82), the matrix elements of ∇ and $\nabla^T \nabla$ do not depend on U_0 nor V_0 and can be written as $\nabla = \mathsf{U}_1 \Sigma_1 \mathsf{V}_1^T$ and $\nabla^T \nabla = \mathsf{V}_1 \Sigma_1^2 \mathsf{V}_1^T$. Consequently, equation (80) can be rewritten as

$$[\mathsf{V}_1 \Sigma_1][\mathsf{U}_1^T \mathsf{H} \mathsf{U}_1][\Sigma_1 \mathsf{V}_1^T]\boldsymbol{\chi}_j + \varepsilon \mathsf{V}_1 \Sigma_1^2 \mathsf{V}_1^T \boldsymbol{\chi}_j = \boldsymbol{u}_j. \tag{84}$$

Since the $K_1 \times K_1$ matrix $\mathsf{U}_1^T \mathsf{H} \mathsf{U}_1$ is antisymmetric, it has the spectral decomposition $\mathsf{U}_1^T \mathsf{H} \mathsf{U}_1 = \imath \mathsf{R}_1 \Lambda_1 \mathsf{R}_1^\dagger$, where Λ_1 is a diagonal, real-valued matrix and R_1 is a unitary matrix, $\mathsf{R}_1^\dagger \mathsf{R}_1 = \mathsf{R}_1 \mathsf{R}_1^\dagger = \mathsf{I}_1$. It follows that

$$\nabla^T \mathsf{H} \nabla = \imath [\mathsf{V}_1 \Sigma_1 \mathsf{R}_1] \Lambda_1 [\mathsf{V}_1 \Sigma_1 \mathsf{R}_1]^\dagger, \quad \nabla^T \nabla = [\mathsf{V}_1 \Sigma_1 \mathsf{R}_1][\mathsf{V}_1 \Sigma_1 \mathsf{R}_1]^\dagger. \tag{85}$$

Consequently, equation (84) can be rewritten as $[\mathsf{V}_1 \Sigma_1 \mathsf{R}_1](\varepsilon \mathsf{I}_1 + \imath \Lambda_1)[\mathsf{V}_1 \Sigma_1 \mathsf{R}_1]^\dagger \boldsymbol{\chi}_j = \boldsymbol{u}_j$. This formula and equation (83) together imply the following analogue of equation (63)

$$\mathsf{V}_1^T \boldsymbol{\chi}_j = \mathsf{V}_1^T \mathsf{Z}_1 (\varepsilon \mathsf{I}_1 + \imath \Lambda_1)^{-1} \mathsf{Z}_1^\dagger \boldsymbol{u}_j, \qquad \mathsf{Z}_1 = \mathsf{V}_1 \Sigma_1^{-1} \mathsf{R}_1. \tag{86}$$

Substituting equation (86) into the functionals $\langle \nabla^T \nabla \boldsymbol{\chi}_j \cdot \boldsymbol{\chi}_k \rangle$ and $\langle \nabla^T \mathsf{H} \nabla \boldsymbol{\chi}_j \cdot \boldsymbol{\chi}_k \rangle$ in equation (81) yields the following analogue of (64) (see Appendix B for details)

$$\mathsf{S}_{jk}^* = \varepsilon(\delta_{jk} + \langle (\varepsilon \mathsf{I}_1 + \imath \Lambda_1)^{-1} \mathsf{Z}_1^\dagger \boldsymbol{u}_j \cdot (\varepsilon \mathsf{I}_1 + \imath \Lambda_1)^{-1} \mathsf{Z}_1^\dagger \boldsymbol{u}_k \rangle), \tag{87}$$
$$\mathsf{A}_{jk}^* = \langle \imath \Lambda_1 (\varepsilon \mathsf{I}_1 + \imath \Lambda_1)^{-1} \mathsf{Z}_1^\dagger \boldsymbol{u}_j \cdot (\varepsilon \mathsf{I}_1 + \imath \Lambda_1)^{-1} \mathsf{Z}_1^\dagger \boldsymbol{u}_k \rangle.$$

The quadratic form $\mathsf{Z}_1^\dagger \boldsymbol{u}_j \cdot \mathsf{Z}_1^\dagger \boldsymbol{u}_k$ arising in (87) yields the following analogue of (65)

$$\mathsf{Z}_1^\dagger \boldsymbol{u}_j \cdot \mathsf{Z}_1^\dagger \boldsymbol{u}_k = \sum_{n=1}^{K_1} \overline{([\boldsymbol{z}_n^1]^\dagger \boldsymbol{u}_j)}([\boldsymbol{z}_n^1]^\dagger \boldsymbol{u}_k) = \sum_{n=1}^{K_1} [\boldsymbol{z}_n^1][\boldsymbol{z}_n^1]^\dagger \boldsymbol{u}_j \cdot \boldsymbol{u}_k, \qquad \boldsymbol{z}_n^1 = \mathsf{V}_1 \Sigma_1^{-1} \boldsymbol{r}_n^1, \tag{88}$$

where $\boldsymbol{r}_n^1$, $n = 1, \ldots, K_1$, are the orthonormal eigenvectors of the matrix $\mathsf{U}_1^T \mathsf{H} \mathsf{U}_1$ which comprise the columns of R_1. From $\nabla = \mathsf{U}_1 \Sigma_1 \mathsf{V}_1^T$ and equations (83) and (88) we have that $\nabla \boldsymbol{z}_n^1 = \mathsf{U}_1 \boldsymbol{r}_n^1$. The orthogonality condition $\boldsymbol{r}_n^1 \cdot \boldsymbol{r}_n^1 = \delta_{nm}$ and equation (83) then imply that the vectors $\boldsymbol{z}_n^1$ satisfy the Sobolev-type orthogonality condition in equation (57), $\nabla \boldsymbol{z}_n^1 \cdot \nabla \boldsymbol{z}_m^1 = \delta_{nm}$. Moreover, since $\sum_n \boldsymbol{r}_n^1 [\boldsymbol{r}_n^1]^\dagger = I_1$, as the vectors $\boldsymbol{r}_n^1$ form an orthonormal basis for $\mathbb{C}^{K_1}$, we also have the following generalization of equation (59)

$$\sum_{n=1}^{K_1} \mathcal{Q}_n^1 = \mathsf{V}_1 \mathsf{V}_1^T, \qquad \mathcal{Q}_n^1 = \boldsymbol{z}_n^1 [\nabla \boldsymbol{z}_n^1]^\dagger \nabla, \qquad \mathcal{Q}_l^1 \mathcal{Q}_m^1 = \mathcal{Q}_l^1 \delta_{lm}, \tag{89}$$

where the matrices $\mathcal{Q}_n^1$, $n = 1, \ldots, K_1$, are self-adjoint with respect to the *discrete* inner-product $\langle \cdot, \cdot \rangle_{1,2}$ defined by $\langle \boldsymbol{\xi}, \boldsymbol{\zeta} \rangle_{1,2} = \langle \nabla \boldsymbol{\xi} \cdot \nabla \boldsymbol{\zeta} \rangle$, i.e., $\langle \mathcal{Q}_n^1 \boldsymbol{\xi}, \boldsymbol{\zeta} \rangle_{1,2} = \langle \boldsymbol{\xi}, \mathcal{Q}_n^1 \boldsymbol{\zeta} \rangle_{1,2}$ for $\boldsymbol{\xi}, \boldsymbol{\zeta} \in \mathbb{C}^{K_1}$.

It follows from equations (87) and (88) that

$$\mathsf{S}_{jk}^* / \varepsilon - \delta_{jk} = \sum_{n=1}^{K_1} \frac{\mathrm{Re}\left[\overline{([\boldsymbol{z}_n^1]^\dagger \boldsymbol{u}_j)}([\boldsymbol{z}_n^1]^\dagger \boldsymbol{u}_k)\right]}{\varepsilon^2 + [\lambda_n^1]^2}, \qquad \mathsf{A}_{jk}^* = \sum_{n=1}^{K_1} \frac{\lambda_n^1 \mathrm{Im}\left[\overline{([\boldsymbol{z}_n^1]^\dagger \boldsymbol{u}_j)}([\boldsymbol{z}_n^1]^\dagger \boldsymbol{u}_k)\right]}{\varepsilon^2 + [\lambda_n^1]^2}, \quad (90)$$

where λ_n^1, $n = 1, \ldots, K_1$, are the eigenvalues of the matrix $-\imath \mathsf{U}_1^T \mathsf{H} \mathsf{U}_1$ corresponding to the eigenvectors $\boldsymbol{r}_n^1$. Here, as in equation (28), we have used the fact that the matrices ∇ and H, as well as the vectors $\boldsymbol{\chi}_1$ and $\boldsymbol{u}_j$, and the molecular diffusivity ε are real valued, so that $\langle \nabla \boldsymbol{\chi}_j \cdot \nabla \boldsymbol{\chi}_k \rangle = \langle \nabla \boldsymbol{\chi}_k \cdot \nabla \boldsymbol{\chi}_j \rangle$ and $\langle \nabla^T \mathsf{H} \nabla \boldsymbol{\chi}_j \cdot \boldsymbol{\chi}_k \rangle = \langle \boldsymbol{\chi}_k \cdot \nabla^T \mathsf{H} \nabla \boldsymbol{\chi}_j \rangle$. Due to the eigenvalues and eigenvectors of the antisymmetric matrix $\mathsf{U}_1^T \mathsf{H} \mathsf{U}_1$ coming in complex conjugate pairs, as in equations (38) and (39), the sums in (90) depend only on a subset of the index set.

We now argue that the mathematical framework developed in equations (80)–(90) generalizes the full rank case in Section VI. Indeed, in the full rank setting, the matrix $\mathsf{V}_1 = \mathsf{V}$ is orthogonal, $\Sigma_1 = \Sigma$ is invertible, and $\mathsf{R}_1 = \mathsf{R}$ is orthogonal, so that the matrix $\mathsf{Z}_1 = \mathsf{Z}$ defined in (86) is given by

$$\mathsf{Z} = \mathsf{V} \Sigma^{-1} \mathsf{R}, \qquad (91)$$

and is invertible with $\mathsf{Z}^{-1} = \mathsf{R}^\dagger \Sigma \mathsf{V}^T$ and satisfies $\mathsf{Z}^{-1} \mathsf{Z} = \mathsf{Z} \mathsf{Z}^{-1} = \mathsf{I}$. Consequently, equation (85) implies that equation (58) is satisfied with $\Lambda_1 = \Lambda$. In this case, equations (63)–(65) are identical to equations (86)–(88), respectively.

We now generalize the mathematical framework developed in Section IV to the case that the matrix ∇ is rank deficient. Using equation (83) and the invertibility of the matrix Σ_1, we can rewrite equation (84) as

$$\mathsf{U}_1 [\mathsf{U}_1^T \mathsf{H} \mathsf{U}_1][\mathsf{U}_1^T \mathsf{U}_1][\Sigma_1 \mathsf{V}_1^T] \boldsymbol{\chi}_j + \varepsilon \mathsf{U}_1 \Sigma_1 \mathsf{V}_1^T \boldsymbol{\chi}_j = \mathsf{U}_1 \Sigma_1^{-1} \mathsf{V}_1^T \boldsymbol{u}_j. \qquad (92)$$

Substituting the formula $\boldsymbol{u}_j = -\nabla^T \mathsf{H} \boldsymbol{e}_j$ of (77) into equation (92) and using $\nabla = \mathsf{U}_1 \Sigma_1 \mathsf{V}_1^T$ yields

$$\left(\varepsilon \mathsf{I} + \Gamma_1 \mathsf{H} \Gamma_1\right) \nabla \boldsymbol{\chi}_j = \boldsymbol{g}_j^1, \qquad \Gamma_1 = \mathsf{U}_1 \mathsf{U}_1^T, \quad \boldsymbol{g}_j^1 = -\Gamma_1 \mathsf{H} \boldsymbol{e}_j, \qquad (93)$$

which analogous to equation (18). As in Section VII, the matrix $\Gamma_1 = \mathsf{U}_1 \mathsf{U}_1^T$ projects subspaces of $\mathbb{R}^N$ onto the *range* of ∇. Since the matrix $\Gamma_1 \mathsf{H} \Gamma_1$ is antisymmetric, it has

the spectral decomposition $\Gamma_1 H \Gamma_1 = \imath W_1 \tilde{\Lambda} W_1^\dagger$, where W_1 is a unitary matrix $W_1^\dagger W_1 = W_1 W_1^\dagger = I$. This and equation (93) yield the resolvent formula for $\nabla \chi_j$ in (35), with corresponding notational changes. In equation (81), write $\langle \nabla^T \nabla \chi_j \cdot \chi_k \rangle = \langle \nabla \chi_j \cdot \nabla \chi_k \rangle$ and $\langle \nabla^T H \nabla \chi_j \cdot \chi_k \rangle = \langle \Gamma_1 H \Gamma_1 \nabla \chi_j \cdot \nabla \chi_k \rangle$, where the second formula follows from $U_1^T U_1 = I_1$ and $\nabla = U_1 \Sigma_1 V_1$ which imply that $\Gamma_1 \nabla = \nabla$. Exactly as in Section IV A, this leads to equations (36) and (37), with corresponding notational changes. This, in turn, leads to the integral representations for S_{jk}^* and A_{jk}^* in equation (28), involving a discrete spectral measure μ_{jk} associated with the function $\mu_{jk}(\lambda) = \langle Q^1(\lambda) g_j^1 \cdot g_j^1 \rangle$, defined by (34) with $Q(\lambda)$ and Q_n substituted by $Q^1(\lambda)$ and Q_n^1, respectively, where $Q_n^1 = [w_n^1][w_n^1]^\dagger$ and w_n^1, $n = 1, \ldots, K_1$, are the eigenvectors of the matrix $\Gamma_1 H \Gamma_1$ which comprise the columns of W_1. In the case that the matrix ∇ is of full rank, we have $U_1 = U$ hence $W_1 = W$. This establishes that the mathematical framework discussed in this paragraph reduces to the mathematical framework in Section IV for the full rank setting and therefore is a generalization.

We now employ the projection method developed in Section IV B to generalize the mathematical framework in Section VII to the rank deficient setting, establishing the equivalence of the two approaches that follow from equations (84) and (93). We stress that the matrix Γ_1 defined in this section is identical to the matrix Γ defined in Section IV B, $\Gamma_1 = \Gamma$, which were given different notations to clarify our discussion here.

Since $\Gamma_1 = U_1 U_1^T$ is a projection matrix, the projection method discussed in Section IV B can be directly applied to equation (93). However, the mathematical framework developed here provides deeper insight into equation (41) of the method. In particular, in Section IV B we wrote $\Gamma = PGP^T$, where P is an orthogonal matrix consisting of the eigenvectors of Γ and the matrix G is defined in equation (41). Moreover, we wrote $P = [P_0 \; P_1]$, where the columns of the matrices P_0 and P_1 are orthonormal eigenvectors that span the null space and range of Γ, respectively. Since the eigenvalues γ_n associated with the eigenvectors in the matrix P_1 satisfy $\gamma_n = 1$, any linear combination of the corresponding eigenvectors is also an eigenvector of Γ with eigenvalue $\gamma_n = 1$. Therefore, since the orthonormal columns of the matrix U_1 span the range of $\Gamma_1 = U_1 U_1^T$, without loss of generality, we may take $P_1 = U_1$ so that $P = [P_0 \; U_1]$. Consequently, we can rewrite equation (42) as

$$U_1^T H U_1 = \imath R_{11} \Lambda_{11} R_{11}^\dagger. \tag{94}$$

From equation (94) and the comment after equation (84), we have that $R_{11} = R_1$ and

$\Lambda_{11} = \Lambda_1$. This and equation (43) establishes that the spectra associated with each of the two approaches are identical. We now establish that the spectral weights associated with both approaches are also identical. From the formula $P = [P_0 \ U_1]$ and equation (43) with $R_{11} = R_1$ and W redefined as W_1, we have that $W_1 = PR = [P_0 \ \ U_1 R_1]$. Consequently, from $\nabla = U_1 \Sigma_1 V_1^T$, equation (83), and the formula $Z_1 = V_1 \Sigma_1^{-1} R_1$ in (86), we have that $\nabla Z_1 = U_1 R_1$, which implies the following generalization of equation (71)

$$W_1 = [P_0 \ \nabla Z_1], \qquad \nabla Z_1 = U_1 R_1. \tag{95}$$

It now follows from $\Gamma_1 P_0 = O$, $\Gamma_1 \nabla = \nabla$, and the formula $\boldsymbol{u}_j = -\nabla^T H \boldsymbol{e}_j$ in (77) that

$$W_1^\dagger \Gamma_1 H \boldsymbol{e}_j \cdot W_1^\dagger \Gamma_1 H \boldsymbol{e}_k = [\nabla Z_1]^\dagger H \boldsymbol{e}_j \cdot [\nabla Z_1]^\dagger H \boldsymbol{e}_k = Z_1^\dagger \boldsymbol{u}_j \cdot Z_1^\dagger \boldsymbol{u}_k. \tag{96}$$

This establishes that the spectral weights associated with both approaches are identical and, in turn, establishes the equivalence of the two approaches following from equations (84) and (93). In Section IX we will use equation (90) to compute the effective diffusivity tensor D^* for various periodic flows and relate spectral characteristics to flow geometry and transport properties.

IX.   COMPUTATIONS OF THE EFFECTIVE DIFFUSIVITY TENSOR

In this section, we employ the mathematical framework developed in Section VIII to provide rigorous computations of the effective diffusivity tensor D^* for various model periodic flows. In particular, we employ equation (90) to compute the symmetric S^* and antisymmetric A^* parts of D^*. As a benchmark test we compute D^* for shear flow, for which the spectral measure is known [3]. We also consider a fluid velocity field that has a free parameter. As the parameter varies, the flow transitions from cellular flow to shear flow in the diagonal x-y direction. This gives rise to fascinating transitional behavior in the spectral measure, which governs transitional behavior in the effective diffusivity tensor D^*. For the sake of brevity, we will focus our attention on the ε behavior of the components S_{jk}^*, $j, k = 1, \ldots, d$, of S^*. Moreover, for computational simplicity, we have restricted our computations to dimension $d = 2$.

A. Numerical Methods

By equation (8), the time-independent fluid velocity field $\boldsymbol{u} = \boldsymbol{u}(\boldsymbol{x})$ is given in terms of an antisymmetric matrix $\mathsf{H} = \mathsf{H}(\boldsymbol{x})$, $\boldsymbol{u} = \boldsymbol{\nabla}\!\cdot\!\mathsf{H}$. For dimension $d = 2$, the matrix H is determined by a stream function $\Psi = \Psi(\boldsymbol{x})$,

$$\mathsf{H} = \begin{bmatrix} 0 & \Psi \\ -\Psi & 0 \end{bmatrix}, \tag{97}$$

yielding $\boldsymbol{u} = [-\partial_y\Psi, \partial_x\Psi]$, where ∂_x denotes partial differentiation in the variable x, for example. In this section we consider two flows with free parameters which transition from cellular flow to shear flow as parameters vary. In particular, we consider BC-flow [9] and "cat's eye" flow [15], which are defined by the following stream functions Ψ_{BC} and Ψ_{CE}, respectively,

$$\Psi_{BC}(\boldsymbol{x}) = B \sin x - C \sin y, \qquad \Psi_{CE}(\boldsymbol{x}) = \sin x \sin y + A \cos x \cos y, \tag{98}$$

where we have denoted $\boldsymbol{x} = (x, y)$. The corresponding fluid velocity fields are

$$\boldsymbol{u}_{BC}(\boldsymbol{x}) = (C \cos y, B \cos x), \tag{99}$$

$$\boldsymbol{u}_{CE}(\boldsymbol{x}) = (-\sin x \cos y + A \cos x \sin y, \cos x \sin y - A \sin x \cos y).$$

The flow geometry of these fluid velocity fields transition from shear to cellular flow structure as the system parameters $A, B, C \in [0, 1]$ vary.

Streamlines of a 2D flow are level sets of the stream function Ψ, which define a family of curves that are instantaneously tangent to the fluid velocity field $\boldsymbol{u}$, since $\boldsymbol{u} = [-\partial_y\Psi, \partial_x\Psi]$ implies that $\boldsymbol{u}\!\cdot\!\boldsymbol{\nabla}\Psi = 0$. In Fig. 1, we display streamlines of the stream functions in equation (98) for various parameter values. The streamlines for cat's eye flow are symmetric about the line $y = x$, which follows from the symmetry of the stream function $\Psi_{CE}(x, y) = \Psi_{CE}(y, x)$. The stream function for BC-flow has a more complicated symmetry $\Psi(x, y; B, C) = -\Psi(y, x; C, B)$. This symmetry indicates that if the values of B and C are interchanged, $B \longleftrightarrow C$, then the original flow is recovered from a 90° rotation $(x \to y,\ y \to -x)$ followed by a reflection about the x-axis $(y \to -y)$. Consequently, flows elongated in the y-direction become flows elongated in the x-direction under the interchange $B \longleftrightarrow C$.
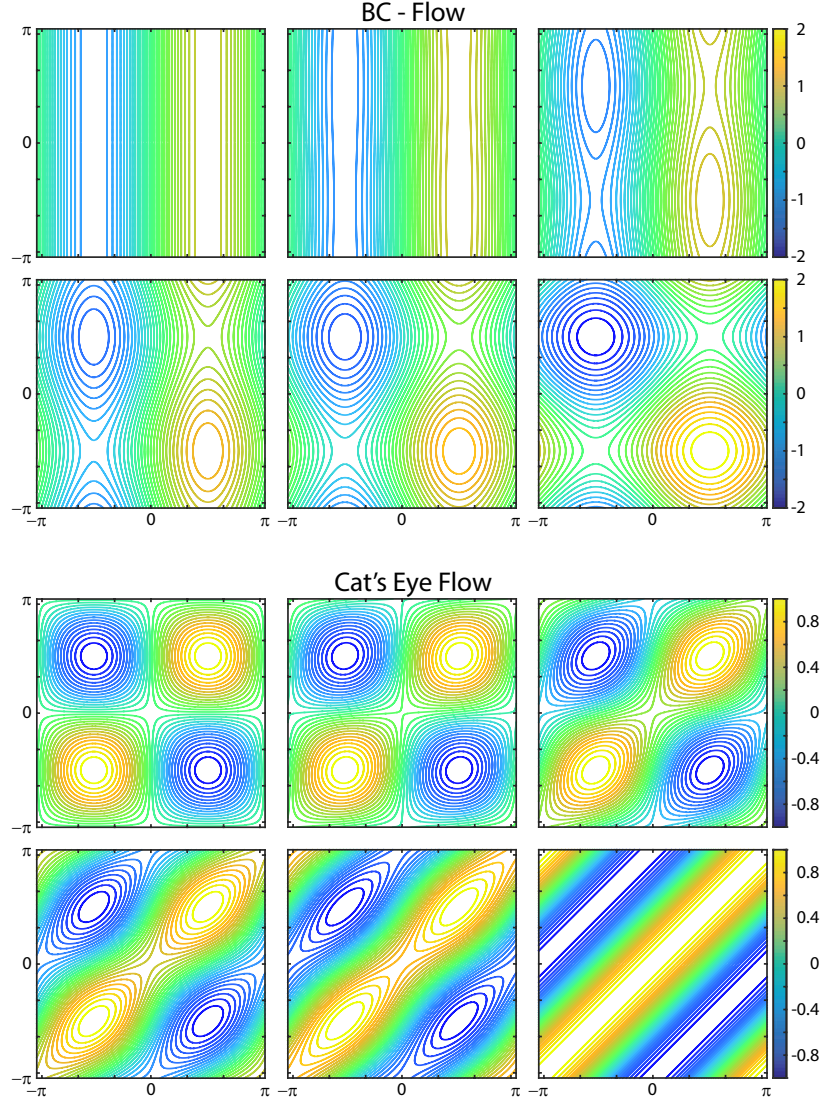
FIG. 1. Transitions in flow structure. The streamlines for BC-flow and cat's eye flow are displayed for various parameter values, transitioning from shear to cell flow structure. From left to right and top to bottom, the parameter values associated with BC-flow are $B = 1$ fixed and $C = 0$, 0.01, 0.1, 0.3, 0.5 and 1, while those for cat's eye flow are $A = 0$, 0.1, 0.3, 0.5, 0.7, and 1.

In equation (6) and the paragraph therein we discussed our non-dimensionalization the advection-diffusion equation in (1). In particular, we mapped $\boldsymbol{u}$ to the non-dimensional fluid velocity field $\boldsymbol{u} \mapsto \boldsymbol{u}/\|\boldsymbol{u}\|$ and ε to the non-dimensional molecular diffusivity $\varepsilon \mapsto \varepsilon/(\ell\|\boldsymbol{u}\|)$, where ℓ is the maximum cell period and $\|\boldsymbol{u}\| = \langle|\boldsymbol{u}|^2\rangle^{1/2}$ is the Hilbert space norm of $\boldsymbol{u}$. For the fluid velocity fields in equation (99), $\mathcal{V} = [0, 2\pi]^2$ and $\ell = 2\pi$. When $\boldsymbol{u}$ in equation (99) is non-random then the underlying Hilbert space is $\mathscr{H} = L^2(\mathcal{V}, \mathrm{m})$, where m denotes the

normalized Lebesgue measure (uniform distribution) on $\mathbb{R}^d$, restricted to $\mathcal{V}$, and $\|\cdot\|$ denotes the $\mathscr{H}$-norm, with

$$\|\boldsymbol{u}_{BC}\|^2 = \frac{B^2 + C^2}{2}, \qquad \|\boldsymbol{u}_{CE}\|^2 = \frac{1 + A^2}{2}. \tag{100}$$

In Section III B we discussed the effective parameter problem for the setting of randomly perturbed, periodic flows. For the sake of brevity, we consider here only the randomly perturbed cat's eye flow, with the parameter A uniformly distributed on the interval $[0, p]$, having second moment $p^2/3$. Numerically, it is natural to set $\mathscr{H} = L^2(\mathrm{m} \times P)$ [26], where P is the probability measure associated with the random variable A. In this case, by Fubini's theorem [18], $\langle \cdot \rangle$ can be considered to denote spatial averaging followed by statistical averaging and the formula for $\|\boldsymbol{u}_{CE}\|^2$ in (100) is replaced by

$$\|\boldsymbol{u}_{CE}\|^2 = \frac{3 + p^2}{6}. \tag{101}$$

We now discuss in more detail our discrete, matrix formulation of the effective parameter problem. To illustrate how to generalize these ideas to dimension d larger than $d = 2$, we will maintain aspects of our general notation. In this discrete setting, the spatial region $\mathcal{V} = [0, 2\pi]^d$, for example, is replaced by a square lattice $\mathcal{V}_L^d$ of size L containing L^d equally spaced points in $\mathcal{V}$. As discussed in the beginning of Section IV A, the differential operators $\boldsymbol{\nabla}$ and $\boldsymbol{\nabla}\cdot$ are replaced by finite difference, matrix operators ∇ and $-\nabla^T$, respectively, with suitable boundary conditions. Periodic boundary conditions will be assumed throughout this section. Since these matrices operate on vectors, the d-dimensional lattice $\mathcal{V}_L^d$ must be bijectively mapped to a one dimensional lattice $\mathcal{V}_N$ of size $N = L^d d$. The specific structure of $\mathcal{V}_N$ and ∇ depend on the bijective mapping Θ chosen. In our computations discussed in this section, we used the mapping Θ described in [37].

Under the mapping Θ, a spatially dependent d-dimensional vector field $\boldsymbol{v}(\boldsymbol{x})$, say, is bijectively mapped to a discretized *constant* vector of length N that contains all of the spatial information of $\boldsymbol{v}(\boldsymbol{x})$ for $\boldsymbol{x} \in \mathcal{V}_L^d$. For example the spatially dependent vector $\boldsymbol{v}(\boldsymbol{x}) = (v_1(\boldsymbol{x}), v_2(\boldsymbol{x}))$ is mapped to $(\boldsymbol{v}_1, \boldsymbol{v}_2)$, where the vectors $\boldsymbol{v}_i$, $i = 1, 2$, are constant and of length L^d. Similarly, the d-dimensional standard basis vector $\boldsymbol{e}_1 = (1, 0, \ldots, 0)$ is mapped to the N-dimensional vector $(\boldsymbol{1}, \boldsymbol{0}, \ldots, \boldsymbol{0})$, where $\boldsymbol{1}$ and $\boldsymbol{0}$ are vectors of ones and zeros of length L^d, respectively, and similarly for the $\boldsymbol{e}_j$ for $j = 2, \ldots, d$. Therefore, the vectors $\hat{\mathbf{e}}_j$,

$j = 1, \ldots, d$, satisfying

$$\hat{\mathbf{e}}_j = \Theta(\mathbf{e}_j)/L^{d/2}, \qquad \hat{\mathbf{e}}_j \cdot \hat{\mathbf{e}}_k = \delta_{jk}, \tag{102}$$

serve as "lattice standard basis vectors." In previous sections, we deferred the description of these vectors to the present section and, for simplicity, used the notation $\mathbf{e}_j$. Now that the specific nature of these vectors has been discussed, we will henceforth use the notation in equation (102). With this convention, the division by $L^{d/2}$ in (102) takes care of the L-scaling in discrete representations of spatial integrals, where the normalized Lebesgue measure $\mathrm{d}\mathbf{x}$ becomes the discrete differential $\mathrm{d}\mathbf{x} = (2\pi/L)^d/(2\pi)^d$ when $\mathcal{V} = [0, 2\pi]^d$ and the spatial average $\langle \xi(\mathbf{x})\, \zeta(\mathbf{x}) \rangle_{\mathcal{V}}$ becomes $\boldsymbol{\xi} \cdot \boldsymbol{\zeta}/L^d$. As another example, under the bijective mapping, the 2×2 matrix H in (97) becomes a $N \times N$ antisymmetric banded matrix, where the stream function $\Psi(\mathbf{x})$ is represented by a diagonal $L^d \times L^d$ matrix and the zero element 0 is represented by a matrix of zeros. In higher dimensions $d > 2$ the discrete representation of the matrix H is also banded. As in previous sections, for notational simplicity, we will not make a notational distinction for the matrix H between the continuum and discrete settings.

In Section VIII we demonstrated that, for the discrete setting, the spectral measure μ_{jk} underlying the Stieltjes integral representation of S_{jk}^* is given by

$$\mathrm{d}\mu_{jk}(\lambda) = \sum_{n:\, \lambda_n^1 \leq \lambda} \langle m_{jk}(n)\, \delta_{\lambda_n^1}(\mathrm{d}\lambda) \rangle, \tag{103}$$

where λ_n^1, $n = 1, \ldots, K_1$, are the eigenvalues of the matrix $-\imath \mathsf{U}_1^T \mathsf{H} \mathsf{U}_1$ in (94), while various equivalent representations of the spectral weights $m_{jk}(n)$, $j, k = 1, \ldots, d$, are given in equation (96). In our computations of μ_{jk}, we used

$$m_{jk}(n) = \mathrm{Re}\,[\, \overline{([\mathbf{r}_n^1]^\dagger \mathsf{U}_1^T \mathsf{H} \hat{\mathbf{e}}_j)} \,([\mathbf{r}_n^1]^\dagger \mathsf{U}_1^T \mathsf{H} \hat{\mathbf{e}}_k)\,], \quad n = 1, \ldots, K_1, \tag{104}$$

which follows from equations (38), (95), and (96). We stress that, for notational simplicity, in this section we denote $\mu_{jk} \equiv \mathrm{Re}\,\mu_{jk}$, $j, k = 1, 2$, as indicated in equation (104). In (104), $\mathbf{r}_n^1$, $n = 1, \ldots, K_1$, are the *complex* eigenvectors of the matrix $-\imath \mathsf{U}_1^T \mathsf{H} \mathsf{U}_1$. Consequently, μ_{kk} is a positive measure and μ_{jk} is a signed measure for $j \neq k$. The size of the matrix ∇ is $N \times L^d$, where $N = L^d d$. For $d = 2$ the nullity of ∇ is 1, therefore, the size of U_1 is $N \times (L^d - 1)$, so that the Hermitian matrix $-\imath \mathsf{U}_1^T \mathsf{H} \mathsf{U}_1$ is of size $K_1 = L^d - 1$.

We denote the spectral weights $m_{jk}(n)$ associated with the decomposition $\mu_{jk} = \mu_{jk}^+ - \mu_{jk}^-$ in (30) by $m_{jk}^+(n)$ and $m_{jk}^-(n)$, where $m_{jk}^\pm(n) \geq 0$. Moreover, we also denote [18] by the

functions $[S_{12}^*]^+$ and $[S_{12}^*]^-$

$$[S_{12}^*]^+(\varepsilon) = \max\{S_{12}^*(\varepsilon), 0\}, \quad [S_{12}^*]^-(\varepsilon) = \max\{-S_{12}^*(\varepsilon), 0\}, \tag{105}$$

for each $0 < \varepsilon < \infty$, so that $S_{12}^* = [S_{12}^*]^+ - [S_{12}^*]^-$, $[S_{12}^*]^\pm(\varepsilon) = S_{12}^*(\varepsilon; \mu_{12}^\pm)$, and $[S_{12}^*]^\pm \geq 0$.

In the case of a non-random fluid velocity field $\boldsymbol{u}$, we used $L = 200$ so that $K_1 = 39,999$. The eigenvalues λ_n^1 and eigenvectors $\boldsymbol{r}_n^1$ of the non-random Hermitian matrix $-\imath U_1^T H U_1$ were computed using the Matlab function *eig()*. In this case, the averaging $\langle \cdot \rangle$ in (103) is interpreted as spatial averaging over the period cell $\mathcal{V}$. In the random setting, we used $L = 100$ so that $K_1 = 9,999$. In this case, the averaging $\langle \cdot \rangle$ in (103) is interpreted as spatial averaging followed by ensemble averaging over $\sim 10^3$ statistical trials.

The numerical accuracy of the eigenvalue problem is determined by the *eigenvalue condition numbers* $\mathcal{K}(\lambda_n^1)$, $n = 1, \ldots, K_1$, which are the reciprocals of the cosines of the angles between the left and right eigenvectors. Large eigenvalue condition numbers of a Hermitian matrix implies that it is near a matrix with multiple eigenvalues, while eigenvalue condition numbers close to 1 imply that the eigenvalue problem is well-conditioned. The eigenvalue problem for the matrix $-\imath U_1^T H U_1$ is extremely well conditioned with $\max_n |1 - \mathcal{K}(\lambda_n^1)| \sim 10^{-14}$ typical, which were computed using Matlab's function *condeig()*.

To our knowledge, Matlab does not provide a function that describes the accuracy of the computed SVD of the matrix $\nabla = U \Sigma V^T$. In order to better understand the numerical accuracy in the entries of the matrix U, which is central to our computational method, we performed the following tests. For the case of Dirichlet boundary conditions, the matrix ∇ is of full rank, hence the matrix Laplacian $\nabla^T \nabla$ is invertible. We computed the matrix $\Gamma = \nabla(\nabla^T \nabla)^{-1} \nabla^T$ directly using Matlab's *mldivide* function $A \backslash B$, i.e., $\Gamma = \nabla((\nabla^T \nabla) \backslash \nabla^T)$, and also using the SVD of the matrix ∇, with $\Gamma = U U^T$. We then computed the component-wise maximum difference $\max_{lm} |[\nabla((\nabla^T \nabla) \backslash \nabla^T) - U U^T]_{lm}|$. When $L = 100$ and $L = 200$ this difference is $\sim 10^{-15}$, which gives an idea of the accuracy of the SVD of ∇ for the rank deficient, periodic setting. In all of our computations, Matlab's sparse architecture was employed wherever possible to reduce roundoff error.

B. Numerical Results

We now discuss our numerical results. It was shown [3] in the continuum setting that for shear flow in the x-direction, the measure μ_{11} is given by a δ-measure concentrated at the spectral origin, while $\mu_{22} \equiv 0$, and similarly for shear flow in the y-direction. As a baseline result, we computed the spectral measures and effective diffusivities for BC-shear-flow in both the x and y-directions, which are obtained for parameter values $(B, C) = (0, 1)$ and $(B, C) = (1, 0)$, respectively. Our computations of the components μ_{jk}, $j, k = 1, 2$, of the spectral measure for BC-shear-flow displayed in Fig. 2 are in agreement with the theoretical prediction in [3].

Fig. 2 displays the streamlines for BC-shear-flow in (a) the x-direction and (b) the y-direction. In Fig. 2c the components S^*_{jk}, $j, k = 1, 2$, of the effective diffusivity tensor are displayed for BC-shear-flow in the x-direction. The analogous result for BC-shear-flow in the y-direction is visually identical to Fig. 2c under the mapping $\mathsf{S}^*_{11} \leftrightarrow \mathsf{S}^*_{22}$, i.e., under the exchange of the colors black $\leftrightarrow$ blue. The components μ_{jk}, $j, k = 1, 2$, of the spectral measure are displayed for BC-shear-flow in (d) the x-direction and (e) the y-direction.

We focus our discussion on the results for BC-shear-flow in the x-direction, as the discussion regarding BC-shear-flow in the y-direction is analogous. For all $n = 1, \ldots, K_1$, the spectral weights $m_{22}(n)$ in Fig. 2d associated with the y-direction satisfy $m_{22}(n) \lesssim 10^{-29}$, while $m_{12}^{\pm}(n) \lesssim 10^{-28}$ in the bulk of the spectrum with a peak near the spectral origin with spectral weights satisfying $m_{12}^{\pm}(n) \lesssim 10^{-16}$. With the effects of finite resolution $L < \infty$ as well as numerical errors in the computed components of the matrix $-\imath \mathsf{U}_1^T \mathsf{H} \mathsf{U}_1$ and its eigenvalue decomposition, associated with roundoff error due to a machine epsilon of $\sim 10^{-16}$, these spectral weights can be considered "numerically zero." The spectral weights for the x-direction satisfy $m_{11}(n) \lesssim 10^{-28}$ in the bulk of the spectrum, while the weights near the spectral origin satisfy $10^{-9} \lesssim m_{11} \lesssim 10^{-1}$, resembling a δ-measure with virtually all of its mass concentrated near the origin. This is consistent with theoretical predictions [3]. Due to the antisymmetry of the *real-valued* matrix $\mathsf{U}_1^T \mathsf{H} \mathsf{U}_1$, its complex eigenvectors and purely imaginary eigenvalues come in complex conjugate pairs [22]. Consequently, the eigenvalues of the Hermitian matrix $-\imath \mathsf{U}_1^T \mathsf{H} \mathsf{U}_1$ come in positive-negative pairs with identical spectral weights, resulting in the symmetry about the y-axis displayed by the spectral measures in Fig. 2.
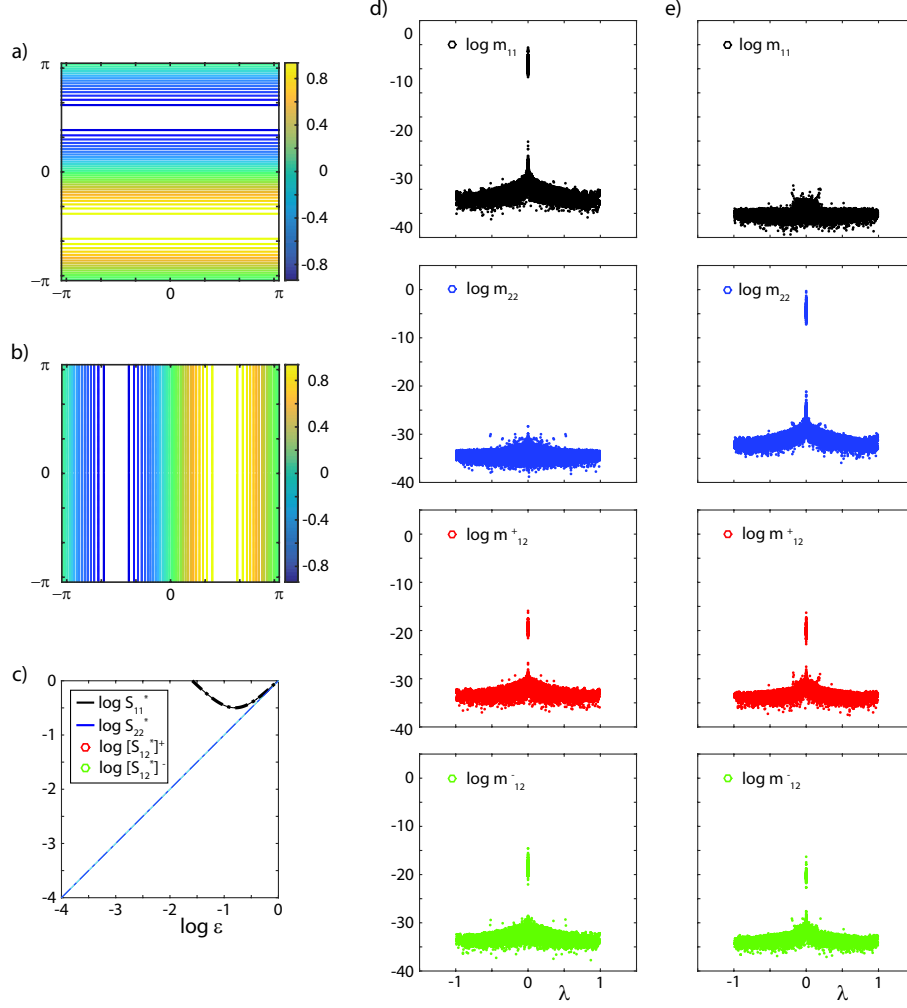
FIG. 2. Shear flow baseline result. The streamlines of BC-shear-flow in (a) the x-direction and (b) the y-direction. (c) The ε behavior of our computations of the components S^*_{jk}, $j,k = 1, 2$, of the effective diffusivity corresponding to shear flow in the x-direction. The spectral weights m_{jk} of the spectral measure Re μ_{jk} for shear flow in (d) the x-direction and (e) the y-direction. Consistent with theoretical predictions, the measure associated with the direction of the flow resembles a delta measure centered at the origin, while the other two components have spectral weights m_{jk} with very small magnitudes.

Due to the high concentration of measure mass in μ_{11} very near the spectral origin, our computation of S^*_{11} displayed in Fig. 2c behaves like it's being governed by a delta function concentrated at the origin. In particular, Fig. 2c shows that the computed ε behavior of S^*_{11} displayed in black color with solid line-style lays right on top of the graph of its upper bound $\varepsilon\left[1 + \mu^0_{kk}/\varepsilon^2\right]$ given in (29), with $\mu^0_{11} \approx 2.5204 \times 10^{-2}$, displayed in black color and dash-dot

line-style. (We had to increase the line-width of the upper bound to be able to distinguish between the two black lines.) Due to the extremely small magnitudes of the spectral weights m_{22} and $m_{12}^{\pm}$, with measure masses $\mu_{22}^0 \approx 2.7050 \times 10^{-30}$, $[\mu_{12}^0]^+ \approx 5.2119 \times 10^{-18}$, and $[\mu_{12}^0]^- \approx 1.6910 \times 10^{-16}$, the upper and lower bounds for S_{22}^* and S_{12}^* in equations (29) and (31) are very close to ε and 0, respectively; The graph of S_{22}^* is virtually right on top of the lower bound ε in cyan color and solid line-style, and the magnitudes of $[\mathsf{S}_{12}^*]^+$ and $[\mathsf{S}_{12}^*]^-$ are so small they don't even appear on the graph. Since the support of the spectral measure is contained in the interval $[-1, 1]$, the components of the effective diffusivity approach their bare molecular diffusivity value $\varepsilon\,\delta_{jk}$ for large ε.

In [38] we developed Fourier methods for the rigorous computation of the spectral measure μ_{jk} for BC-cell flow, with $B = C = 1$. In particular, the eigenvalue problem $A\varphi_n = \lambda_n\varphi_n$ associated with the operator $A = \Delta^{-1}[\boldsymbol{u}\cdot\boldsymbol{\nabla}]$ was transformed into an infinite algebraic system of equations, defining a discrete, generalized eigenvalue problem. The Fourier coefficients of the eigenfunctions φ_n, $n = 1, 2, 3, \ldots$, for the continuum setting comprised the components of the generalized eigenvectors in the discrete setting. Moreover, motivated by the theoretical findings in the current work, we provided a rigorous extension of the results given here to the setting of a time-dependent fluid velocity field, where $A = \Delta^{-1}[\partial_t + \boldsymbol{u}\cdot\boldsymbol{\nabla}]$ and ∂_t denotes partial differentiation in time. Furthermore, we used abstract methods of functional analysis to generalize Lemma 1 to the continuum, steady and dynamic settings. The Fourier methods in [38] were also generalized to the setting of a time-dependent fluid velocity field. Since we already treated BC-cell flow in [38], and for the sake of brevity, we now turn our attention to a discussion regarding our results for "cat's eye flow."

Since the streamlines for cat's eye flow in Fig. 1 are symmetric about the line $y = x$, as discussed above, we anticipate that $\mu_{11} = \mu_{22}$. Our computations of the components μ_{jk}, $j, k = 1, 2$, of the spectral measure displayed in Figures 3 and 4, for non-random A, indicate that this is indeed the case. A closer look at these figures reveals a deeper symmetry, namely that $\mu_{11} = \mu_{22} = |\mu_{12}|$, where $|\mu_{12}| = \mu_{12}^+ + \mu_{12}^-$ is the total variation of the signed measure μ_{12} introduced in equation (30).

Since the operator $A = \Delta^{-1}[\boldsymbol{\nabla}\cdot\boldsymbol{u}]$ is compact [8], its spectra is discrete with a limit point at the spectral origin $\lambda = 0$ [49]. This limit point behavior of the measures μ_{jk}, $j, k = 1, 2$, can be seen in all of the panels of Fig. 3. When the parameter $A = 0$, the streamlines of cat's eye flow are closed cell structures, as shown in Fig. 1, so that large scale transport
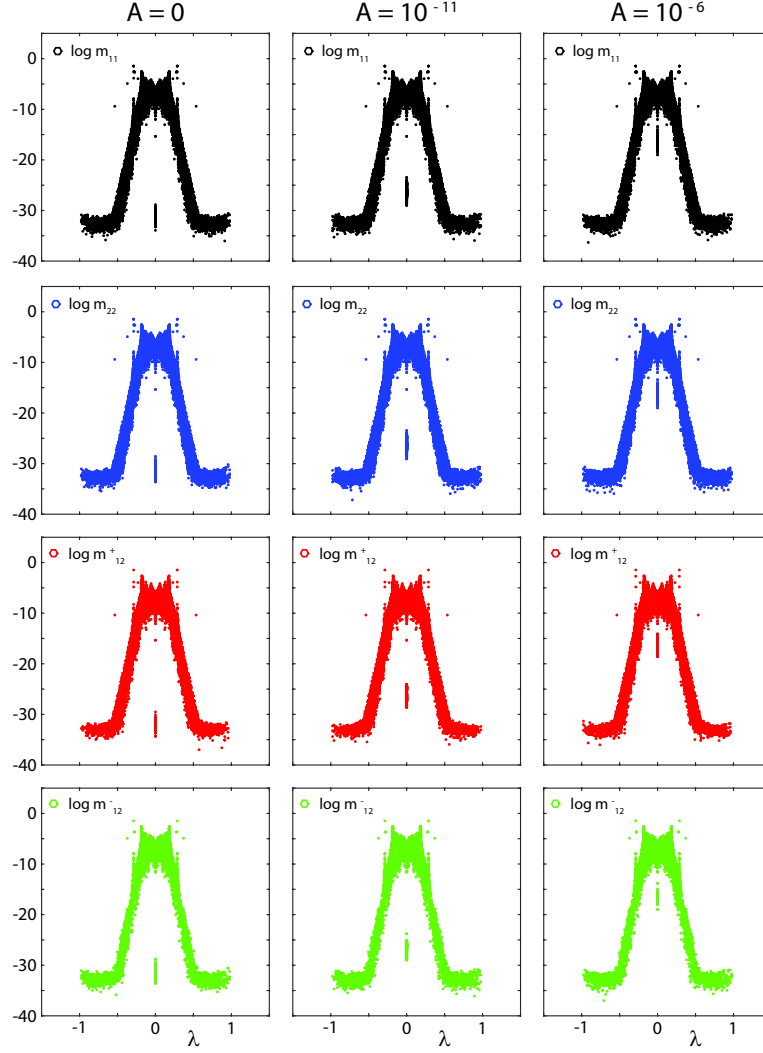
FIG. 3. Transition away from cat's eye cell flow. The spectral weights m_{jk} for the components Re μ_{jk}, $j,k = 1,2$, of the spectral measure are displayed with increasing values of the free parameter A from left to right. As the parameter A increases, the streamlines of the flow transition away from cell structures to open channels. This is reflected in the measure by a dramatic increase in the magnitude of the spectral weights m_{jk} associated with the limit point of the measure at $\lambda = 0$, while the other weights change only slightly.

occurs only when $\varepsilon > 0$ [15]. In this case, the magnitude of the spectral weights $m_{kk}(n)$ and $m_{jk}^{\pm}(n)$, $n = 1,\ldots,K_1$, associated with this limit point at $\lambda = 0$ are $\lesssim 10^{-28}$, as shown in Fig. 3. When $A > 0$, open channels connect neighboring cells and large scale transport takes place both in thin boundary layers and within the channels [15]. This is reflected in the spectral measure by a dramatic increase in the magnitude of the spectral weights $m_{kk}(n)$
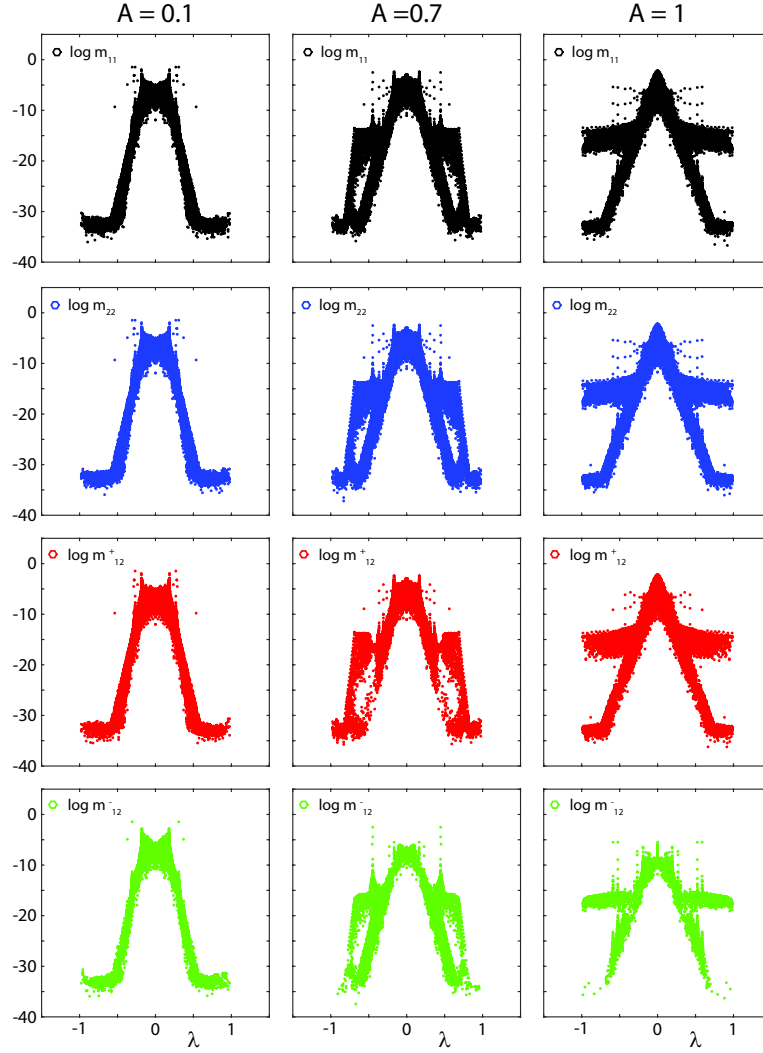
FIG. 4. Transition toward cat's eye shear flow. The spectral weights m_{jk} for the components Re μ_{jk}, $j, k = 1, 2$, of the spectral measure are displayed with increasing values of the free parameter A from left to right. As the value of the parameter A increases, the streamlines become more elongated in the x-y diagonal direction, becoming shear flow when $A = 1$. This is reflected in the spectral measure by an increase in the breadth of the spectral region with significant measure mass.

and $m_{jk}^{\pm}(n)$ associated with the limit point at $\lambda = 0$, by more than *15 orders of magnitude* for a change of only 10^{-6} in the magnitude of A, while the spectral weights associated with the bulk of the spectrum change only subtlety, as shown in Fig. 3.

As the value of A increases into the range $(10^{-2}, 10^0)$, the limit point near $\lambda = 0$ persists. However, the increase in the magnitudes of the associated spectral weights stops, with values

in the range $(10^{-11}, 10^{-5})$ for all $A \in (10^{-2}, 10^0)$. In this regime, the limit point of the spectral measure is closely surrounded by spectrum in the bulk having spectral weights with comparable magnitudes. As A increases in the range $(10^{-1}, 10^0)$, a significant transitional behavior arises in the spectral measure in the bulk of the spectrum, as shown in Fig. 4. In particular, a plateau forms in the spectral measure for $\lambda \in (-1, -0.5) \cup (0.5, 1)$ with spectral weights having magnitudes $\lesssim 10^{-13}$. Another feature also arises that has a more significant influence on the behavior of the effective diffusivity S^*. Namely, the appearance of spectra $\lambda \in (-0.5, -0.2) \cup (0.2, 0.5)$ with measure masses in the range $(10^{-10}, 10^{-2})$, as shown in Fig. 4. This broadening of the region having spectral weights with magnitudes as large as 10^{-2} from $\lambda \in (-0.2, 0, 2)$, present for all $A \in [0, 1]$, to $\lambda \in (-0.5, 0, 5)$ has a significant influence on the behavior of the effective diffusivity S^*, as shown in Fig. 5.

Our computations of the components S^*_{jk}, $j, k = 1, 2$, for cat's eye flow are displayed in Fig. 5 along with their upper bounds given in the same color and dash-dot line-style. Since the support of μ_{jk} is contained in the interval $[-1, 1]$, the components S^*_{jk} of the effective diffusivity approach their bare molecular diffusivity value $\varepsilon \delta_{jk}$ for large ε. We discussed above that our computations of the components μ_{jk}, $j = 1, 2$, of the spectral measure display the symmetry $\mu_{11} = \mu_{22} = |\mu_{12}|$. Since the behavior of the μ_{jk} govern the behavior of the corresponding components of the effective diffusivity S^*_{jk}, the symmetry $\mu_{11} = \mu_{22} = |\mu_{12}|$ between the measures gives rise to the symmetry $\mathsf{S}^*_{11}(\varepsilon) = \mathsf{S}^*_{22}(\varepsilon) = \varepsilon + X(\varepsilon; \mu_{12}^+) + X(\varepsilon; \mu_{12}^-)$ between the components of the effective diffusivity, where we have denoted by $X(\varepsilon; \nu) = \int \mathrm{d}\nu(\lambda)/(\varepsilon^2 + \lambda^2)$, e.g., $\mathsf{S}^*_{11}(\varepsilon) = \varepsilon + X(\varepsilon; \mu_{11})$. The symmetry $\mathsf{S}^*_{11} = \mathsf{S}^*_{22}$ can be clearly seen in our computations of S^*_{jk}, $j, k = 1, 2$, displayed in Fig. 5; The two curves lay right on top of one another, as do their upper bounds as $\mu_{11}^0 = \mu_{22}^0$. The lower bounds for S^*_{kk}, $k = 1, 2$, have been omitted in the figure panels, as they are virtually right on top of the looser lower bound ε (displayed in cyan color) due to the small measure masses $\lesssim 10^{-3}$. We have also numerically explored the approximate relationship $\mathsf{S}^*_{11} \approx \varepsilon + [\mathsf{S}^*_{12}]^+ + [\mathsf{S}^*_{12}]^-$ by plotting S^*_{11}, S^*_{22}, and $\varepsilon + [\mathsf{S}^*_{12}]^+ + [\mathsf{S}^*_{12}]^-$ on one graph. For most values of A and ε considered, the three curves lay virtually on top of each other (not shown), and when there is a deviation of $\varepsilon + [\mathsf{S}^*_{12}]^+ + [\mathsf{S}^*_{12}]^-$ from S^*_{11}, it is slight.

Recall, we demonstrated in Fig. 3 that for $A \in (0, 10^{-2})$, the limit point $\lambda = 0$ of the spectral measure μ_{jk} has weights m_{jk} with magnitudes that increase dramatically as A increases from zero, with magnitudes in the interval $(10^{-11}, 10^{-5})$ when $A \sim 10^{-2}$. However,
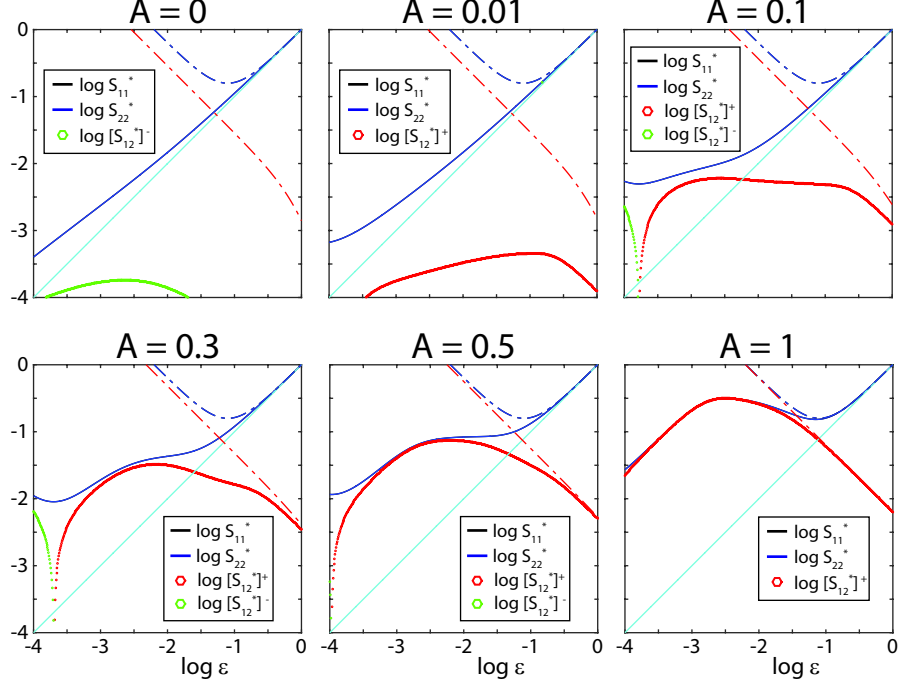
FIG. 5. Transitional behavior of the effective diffusivity from cat's eye cell flow to shear flow. The behavior of the components S^*_{jk}, $j, k = 1, 2$, of the effective diffusivity as a function of the molecular diffusivity ε and increasing values of the parameter A from left to right and top to bottom. The upper bounds corresponding to S^*_{jk} are in dash-dot line-style and are the same color for S^*_{kk} and red for S^*_{12}, while the lower bound ε for S^*_{kk} is in cyan color and solid line-style. For small values of the parameter A, the enhancement in the effective diffusivity is more pronounced for small values of ε. However, as the value of the parameter A increases and the flow transitions from cell to shear structure, there is a substantial enhancement in the effective diffusivity for larger values of ε. This is due to the behavior of the spectral measure discussed in Figures 3 and 4.

in the bulk of the spectrum, the magnitudes of the spectral weights change only subtlety. Consequently, for $A \in (0, 10^{-2})$ this transitional behavior of the spectral measure μ_{kk} governs primarily the small ε behavior of S^*_{kk}, as shown in the panels of Fig. 5 corresponding to $A = 0$ and $A = 10^{-2}$. The transitional behavior of S^*_{12} is more pronounced due to the lack of the $\varepsilon \, \delta_{jk}$ term for $j \neq k$.

Recall, we demonstrated in Fig. 4 that when the parameter A increases in the interval $(10^{-1}, 10^0)$, spectra $\lambda \in (-0.5, -0.2) \cup (0.2, 0.5)$ appear with measure masses in the range $(10^{-10}, 10^{-2})$. This broadens the influence of the spectral measure μ_{jk} over the effective
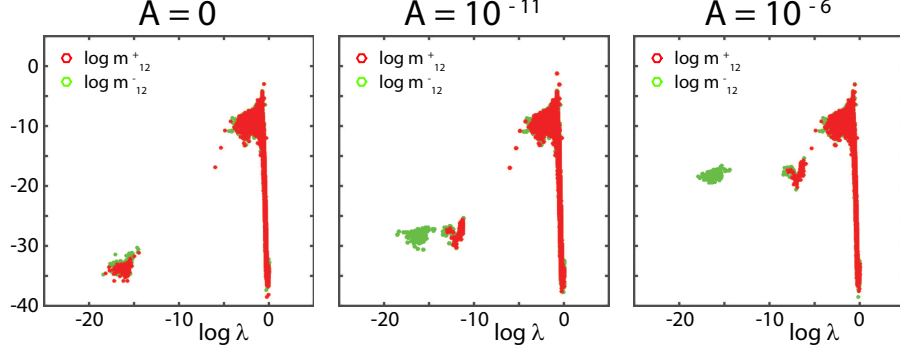
FIG. 6. Migration of positive measure mass from the limit point at the spectral origin. As the free parameter A of cat's eye flow increases from zero, the magnitude of the spectral weights $m_{12}^{\pm}$ increase dramatically. Moreover, the spectra associated with the positive weights m_{12}^{+} migrate away from the spectral origin until the limit point is comprised only of negative valued mass.

diffusivity S_{jk}^{*} to larger values of ε, greatly enhancing it above its bare molecular diffusivity value $\varepsilon\,\delta_{jk}$, as shown in the panels of Fig. 5 for $A \geq 0.1$. Note that, since $\mu_{11} = \mu_{22} = |\mu_{12}|$, we have the inequalities $S_{11}^{*} \geq \varepsilon + [S_{12}^{*}]^{+}$ and $S_{11}^{*} \geq \varepsilon + [S_{12}^{*}]^{-}$, with $S_{11}^{*} = S_{22}^{*}$, as shown in Fig. 5.

When the figure panels associated with μ_{12} in Fig. 3 are plotted in log-log scale as shown in Fig. 6, the following is revealed. As A increases from zero, the spectra of the limit point with positive measure mass migrates away from $\lambda = 0$, so that the limit point eventually consists of spectra with only negative measure mass. Consequently, as ε decreases below 10^{-3}, this influence of μ_{12} on S_{12}^{*} becomes more dominant and S_{12}^{*} changes sign, becoming negative, as shown in Fig. 5. As the value of ε approaches the location of this limit point, the numerical approximation breaks down due to effects of finite resolution L.

We now discuss our computations of the components μ_{jk} and S_{jk}^{*}, $j, k = 1, 2$, of the spectral measure and effective diffusivity, respectively, for cat's eye flow with random parameter A uniformly distributed on the interval $[0, p]$. For each statistical trial of a sample space Ω_0 of $\sim 10^{3}$ statistical trials and a system resolution $L = 100$, we computed *every* eigenvalue λ_n^1 and eigenvector r_n^1, $n = 1, \ldots, K_1$, of the matrix $-\imath U_1^T H U_1$ to form the spectral measure μ_{jk} in equation (103). In order to visually determine the behavior of the function $\mu_{jk}(\lambda) = \langle \mathbf{Q}(\lambda)\hat{e}_j, \hat{e}_k \rangle$ underlying the spectral measure μ_{jk}, we plot a histogram representation of $\mu_{jk}(\lambda)$ called the *spectral function*, which we will also denote by $\mu_{jk}(\lambda)$.
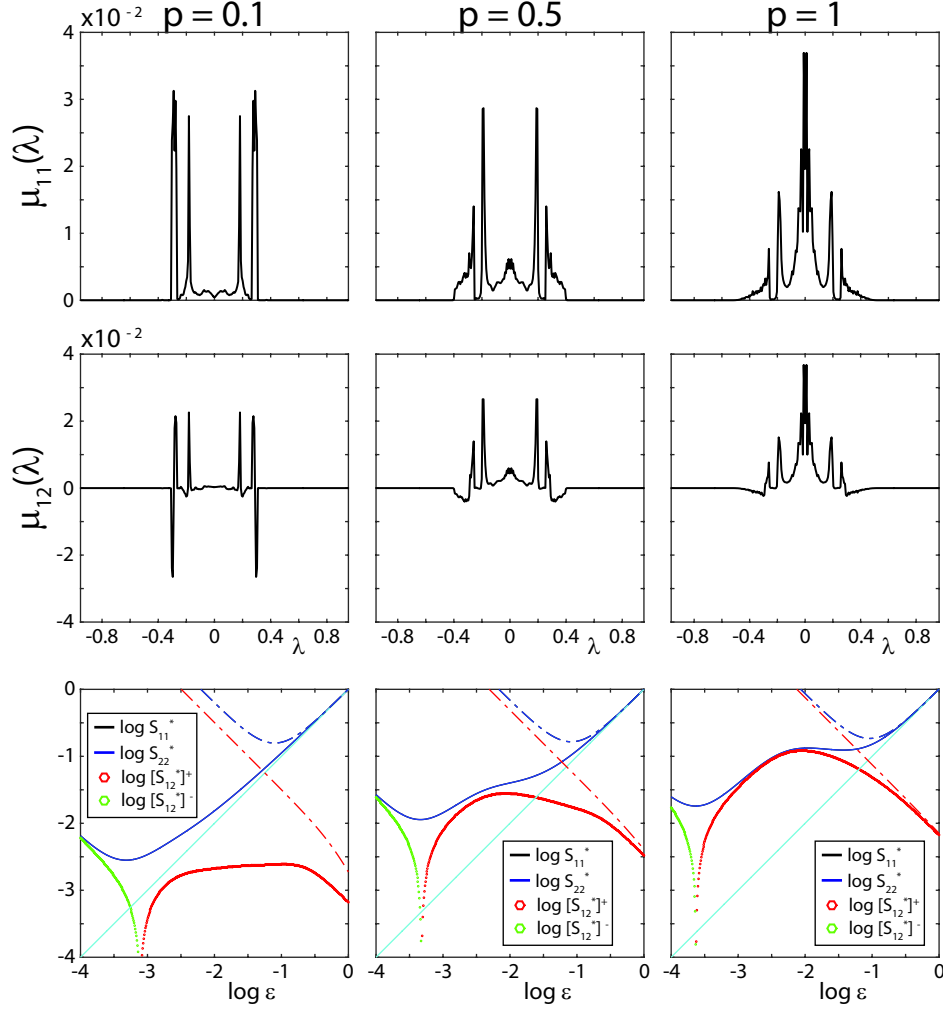
FIG. 7. Spectral functions and effective diffusivities for randomly perturbed cat's eye flow. The random parameter A is uniformly distributed on the interval $[0, p]$. The spectral functions $\mu_{jk}(\lambda)$ are displayed with corresponding effective diffusivities S_{jk}^* directly below for various values of p, increasing from left to right. As p increases and the streamlines of the flow become more elongated in the x-y direction, on average, the region about the spectral origin $\lambda = 0$ with substantial measure mass increases in breadth and magnitude. This gives rise to a substantial enhancement in the components S_{jk}^* of the effective diffusivity for larger values of the molecular diffusivity ε. The color scheme of the panels for S_{jk}^* is the same as that in Fig. 5.

We now describe how we computed this graphical representation of the measure μ_{jk}. First, the spectral interval $I \supseteq \Sigma$ was divided into V sub-intervals I_v, $v = 1, \ldots, V$, of equal length $1/V$. Second, for fixed v, we identified all of the eigenvalues that satisfy $\lambda_n^1(\omega) \in I_v$, for $n = 1, \ldots, K_1$ and $\omega \in \Omega_0$. The assigned value of $\mu_{jk}(\lambda)$ at the midpoint λ of the interval

I_v, is the sum of the spectral weights $m_{jk}(\omega)$ associated with all such $\lambda_n^1(\omega) \in I_v$. In our computations of the spectral functions, we typically used $V \sim 10^2$.

Consistent with the symmetries of the random flow, our computations of the spectral function satisfies $\mu_{11}(\lambda) = \mu_{22}(\lambda)$, hence the ensemble averaged components S_{jk}^* of the effective diffusivity also satisfy $\mathsf{S}_{11}^* = \mathsf{S}_{22}^*$, as shown in Fig. 7. Similar to our computations for non-random A, when $p = 0.1$ the measure mass of μ_{jk}, $j, k = 1, 2$, near the spectral origin is quite small and, on average, the region with significant magnitude increases in breadth as p increases. This average increase in the breadth of the region with significant mass gives rise to a substantial enhancement of the components S_{jk}^* of the effective diffusivity above the bare molecular diffusivity values $\varepsilon \, \delta_{jk}$. Our results for cat's eye flow with random A also demonstrate the influence of resolution L in the numerical computations. In particular, with a decrease in resolution L from $L = 200$ in Figures 3 and 4 to $L = 100$ in Fig. 7, we see that the accuracy of the numerical computations break down for $\varepsilon \sim 10^{-3}$ with $L = 100$ instead of $\varepsilon \sim 10^{-4}$ with $L = 200$, indicated by a $1/\varepsilon$ divergence. For the continuum setting, the limit point of the spectrum at $\lambda = 0$ can be discrete with finite or infinite multiplicity, and can even be continuous [51].

X.   CONCLUSIONS

In Section III we adapted and extended a method [2, 3] that provides the rigorous Stieltjes integral representations for the symmetric S^* and antisymmetric A^* parts of effective diffusivity tensor D^* shown in equation (28). These integral representations involve the molecular diffusivity ε and a spectral measure μ_{jk} of a self-adjoint operator that acts on the Hilbert space of curl-free vector fields. In Section IV we considered a discrete formulation of Section III for the case that the matrix Laplacian is of full rank, hence invertible. A matrix analysis showed that the spectral measure is given in terms of the eigenvalues and eigenvectors of a Hermitian matrix. In Section IV B we provided a projection method which revealed that many of the spectral weights of the discrete spectral measure are identically zero, while the others are determined by a much smaller Hermitian matrix. This method stabilizes and increases the efficiency of numerical computations of μ_{jk}, which enables more accurate computations of the effective diffusivity tensor D^*.

In Section V we returned to the continuum setting, adapting and extending a different

method [8, 41] that provides the rigorous Stieltjes integral representations in equation (28), involving the molecular diffusivity ε and a (possibly different) spectral measure μ_{jk} of a self-adjoint operator that acts on a Sobolev space of scalar fields. In Section VI we considered a discrete formulation of Section V for the case that the matrix Laplacian is of full rank. A matrix analysis showed that the spectral measure is given in terms of the *generalized* eigenvalues and eigenvectors associated with a pair of Hermitian matrices of the same size as that arising in the above mentioned projection method.

In Section VII we used properties of the singular value decomposition of the matrix gradient ∇ to reveal symmetries between the two discrete approaches formulated in Sections IV and VI, establishing in Lemma 1 that the two approaches yield equivalent spectral representations of the effective diffusivity tensor D^* when the matrix Laplacian is of full rank. In particular, we established in the proof of Lemma 1 that the eigenvalues and generalized eigenvalues underlying the spectral measures for each method are in fact eigenvalues of a Hermitian matrix arising in both methods. Moreover, the eigenvectors $\boldsymbol{w}_n$ and generalized eigenvectors $\boldsymbol{z}_n$ of the two methods are related by $\boldsymbol{w}_n = \nabla \boldsymbol{z}_n$, which leads to the equivalence of the discrete spectral measures of the two approaches.

In Section VIII we generalized Lemma 1 to the case that matrix Laplacian is rank deficient, hence non-invertible. This extends the numerical methods developed in Sections IV and VI to the setting of periodic boundary conditions, for which the matrix Laplacian is singular. In over 25 years since the formulation [2, 3] of Stieltjes integral representations for the effective diffusivity tensor D^*, analytical calculations of D^* have been obtained for only a few simple flows, such as shear flow. Our results of Section VIII help overcome this limitation by providing a mathematical foundation for rigorous computation of D^*.

In Section IX we employed the numerical methods formulated in Section VIII to compute the components S_{jk}, $j, k = 1, \ldots, d$, of S^* for some model 2D periodic flows, by directly computing the associated spectral measure Re μ_{jk}. As a baseline result, we computed S_{jk} and Re μ_{jk} for BC-shear-flow, for which the spectral measure is known [3]. Our numerical results are in good agreement with the theoretical result. We also computed the transitional behavior of S_{jk} and Re μ_{jk} for "cat's eye" flow as a function of a free parameter, both for the random and non-random settings. Consistent with the symmetries of the flow, our computations indicate that Re $\mu_{11} = $ Re μ_{22}. Our computations of Re μ_{jk}, $j, k = 1, 2$, for cat's eye flow also reveal a deeper symmetry, namely Re $\mu_{11} = $ Re $\mu_{22} = |$Re $\mu_{12}|$, where $|$Re $\mu_{12}|$

is the total variation of the measure Re μ_{12}. Our computations of S_{jk} are consistent with these symmetries, as well as rigorous bounds that we derived from the analytic properties of the Stieltjes integral representation for S_{jk} and the associated measures.

Motivated by the theoretical findings in the current work, in [38] we provided a rigorous extension of the results given here to the setting of a time-dependent fluid velocity field $\boldsymbol{u} = \boldsymbol{u}(t, \boldsymbol{x})$. Furthermore, we used abstract methods of functional analysis to generalize Lemma 1 to the continuum, steady and dynamic settings. We are currently exploring the extension of these methods to the time-stochastic setting, which is relevant to atmospheric and oceanic flows.

XI.   ACKNOWLEDGMENTS

Appendix A: Properties of the linear operator A

In this section we derive various properties of the linear operator $A = \Delta^{-1}[\boldsymbol{u}\cdot\boldsymbol{\nabla}]$ defined in equation (48). In particular, we demonstrate that A is antisymmetric on the Hilbert space $\mathcal{H}^{1,2}$ defined in (46). Moreover, we show that A is bounded on $\mathcal{H}^{1,2}$ and we provide an upper bound for $\|A\|_{1,2}$ when $\boldsymbol{u}$ is uniformly bounded on the period cell $\mathcal{V}$.

We first show that the incompressibility condition $\boldsymbol{\nabla}\cdot\boldsymbol{u} = 0$ implies that the operator A is antisymmetric on $\mathcal{H}^{1,2}$ [8], $\langle Af, h\rangle_{1,2} = -\langle f, Ah\rangle_{1,2}$. On the Hilbert space $\mathcal{H}$ defined in (45) the linear operator Δ^{-1} satisfies $\langle \Delta\Delta^{-1}f, h\rangle = \langle f, h\rangle$ in a distributional sense, for all

$f, h \in \mathcal{H}$ [17, 33]. Consequently, for all $f, h \in \mathcal{H}^{1,2}$ we have

$$\langle Af, h \rangle_{1,2} = \langle [\boldsymbol{\nabla}(\Delta^{-1})(\boldsymbol{u}\boldsymbol{\cdot}\boldsymbol{\nabla})f]\boldsymbol{\cdot}\boldsymbol{\nabla} h \rangle \tag{A1}$$

$$= -\langle [(\boldsymbol{u}\boldsymbol{\cdot}\boldsymbol{\nabla})f], h \rangle$$

$$= -\langle [\boldsymbol{\nabla}\boldsymbol{\cdot}(\boldsymbol{u}f)], h \rangle$$

$$= \langle f, [(\boldsymbol{u}\boldsymbol{\cdot}\boldsymbol{\nabla})h] \rangle$$

$$= \langle f, [\Delta(\Delta^{-1})(\boldsymbol{u}\boldsymbol{\cdot}\boldsymbol{\nabla})h] \rangle$$

$$= -\langle \boldsymbol{\nabla} f\boldsymbol{\cdot}[\boldsymbol{\nabla}(\Delta^{-1})(\boldsymbol{u}\boldsymbol{\cdot}\boldsymbol{\nabla})h] \rangle$$

$$= -\langle f, Ah \rangle_{1,2}.$$

Now, we derive the bound on $\|A\|$ given in equation (52). From the Cauchy-Schwartz inequality $|\langle f, h \rangle| \leq \|f\| \|h\|$ we have that

$$\|Af\|_{1,2}^2 = |\langle \boldsymbol{\nabla}[\Delta^{-1}(\boldsymbol{u}\boldsymbol{\cdot}\boldsymbol{\nabla} f)]\boldsymbol{\cdot}\boldsymbol{\nabla}[\Delta^{-1}(\boldsymbol{u}\boldsymbol{\cdot}\boldsymbol{\nabla} f)] \rangle| \tag{A2}$$

$$= |-\langle [\Delta^{-1}(\boldsymbol{u}\boldsymbol{\cdot}\boldsymbol{\nabla} f)], (\boldsymbol{u}\boldsymbol{\cdot}\boldsymbol{\nabla} f) \rangle|$$

$$\leq \|\Delta^{-1}(\boldsymbol{u}\boldsymbol{\cdot}\boldsymbol{\nabla} f)\| \|\boldsymbol{u}\boldsymbol{\cdot}\boldsymbol{\nabla} f\|$$

$$\leq \|\Delta^{-1}\| \|\boldsymbol{u}\boldsymbol{\cdot}\boldsymbol{\nabla} f\|^2.$$

We now provide an upper bound for $\|\boldsymbol{u}\boldsymbol{\cdot}\boldsymbol{\nabla} f\|$ when the components u_k, $k = 1, \ldots, d$, of the fluid velocity field $\boldsymbol{u}$ are uniformly bounded on the period cell $\mathcal{V}$. By the Cauchy-Schwartz inequality, $|\boldsymbol{\xi}\boldsymbol{\cdot}\boldsymbol{\zeta}| \leq |\boldsymbol{\xi}| |\boldsymbol{\zeta}|$, we have

$$\|\boldsymbol{u}\boldsymbol{\cdot}\boldsymbol{\nabla} f\|^2 = \langle |\boldsymbol{u}\boldsymbol{\cdot}\boldsymbol{\nabla} f|^2 \rangle \leq \langle |\boldsymbol{u}|^2 |\boldsymbol{\nabla} f|^2 \rangle \leq \sup_{\boldsymbol{x} \in \mathcal{V}} |\boldsymbol{u}(\boldsymbol{x})|^2 \|f\|_{1,2}^2. \tag{A3}$$

The result in equation (52) is now clear.

Appendix B: Derivation of equation (87)

In this section we provide a derivation of equation (87). Equation (85) allows equation (80) to be written as $[\mathsf{V}_1\Sigma_1\mathsf{R}_1](\varepsilon\mathsf{I}_1 + \imath\Lambda_1)[\mathsf{V}_1\Sigma_1\mathsf{R}_1]^\dagger \boldsymbol{\chi}_j = \boldsymbol{u}_j$. This and equation (83) imply that

$$\mathsf{V}_1^T \boldsymbol{\chi}_j = \Sigma_1^{-1}\mathsf{R}_1(\varepsilon\mathsf{I}_1 + \imath\Lambda_1)^{-1}\mathsf{R}_1^\dagger\Sigma_1^{-1}\mathsf{V}_1^T\boldsymbol{u}_j. \tag{B1}$$

This formula and $\nabla = \mathsf{U}_1\Sigma_1\mathsf{V}_1^T$ imply that

$$\nabla\boldsymbol{\chi}_j = \mathsf{U}_1\mathsf{R}_1(\varepsilon\mathsf{I}_1 + \imath\Lambda_1)^{-1}\mathsf{R}_1^\dagger\Sigma_1^{-1}\mathsf{V}_1^T\boldsymbol{u}_j. \tag{B2}$$

Therefore, since $\mathsf{U}_1^T\mathsf{U}_1 = \mathsf{I}_1$ and $\mathsf{R}_1^\dagger\mathsf{R}_1 = \mathsf{I}_1$, we clearly have the first formula in (87) for S_{jk}^* with $\mathsf{Z}_1^\dagger = \mathsf{R}_1^\dagger\Sigma_1^{-1}\mathsf{V}_1^T$. From equation (85) we have that

$$\langle\nabla^T\mathsf{H}\nabla\boldsymbol{\chi}_j{\cdot}\boldsymbol{\chi}_k\rangle = \langle\imath[\mathsf{V}_1\Sigma_1\mathsf{R}_1]\Lambda_1[\mathsf{R}_1^\dagger\Sigma_1\mathsf{V}_1^T]\boldsymbol{\chi}_j{\cdot}\boldsymbol{\chi}_k\rangle = \langle\imath[\Sigma_1\mathsf{R}_1\Lambda_1\mathsf{R}_1^\dagger\Sigma_1]\mathsf{V}_1^T\boldsymbol{\chi}_j{\cdot}\mathsf{V}_1^T\boldsymbol{\chi}_k\rangle. \tag{B3}$$

This formula, $\mathsf{R}_1^\dagger\mathsf{R}_1 = \mathsf{I}_1$, $\Sigma_1^T = \Sigma_1$, and equation (B1) clearly imply the second formula for A_{jk}^* in equation (87), with $\mathsf{Z}_1^\dagger = \mathsf{R}_1^\dagger\Sigma_1^{-1}\mathsf{V}_1^T$.

---

[1] G.S. Aslanyan, I.L. Maikov, and I.Z. Filimonova. Simulation of pulverized coal combustion in a turbulent flow. *Combust., Expl., Shock Waves*, 30(4):448–453, 1994.

[2] M. Avellaneda and A. Majda. Stieltjes integral representation and effective diffusivity bounds for turbulent transport. *Phys. Rev. Lett.*, 62:753–755, 1989.

[3] M. Avellaneda and A. Majda. An integral representation and bounds on the effective diffusivity in passive advection by laminar and turbulent flows. *Comm. Math. Phys.*, 138:339–391, 1991.

[4] M. Avellaneda and M. Vergassola. Stieltjes integral representation of effective diffusivities in time-dependent flows. *Phys. Rev. E*, 52(3):3249–3251, 1995.

[5] G. A. Baker and P. R. Graves-Morris. *Padé Approximants*. Encyclopedia of Mathematics and its Applications. Cambridge University Press, 1996.

[6] A. Bensoussan, J.-L. Lions, and G. Papanicolaou. *Asymptotic Analysis for Periodic Structures*. North-Holland, Amsterdam, 1978.

[7] M.R. Beychok. *Fundamentals of Stack Gas Dispersion: Guide*. The Author, 1994.

[8] R. Bhattacharya. Multiscale diffusion processes with periodic coefficients and an application to solute transport in porous media. *Ann. Appl. Probab.*, 9(4):951–1020, 1999.

[9] L. Biferale, A. Crisanti, M. Vergassola, and A. Vulpiani. Eddy diffusivities in scalar transport. *Phys. Fluids*, 7:2725–2734, 1995.

[10] R. W. Bilger, S. B. Pope, K. N. C. Bray, and J. F. Driscoll. Paradigms in turbulent combustion research. *Proc. Combust. Inst.*, 30:21–42, 2005.

[11] K. F. Bowden. Horizontal mixing in the sea due to a shearing current. *J. Fluid Mech.*, 21(1):83– 95, 1965.

[12] G. T. Csanady. Turbulent diffusion of heavy particles in the atmosphere. *J. Atmos. Sci.*, 20(3):201–208, 1963.

[13] J. W. Demmel. *Applied Numerical Linear Algebra*. SIAM, 1997.

[14] E. Di Lorenzo, D. Mountain, H. P. Batchelder, N. Bond, and E. E. Hofmann. Advances in marine ecosystem dynamics from us globec: The horizontal-advection bottom-up forcing paradigm. *Oceanography*, 26(4):22–33, 2013.

[15] A. Fannjiang and G. Papanicolaou. Convection enhanced diffusion for periodic flows. *SIAM Journal on Applied Mathematics*, 54(2):333–408, 1994.

[16] A. Fannjiang and G. Papanicolaou. Convection-enhanced diffusion for random flows. *J. Stat. Phys.*, 88(5-6):1033–1076, 1997.

[17] G. B. Folland. *Introduction to Partial Differential Equations*. Princeton University Press, Princeton, NJ, 1995.

[18] G. B. Folland. *Real Analysis: Modern Techniques and Their Applications*. Wiley–Interscience, New York, NY, 1999.

[19] K. M. Golden and G. Papanicolaou. Bounds for effective parameters of heterogeneous media by analytic continuation. *Commun. Math. Phys.*, 90:473–491, 1983.

[20] Y. Gorb, D. Nam, and A. Novikov. Numerical simulations of diffusion in cellular flows at high Péclet numbers. *Discrete Contin. Dyn. Syst. Ser. B*, 15(1):75–92, 2011.

[21] E. E. Hofmann and E. J. Murphy. Advection, krill, and antarctic marine ecosystems. *Antarctic Science*, 16(04):487–499, 12 2004.

[22] R. A. Horn and C. R. Johnson. *Matrix Analysis*. Cambridge University Press, 1990.

[23] M. B. Isichenko and J. Kalda. Statistical topography II. 2D transport of passive scalar. *J. Nonlinear Sci.*, 4:375–397, 1991.

[24] J. D. Jackson. *Classical Electrodynamics*. John Wiley and Sons, Inc., New York, 1999.

[25] J. P. Keener. *Principles of Applied Mathematics: Transformation and Approximation*. Advanced book program. Westview Press, Cambridge, MA, 2000.

[26] D. Khoshnevisan. *Probability*. Graduate studies in mathematics. American Mathematical Society, 2007.

[27] G. Kullenberg. Apparent horizontal diffusion in stratified vertical shear flow. *Tellus*, 24(1):17–28, 1972.

[28] J. V. Lukovich, D. G. Babb, and D. G. Barber. On the scaling laws derived from ice beacon trajectories in the southern beaufort sea during the international polar year - circumpolar flaw lead study, 2007–2008. *J. Geophys. Res.-Oceans*, 116(C9):C00G07 (16pp.), 2011.

[29] A. Majda and P. R. Kramer. *Simplified Models for Turbulent Diffusion: Theory, Numerical Modelling, and Physical Phenomena.* Physics reports. North-Holland, 1999.

[30] A. J. Majda and P. E. Souganidis. Large scale front dynamics for turbulent reaction-diffusion equations with separated velocity scales. *Nonlinearity*, 7(1):1–30, 1994.

[31] D. McLaughlin, G. Papanicolaou, and O. Pironneau. Convection of microstructure and related problems. *SIAM J. Appl. Math.*, 45:780–797, 1985.

[32] R. M. McLaughlin and M. G. Forest. An anelastic, scale-separated model for mixing, with application to atmospheric transport phenomena. *Phys. Fluids*, 11(4):880–892, 1999.

[33] R. C. McOwen. *Partial differential equations: methods and applications.* Prentice Hall PTR, 2003.

[34] Y. A. Melnikov, Y. A. Melnikov, and M. Y. Melnikov. *Green's Functions: Construction and Applications.* De Gruyter studies in mathematics. De Gruyter, 2012.

[35] G. W. Milton. *Theory of Composites.* Cambridge University Press, Cambridge, 2002.

[36] H. K. Moffatt. Transport effects associated with turbulence with particular attention to the influence of helicity. *Rep. Prog. Phys.*, 46(5):621–664, 1983.

[37] N. B. Murphy, E. Cherkaev, C. Hohenegger, and K. M. Golden. Spectral measure computations for composite materials. *Commun. Math. Sci.*, 13(4):825–862, 2015.

[38] N. B. Murphy, E. Cherkaev, J. Xin, J. Zhu, and K. M. Golden. Spectral analysis and computation of effective diffusivities in space-time periodic incompressible flows. Submitted, 2016.

[39] G. Papanicolaou and S. Varadhan. Boundary value problems with rapidly oscillating coefficients. In *Colloquia Mathematica Societatis János Bolyai 27, Random Fields (Esztergom, Hungary 1979)*, pages 835–873. North-Holland, 1982.

[40] B. N. Parlett. *The Symmetric Eigenvalue Problem.* Prentice-Hall, Inc., Upper Saddle River, NJ, USA, 1998.

[41] G. A. Pavliotis. *Homogenization theory for advection-diffusion equations with mean flow.* PhD thesis, Rensselaer Polytechnic Institute Troy, New York, 2002.

[42] G. A. Pavliotis. Asymptotic analysis of the Green–Kubo formula. *IMA J. Appl. Math.*, 75:951–967, 2010.

[43] N. Peters. *Turbulent Combustion.* Cambridge Monographs on Mechanics. Cambridge University Press, 2000.

[44] P. Rampal, J. Weiss, D. Marsan, and M. Bourgoin. Arctic sea ice velocity field: General circulation and turbulent-like fluctuations. *J. Geophys. Res.-Oceans*, 114(C10):C10014 (17pp.), 2009.

[45] P. Rampal, J. Weiss, D. Marsan, R. Lindsay, and H. Stern. Scaling properties of sea ice deformation from buoy dispersion analysis. *J. Geophys. Res.-Oceans*, 113(C3):C03002 (12pp.), 2008.

[46] M. C. Reed and B. Simon. *Functional Analysis.* Academic Press, San Diego CA, 1980.

[47] W. Rudin. *Real and Complex Analysis.* McGraw-Hill, Inc., New York, NY, 1987.

[48] P. J. Samson. Atmospheric transport and dispersion of air pollutants associated with vehicular emissions. In A. Y. Watson, R. R. Bates, and D. Kennedy, editors, *Air Pollution, the Automobile, and Public Health*, pages 77–97. National Academy Press (US), 1988.

[49] I. Stakgold. *Boundary Value Problems of Mathematical Physics.* Classics in Applied Mathematics. SIAM, 2000. 2-volume set.

[50] T.-J. Stieltjes. Recherches sur les fractions continues. *Annales de la faculté des sciences de Toulouse*, 4(1):J1–J35, 1995.

[51] M. H. Stone. *Linear Transformations in Hilbert Space.* American Mathematical Society, Providence, RI, 1964.

[52] R. J. Tabaczynski. Turbulent flows in reciprocating internal combustion engines. In J. H. Weaving, editor, *Internal Combustion Engineering: Science & Technology*, pages 243–285. Springer Netherlands, 1990.

[53] G. I. Taylor. Eddy motion in the atmosphere. *Phil. Trans. R. Soc. Lond. A*, 215(523–537):1–26, 1915.

[54] G. I. Taylor. Diffusion by continuous movements. *Proc. London Math. Soc.*, 2:196–211, 1921.

[55] W. M. Washington and C. L. Parkinson. *An Introduction to Three-dimensional Climate Modeling.* University Science Books, 1986.

[56] E. Watanabe and H. Hasumi. Pacific water transport in the western Arctic Ocean simulated by an eddy-resolving coupled sea ice–ocean model. *J. Phys. Oceanogr.*, 39(9):2194–2211, 2009.

[57] F. A. Williams. *Turbulent Combustion*, chapter 3, pages 97–131. Frontiers in Applied Mathematics. Society for Industrial and Applied Mathematics, SIAM, 3600 Market Street, Floor 6,

Philadelphia, PA 19104, 1985.

[58] J. Xin. *An Introduction to Fronts in Random Media.* Surveys and Tutorials in the Applied Mathematical Sciences. Springer New York, 2009.

[59] W. R. Young, P. B. Rhines, and C. J. R. Garrett. Shear-flow dispersion, internal waves and horizontal mixing in the Ocean. *J. Phys. Oceanogr.*, 12:515–527, 1982.